SECOND HARMONIC GENERATION IN PROTON-EXCHANGED LITHIUM NIOBATE OPTICAL WAVEGUIDES

A Thesis submitted to the

Faculty of Engineering at the

University of Glasgow

for the degree of

Doctor of Philosophy

by

Robert W. Keys

May 1991

ProQuest LLC.
789 East Eisenhower Parkway
P.O. Box 1346
Ann Arbor, MI 48106 – 1346

Dedicated to Alison

ACKNOWLEDGEMENTS

I would like to express my gratitude to my academic supervisor and friend Professor Richard De La Rue for his extremely valuable help, encouragement and many useful and enlightening discussions. I am also greatly indebted to my friend Doctor Armando Loni for his technical assistance and advice throughout the duration of my study.

I am extremely grateful to Professor John Lamb for the encouragement and support he has given me over the last three years and for the use of the facilities in the Department of Electronic and Electrical Engineering.

The help and assistance of the members of the mechanical and electrical workshops was greatly appreciated. Special thanks must go to Kaz Piechowiak for his polishing work, to Robert Harkins for provision of the photolithographic masks and to Lois Hobbs, George Boyle, Jimmy Young, Dave Clifton and Harry Anderson for their invaluable and expert assistance.

I would like to express my extreme gratitude to my colleagues in the Optical Materials and Applications group at Bell Northern Research Europe / Standard Telecommunications Laboratories for their encouragement during the writing of this thesis. Special thanks must go to Doctor Mike Scott for allowing me the use of the computing facilities which enabled this thesis to be written.

Finally, I would like to thank all of my colleagues who made my stay at Glasgow University an enjoyable one.

Thesis Outline

The object of this thesis is to investigate second order nonlinear optical processes in proton–exchanged lithium niobate waveguides. In particular it is to investigate the effects of different waveguide fabrication parameters on the conversion efficiency for second harmonic generation with the aim of optimizing the conversion efficiency.

Chapter one gives a brief account of nonlinear optical processes in dielectric materials and, in particular, reviews the properties of lithium niobate which make it such an effective crystal for nonlinear processes. Nonlinear processes in bulk crystals are first explained. This is extended to include the effects of constraining the light inside a waveguiding structure and to show how this approach leads to more efficient interactions. Techniques for producing low–loss waveguides in lithium niobate are then discussed with the emmphasis being on the proton–exchange process. Finally, the possibility of constructing efficient miniature, Q–switched, self–frequency doubled lasers in doped lithium niobate is discussed.

Chapter two explains the Cerenkov phase–matching scheme for second harmonic generation in proton–exchanged waveguides. A brief review of the published theoretical studies of Cerenkov SHG is given. This is followed by an outline of a coupled mode analysis of the problem derived by the author. The results of this analysis are compared to the published results.

Chapter three is concerned with the investigation of the proton–exchange fabrication parameters on the efficiency of second harmonic generation in planar waveguides. The need to choose on optimum depth to maximise the conversion efficiency is shown, followed by an investigation into the effect of annealing the waveguide. Low power c.w. second harmonic generation in stripe waveguides is then investigated and demonstrated using both a Nd:YAG laser and a semiconductor laser.

Chapter four describes experimental work undertaken to compare and contrast the conversion efficiency for second harmonic generation in waveguides fabricated with two different acids. It has been claimed that waveguides fabricated with phosphoric acid have a higher refractive index than those fabricated with benzoic acid and consequently could give waveguides with a higher conversion efficiency. These claims are investigated for both congruent and magnesium oxide doped

lithium niobate.

In chapter five the application of grating structures to second order nonlinear interactions is investigated. Firstly, a novel technique for the production of first−order pratings on the −c− face of the lithium niobate substrate is described. Such grating structures should allow efficient second harmonic generation via quasi phasematching. The determination of the correct period for the grating and the fabrication of the grating is described. Secondly, the application of grating structures to the measurement of the second order nonlinear d_{33} coefficient of proton−exchanged lithium niobate is described. Using this technique the d_{33} coefficient was measured as well as the effect of annealing on the magnitude of the coefficient.

Finally, in chapter six, a summary, with conclusions, of the thesis is presented.

CONTENTS

CHAPTER FIVE

GRATING STRUCTURES AND THE NONLINEAR d_{33} COEFFICIENT

CHAPTER SIX

CONCLUSIONS

CHAPTER 1.

NONLINEAR INTEGRATED OPTICS IN LITHIUM NIOBATE OPTICAL WAVEGUIDES

1.1 Introduction.

The aim of this chapter is to outline some of the background to nonlinear interactions in lithium niobate waveguides. Nonlinear interactions in other materials, such as organic crystals or III–V semiconductors, will be mentioned only briefly.

The chapter splits naturally into four sections. In the first section, a brief history of nonlinear optics is presented. The potential of integrated optical waveguide structures for the efficient exploitation of nonlinear effects will then be discussed. Standard results from the theory of second harmonic generation will be quoted throughout the text. No attempt has been made to justify the quoted results as the derivations are well known and, in chapter two, the theory of second harmonic generation in proton–exchanged waveguides will be explained in more detail.

A brief overview of the properties of lithium niobate will then be given in the second section of the chapter followed, in the third section of the chapter, by an outline of the proton–exchange process for waveguide fabrication. The properties of the waveguides which are important for nonlinear applications will be highlighted. Included in this section will be a short review of previous work on nonlinear integrated optics in proton–exchanged waveguides.

A short section then reviews some of the new applications for nonlinear effects in specially–doped lithium niobate substrates. These applications include diode–pumped solid state lasers which can exploit the nonlinear properties of lithium niobate and the advantages of integrated optical waveguiding structures.

Finally, to conclude the chapter, a brief, chapter–by–chapter, review of the contents of this thesis is presented.

1.2 Nonlinear optical frequency conversion in optical waveguides

1.2.1 Nonlinear optics: A brief review

The branch of optics now commonly referred to as "nonlinear optics" only really began to develop significantly after the invention of the laser in the early part of te 1960's. Although nonlinear optical effects were known and had been extensively researched before the invention of the laser, for example optical pumping, the unique properties of the laser allowed the exploitation of optical effects which had previously been unobtainable with even the highest power light sources of the day. Shortly after the invention of the laser, Franklin and co-workers demonstrated ultra-violet generation by the frequency doubling of a ruby laser [1]. This led to an intensive study of nonlinear effects in crystals and the discovery of many new phenomenon. The high intensity laser sources required to exploit the nonlinearity of crystals limited the development of practical devices for commercial use, with the consequence that nonlinear optics remained, on the whole, in the laboratory. With the emergence of integrated optics in the 1970s, many nonlinear effects could be observed easily using low power laser sources, due to the power confinement capability of an optical waveguide which leads to a high beam intensity even at low powers. Many practical devices have now been demonstated using semiconductor lasers as the pump source.

When a dielectric medium is subjected to an electric field the electrons in the medium are polarised. For weak electric fields the induced polarisation is linearly proportional to the applied electric field [2]:-

$$\mathbf{P} = \epsilon_0 . \chi^{(1)} . \mathbf{E} \qquad (1.1)$$

where $\chi^{(1)}$ is the linear optical susceptibility, related to the refractive index of the medium by $\chi^{(1)} = n^2 - 1$. A linear polarisability is an approximation to the true constitutive relation which can be written as a Taylor expansion of the optical field [2]:-

$$\mathbf{P} = \epsilon_0 . \mathbf{E} . \{ \chi^{(1)} + \chi^{(2)} \mathbf{E} + \chi^{(3)} \mathbf{E} . \mathbf{E} + \ldots\ldots \} \qquad (1.2)$$

where $\chi^{(n)}$ is the n-th order nonlinear susceptibilty. The n-th order susceptibilities are in general (n+1) order tensors. Table 1 lists some of the effects which can arise due to the second and third order nonlinear

susceptibilities. In this project, only effects due to $\chi^{(2)}$ have been studied and no further mention will be made of third order effects.

Table 1.

Nonlinear coefft.	Effects	Uses
$\chi^{(2)}$	SHG	frequency doublers
	frequency mixing $\omega_1 \pm \omega_2 = \omega_3$	optical mixers
	parametric amplification	optical parametric oscillators
$\chi^{(3)}$	Kerr effect	optical switches
	optical bistability	optical logic gates etc.

Figure 1.1 illustrates two of the second order effects, namely second harmonic generation and parametric amplification.

second harmonic generation

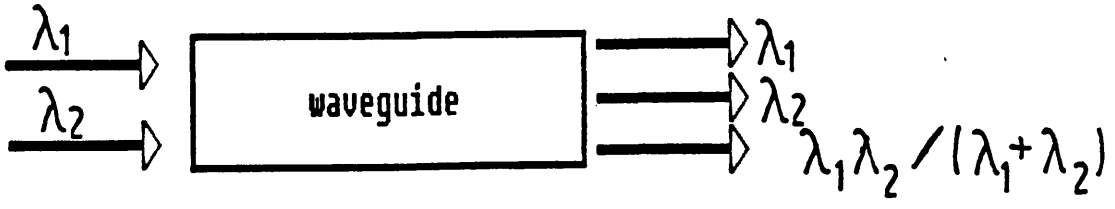

parametric amplification / 3-wave mixing

figure 1.1

In general, the n interacting fields may have n different frequencies. A superposition of sinusiodal electric fields may be written as:—

$$E(r,t) = \sum_{\omega}\sum_{i} e_i.(1/2).[E_i(\omega).e^{j(\omega t - k.r)} + c.c.] \qquad (1.3)$$

where E_i is the complex field amplitude in the direction of the unit vector e_i. The n fields interact through the nonlinear susceptibility of the material (which may be represented as a tensor of order n+1). The nonlinear polarization can be expanded similarly:—

$$P(r,t) = P^{(1)}(r,t) + P^{(2)}(r,t) + ... \qquad (1.4)$$

where:—

$$P^{(n)}(r,t) = \sum_{\omega}\sum_{i} e_i.(1/2).[P_i^{(n)}(\omega).e^{j(\omega t - k.r)} + c.c.] \qquad (1.5)$$

Each $P^{(n)}(r,t)$ can be related to the electric fields producing it via the appropriate susceptibility tensor. Each $P^{(n)}(r,\omega)$ can be related to the electric fields producing it via the appropriate susuceptibility tensor. The second order term is:—

$$P_f^{2\omega}(r,\omega_3) = \epsilon_0.\sum_{jk}\chi_{jk}^{(2)}(\omega_3:\omega_1,\omega_2).E_j(\omega_1).E_k(\omega_2).e^{-K.r} \qquad (1.6)$$

where:—

$$K = k_1 + k_2 \qquad (1.7)$$

with k_i being the wavevector for the i—th wave at frequency ω_i. It has been customary to describe the second order susceptibility by writing the polarization density at the second harmonic in the form:—

$$P_j^{2\omega} = \epsilon_0.\sum_{jk} d_{ijk}.E_j^{\omega}.E_k^{\omega} \qquad (1.8)$$

The components of the nonlinear susceptibility tensor, $\chi^{(2)}$, defined by equation 6, can be related to the components of the nonlinear d tensor by [2]:—

$$\chi_{ijk} = 2.d_{ijk} \qquad (1.9)$$

The coefficients of the nonlinear d tensor have units mV^{-1}. The physical basis of the nonlinear effect is in the asymmetric structure of the crystalline material. Theories exist that allow a calculation of the nonlinear tensor coefficients. The most basic of these theories, the anharmonic oscillator model, treats the electrons as being in an asymmetric potential well. This theory allows a simple calculation of d_{ijk}. A proper derivation of the n−th order nonlinear coefficients involves a detailed quantum mechanical treatment using density matrix theory. Details of such theories are outwith the scope of this thesis.

1.2.2 Second harmonic generation; Comparison of bulk and guided wave configurations

Nonlinear interactions, in particular second harmonic generation, have been studied in great depth using bulk crystals. The conversion efficiency for second harmonic generation is defined as:−

$$\eta = P^{2\omega} / P^{\omega} \qquad (1.10)$$

where $P^{2\omega}$, P^{ω} are the powers of the harmonic and fundamental waves respectively. In chapter two the theory of second harmonic generation will be discussed in more detail but, in order to compare bulk optics with integrated optics, the main results will be outlined in this section.

In bulk nonlinear optics, the electric field of the laser at the fundamental wavelength will usually be described by a Gaussian distribution. To simplify the analysis, consider the case of plane waves. In the limit of low conversion efficiencies, i.e. the fundamental beam is undepleted, the conversion efficiency can be shown to be given by [3]:−

$$\eta = 2.\frac{\omega^2}{n_\omega^2 n_{2\omega} c^3 \epsilon_0}.d_{eff}^2.L^2.\frac{P^{\omega}}{A}\frac{\sin^2(0.5\Delta kL)}{(0.5\Delta kL)^2} \qquad (1.11)$$

where d_{eff} is the effective nonlinear coefficient, L is the interaction length, $\Delta k = k^{2\omega} - k^{\omega}$ is the phase mis−match and all other terms have their usual meaning.

For the case of second harmonic generation in an integrated optical waveguide, the electric fields are given by the modal field solutions of Maxwells equations under the boundary conditions imposed by the waveguide structure. The

conversion efficiency for second harmonic generation is given by:—

$$\eta = C.\mathrm{sinc}^2(0.5\Delta kL).I^2 \qquad (1.12)$$

where C is given by:—

$$C = 2.\frac{\omega^2}{n_\omega^2 n_{2\omega} c^3 \epsilon_0}.d_{eff}^2.L^2.P^\omega.\frac{\sin^2(0.5\Delta\beta L)}{(0.5\Delta\beta L)^2} \qquad (1.13)$$

and I, known as the overlap integral is given by:—

$$I\ (m^{-1}) = \int(E_{2\omega}).(E_\omega)^2.dxdy \qquad (1.14a)$$

$E_{2\omega}$ and E_ω are the normalised electric field distributions at the harmonic and fundamental frequencies; that is

$$\int(E_{\omega,2\omega})^2 dxdy = 1 \qquad (1.14b)$$

The overlap of a fundamental field and a harmonic field is illustrated in figure 1.2. The overlap changes as the field distributions change. Thus the conversion efficiency is stongly dependent on the waveguide parameters through this overlap integral. Figure 1.3 illustrates both situations of a guided—guided mode interaction as in conventional phasematching and also guided—radiation mode interaction as found in the Cerenkov phasematching scheme. In bulk nonlinear optics, the phase mis—match can be compensated for by temperature tuning the birefringence of the crystal [4] or by angle tuning the direction of propagation in the crystal [4].

Integrated optical waveguide structures are very interesting because they allow alternative solutions to the problem of efficient second harmonic generation. In crystals where the natural birefringence does not permit phasematching, guided wave optics allow the use of modal dispersion to arrange for the phase mis—match to be $\Delta k = 0$. As phasematching is essential for an efficient interaction, integrated optics may allow the use of materials which cannot otherwise be phasematched, but which are nonetheless nonlinear.

To continue the comparison, consider the case of a phasematched interaction in both the bulk and guided wave interactions. In this case the essential advantage of the guided wave arises from the ability of the waveguide to confine the optical power density over a long interaction length. In bulk crystals, the fundamental beam must be focussed down to increase the power density. The optimum

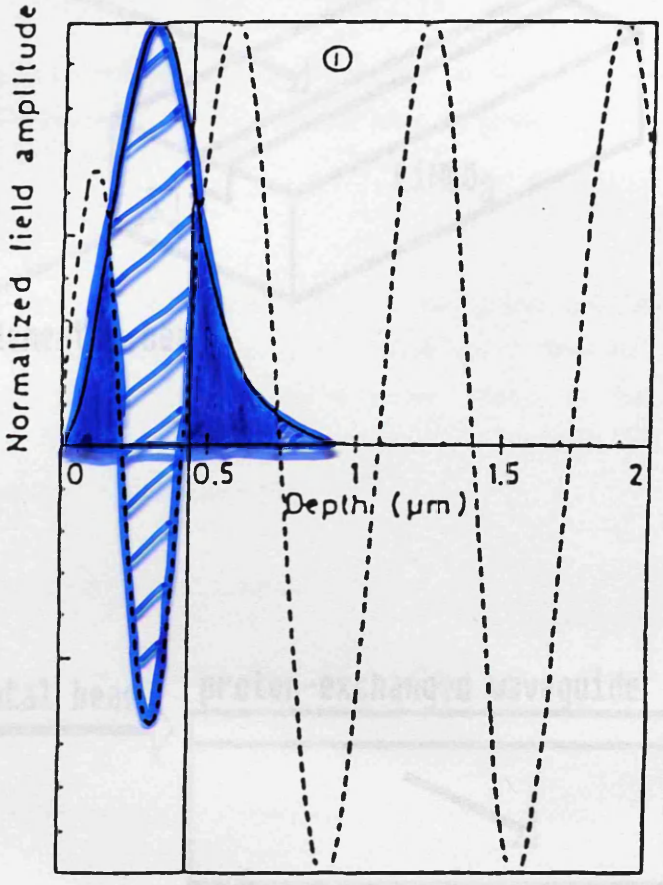

Normalized field amplitudes as a function of depth (in the direction of waveguide thickness). The solid curve is for a squared of a fundamental wave TM guided mode and the dashed curve is for a second harmonic radiation mode.

After H. Tamada "Coupled mode analysis of SHG in the form of Cerenkov radiation from a planar optical waveguide"; IEEE Jnl Quantum Electronics 27(3), pp.502-508, 1991.

figure 1.2 overlap of the fundamental and harmonic modes. The dark shaded areas represent a positive contribution to the overlap intgral, the hatched areas a negative contribution.

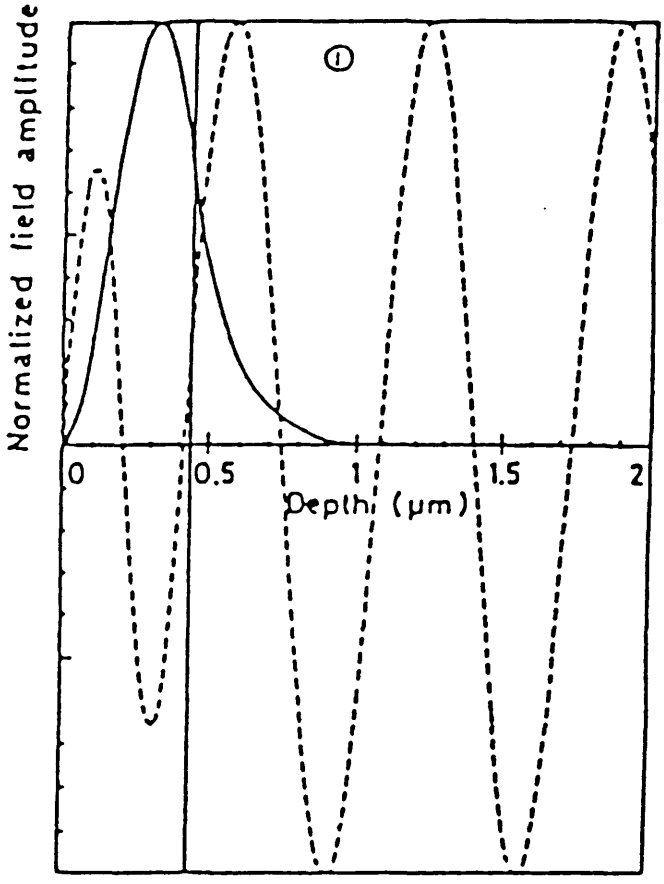

Normalized field amplitudes as a function of depth (in the direction of waveguide thickness). The solid curve is for a squared of a fundamental wave TM guided mode and the dashed curve is for a second harmonic radiation mode.

After H. Tamada "Coupled mode analysis of SHG in the form of Cerenkov radiation from a planar optical waveguide"; IEEE Jnl Quantum Electronics 27(3), pp.502-508, 1991.

figure 1.2 overlap of the fundamental and harmonic modes. The dark shaded areas represent a positive contribution to the overlap intgral, the hatched areas a negative contribution.

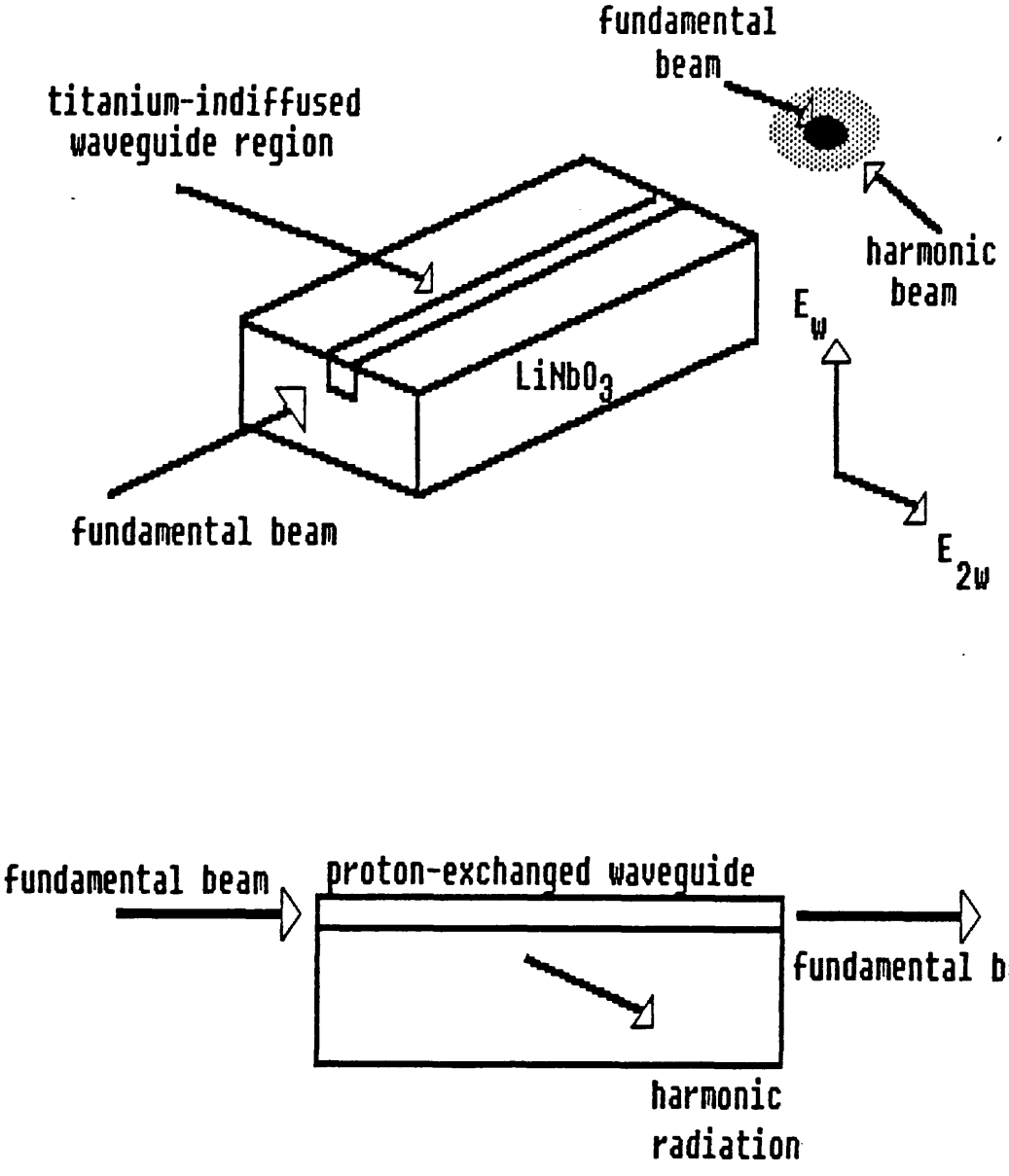

figure 1.3 SHG in optical waveguides in lithium niobate. Top:- guided-guided mode interaction. Bottom:- guided-radiation mode interaction.

arrangement for this is the so-called confocal focussing arrangement, in which case Eq. 1.11 must be derived in a more rigorous fashion. For a Gaussian beam distribution, in the confocal focussing arrangement, the conversion efficiency can be shown to be given by:-

$$\eta = 4.\frac{\omega^2}{n_\omega n_{2\omega} c^3 \epsilon_0}.d_{eff}^2.\frac{L}{\lambda}P_\omega.\frac{\sin^2(0.5\Delta kL)}{(0.5\Delta kL)^2} \qquad (1.15)$$

Comparing the confocal beam configuration to that of guided waves, the ratio of the guided wave term to the confocal term is given by:-

$$GW/CF = (L.\lambda/2N_{eff}).I^2 \qquad (1.16)$$

For values appropriate to lithium niobate waveguides this leads to an improvement factor of around 200 for the guided wave case. However, the efficiency of the guided wave case is reduced by a factor known as the overlap integral (see chapter 2). This "reduction" is actually multiplication by the overlap integral factor which is less than one [3].

1.2.3 Choice of nonlinear material

For bulk nonlinear optical applications the crystals should (ideally) possess the following properties [5]:-

(1) non-centrosymmetry for exploitation of $\chi^{(2)}$ effects,

(2) optical transparency in the wavelength ranges of use, i.e. at both the fundamental and harmonic (or sum/difference) wavelengths of interest,

(3) birefringence,

(4) resistance to optical damage.

For nonlinear integrated optics the above conditions can, under given conditions, be relaxed. For example, the requirement for birefringence need no longer hold as the waveguide dispersion can allow an extra degree of freedom for phasematching as discussed above. However, an extra constraint is that it must be possible to fabricate good quality, low loss, waveguides in a reproducible manner.

Ferroelectric lithium niobate has long been known to possess large optical nonlinearities and, as such, has routinely been used for nonlinear optical applications. Furthermore, it is possible to fabricate low-loss waveguides by either titanium-indiffusion, proton-exchange or a combination of both. For these reasons, lithium niobate was the crystal chosen as the nonlinear material. One disadvantage of using lithium niobate is that it is photorefractive, i.e. it is susceptible to optical damage, even at moderate input powers. The waveguide fabrication technique used throughout the thesis was proton-exchange and it is known that the photorefractive susceptibility of proton-exchanged lithium niobate is lower than that of the bulk crystal.

1.2.4 The crystal structure of lithium niobate

Lithium niobate is a man-made compound that does not occur naturally. The growth of lithium niobate by the Czochralski technique was reported independently by Ballman [6] and Fedulov [7] in 1964 and since then this technique has become the standard method for the commercial growth of lithium niobate. It is ferroelectric, with a three-fold rotational symmetry about the c-axis, making it a member of the trigonal crystal system. It also has mirror symmetry about three planes 60^0 apart rotated about the c-axis and is thus classified as a member of the 3m point group. Crystals which belong to the trigonal group can be structurally classified using either a hexagonal or a rhombohedral unit cell. For an in-depth study of the lithium niobate crystal structure a series of five papers by Nassau, Abrahams et al [8,9,10,11,12], concerned with the growth, crystal structure and other material aspects published in 1966 is considered an important piece of research work. Other general reviews on the properties of lithium niobate have been published by Rauber [13], by Weis and Gaylord [14] as well as an INSPEC volume devoted entirely to lithium niobate [14b].

Lithium niobate has been shown to have a large deviation in the stoichiometry dependent upon the crystal growth conditions. The dependence of the stoichiometry upon crystal growth has been well studied by many workers [15, 16]. Many of the physical properties of lithium niobate are dependent on the crystal stoichiometry and so, also, is the crystal homogeneity. It is now well understood that the extraordinary refractive index is strongly dependent on the stoichiometry but that the ordinary index is not dependent. This implies that the phasematching temperature for second harmonic generation is dependent on the crystal stoichiometry. By growing crystals in which the initial melt composition is 48.6 mole% Li_2O, congruent lithium niobate is grown. The congruent crystals are

very homogeneous and consequently the physical properties of lithium niobate are very close to constant throughout the crystal.

1.2.5 Nonlinear properties of lithium niobate

As was stated in the previous section, lithium niobate is a member of the 3m point group. General crystallographic symmetry considerations indicate that there should be four nonlinear coefficients d_{15}, d_{22}, d_{31}, and d_{33}. Applying the Kleinmann symmetry rule [4] indicates that $d_{31} = d_{15}$ and, consequently, for lithium niobate, there are only three independent second order nonlinear coefficients. The components of the second harmonic polarization can be written, in the reduced matrix notation, as follows:—

$$\begin{bmatrix} P_x \\ P_y \\ P_z \end{bmatrix} = \begin{bmatrix} 0 & 0 & 0 & 0 & d_{31} & -d_{22} \\ -d_{22} & d_{22} & 0 & d_{31} & 0 & 0 \\ d_{31} & d_{31} & d_{33} & 0 & 0 & 0 \end{bmatrix} \begin{bmatrix} E_x^2 \\ E_y^2 \\ E_z^2 \\ 2E_yE_z \\ 2E_xE_z \\ 2E_xE_y \end{bmatrix} \qquad (1.17)$$

Equation 1.17 allows the nonlinear polarisation fields to be calculated for a given polarisation of fundamental field. For example consider an electric field poarised in the x—direction. It can be seen that this field can couple to an electric polarised field in the z—direction via the d_{31} coefficient and also to a y—polarised field via d_{22}. Phasematching then determines which field dominates at the output face of the crystal (see figure 1.3).

The magnitude of the coefficients (in pmV^{-1}) are as follows [13]:—

$d_{33} = 34.4$

$d_{31} = 5.95$

Experimentally, the value of d_{22} is subject to large errors because it can only be determined from a difference of large numbers [13]. As d_{22} is of little interest for the work of this thesis no value of the magnitude will be quoted. The magnitudes quoted above are for a fundamental wavelength of 1.06μm. However, as expected, there is little variation in the magnitude of the coefficients over the visible and near IR spectrum. As was mentioned in 1.2.4 above, the physical properties of lithium niobate are dependent on the crystal stoichiometry. This indicates that the nonlinear coefficients may be dependent on the stoichiometry.

Miller and Norland [17] have reported that only the d_{31} coefficient is strongly dependent on the initial melt composition. This dependence emphasises the need for congruent crystals for nonlinear applications in which the d_{31} coefficient is to be used.

1.3 Fabrication of optical waveguides by proton–exchange

Only proton–exchanged waveguides were used in the work presented in this thesis. There are several other techniques for waveguide fabrication in lithium niobate and it is outside the scope of this thesis to discuss these. Several articles have been published reviewing waveguide fabrication techniques in lithium niobate [21,22]. A brief overview of the proton–exchange process will be given. For a review of the alternative techniques the reader is referred to the cited articles.

Proton–exchange using benzoic acid was first demonstrated by Jackel at al [18], in 1982 and developed from earlier work on ion–exchange involving $AgNO_3$ [19] and $TlNO_3$ [20] melts. The ion–exchange process resulted in generally unreproducible high index guides and was initially believed to be due to an exchange between the lithium ions and the Ag or Tl ions. The index change was later recognised to be due to an exchange process between hydrogen ions (protons) from water impurities in the molten salts and the lithium ions [20].

Proton–exchange involves an exchange between lithium ions from the substrate with hydrogen ions (protons) from the acid source. Chemically, the proton–exchange process can be written as:–

$$LiNbO_3 + xH \longrightarrow H_xLi_{1-x}NbO_3 + xLi \qquad (1.18)$$

A number of acid sources have been used, the most widely studied being benzoic acid (C_6H_5COOH), for several reasons. Firstly, it has a convenient working range, the melting and boiling points of the acid being $\simeq$122 °C and $\simeq$249 °C respectively [21]. It is also non–toxic, easy to handle and is relatively inexpensive. Other acids used have included pyro– and orthophosphoric acid [22,23], sulphuric acid [24] and oleic acid [25]. The resulting waveguide properties are essentially independent of the acid used. It has been claimed that waveguides fabricated using the phosphoric acid have a larger refractive index change than those made with benzoic acid [22], although recent work has questioned these claims [26]. Waveguide fabrication using pyrophosphoric acid will be discussed in more detail in chapter 4.

The proton–exchange process results in a waveguide with a step–index profile with an increase in the extraordinary index and a slight decrease in the ordinary index. At a wavelength of 0.6328μm the refractive index changes are given by:–

$\Delta n_e \simeq 0.12$

$\Delta n_o \simeq -0.04$

Proton–exchanged waveguides will therefore only support optical modes which have their electrical field directed along the c–axis, i.e. TE modes for x–cut lithium niobate and TM modes for z–cut material. The origin of the refractive index change is not clearly understood. Rice has hypothesised that it may be related to a change in the polarizability of the oxygen ions in the crystal lattice [27] by the inclusion of protons. Loni et al [28] have used infrared spectroscopy to monitor the isotopic exchange of ^1H and ^2H and atomic absorption spectroscopy to establish the concentration of lithium present in the benzoic acid after the exchange. From the results of the study they concluded that the uptake of hydrogen as hydroxyl groups provides charge compensation, while the depletion of lithium determines the refractive index profile.

The extent of proton–exchange is dependent on the exchange time and the temperature of the acid. Only partial exchange is necessary for waveguide formation. For a typical optical waveguide fabricated using benzoic acid, Loni et al [29] have found that the "x" value lies between the limits $0.4 < x < 0.5$, although this probably represents a lower limit. Other workers [30] have estimated x to be closer to 0.7. Complete exchange results in a transformation from the rhombohedral lithium niobate structure to the cubic hydrogen niobate structure [31]. Although the exchange is apparently only partial, it has been reported that a structural transformation takes place within the waveguide region [32]. The structural transformation has its origins in the stress induced in the crystal by the replacement of lithium ions by protons. The direction of the stress is along the c–axis with a reported magnitude of $\Delta c/c = 0.47\%$ [32]. It is this induced stress which prevents fabrication of proton–exchanged waveguides on the y–face of lithium niobate [33]. Waveguides can be fabricated on the y–face if prior steps are taken to reduce the stress, such as titanium–indiffusion or melt dilution.

Several methods have been used to characterise the exact structural changes which occur during proton–exchange and post–annealing processes. In a comprehensive

study Canali et al [34] have employed Rutherford backscattering spectrometry, nuclear reactions, secondary ion mass spectrometry, scanning electron microscopy and x-ray diffraction to measure the lattice distortions and atomic composition profiles of the proton-exchanged regions. From this work it was concluded that the hydrogen depth profile had a step-like profile, in agreement with the refractive index profile.

Many problems have been identified with proton-exchanged waveguides. Yi-Yan has observed index instability [35] and that the waveguides can have a high propagation loss due to severe in-plane scattering [36]. Other important problems which have been reported include a DC-extinction effect, reduced electro-optic and second order nonlinear coefficients [37,38,39,40,41].

Many of these problems can be avoided by annealing the waveguides or by using dilute melts [42]. A dilute melt is the exchange acid with a small amount of a lithium containing salt (e.g. lithium benzoate) added as a buffer. The effect of the buffer is to slow the effective diffusion of protons into the substrate [42]. The percentage that benzoic acid is diluted by the addition of lithium benzoate is defined by:-

$$X = \frac{\{\text{lithium benzoate}\}}{\{\text{lithium benzoate}\} + \{\text{benzoic acid}\}} \times 100\% \qquad (1.19)$$

where {..} denotes the number of moles of the chemical.

The refractive index difference between proton-exchanged waveguides and the substrate leads to tight confinement of the radiation within the waveguide structure. This is advantageous for nonlinear applications or for curved structures such as bends or ring resonators [43]. The negative change in the ordinary index means that proton-exchanged waveguides can be used as polarisation selective elements [44]. An important property of proton-exchanged waveguides is that they exhibit a significantly reduced photo-refractive effect [45], thus avoiding a problem encountered with titanium-indiffused waveguides [46].

The proton-exchange process has been used to fabricate a wide range of integrated optical devices. Passive structures have included various types of gratings and lenses [47,48], and polarisers and ring resonators as mentioned above. Active devices have included electro-optic phase-modulators [32,37] and intensity modulators [49], acousto-optic devices [50] and interferometric sensors [51].

Recently, there has been a great deal of work carried out to investigate the properties of proton–exchanged waveguides for nonlinear optical devices. Because the high refractive index difference between the waveguide and the substrate gives strong confinement, the power density in the waveguide can be very high even for low power levels. This has the potential to allow efficient frequency doubling of low power semiconductor lasers. Neveu et al [52] were the first to investigate frequency doubling in proton–exchanged waveguides. They achieved phase–matching by angle tuning the direction of propagation in a planar waveguide. The observed conversion efficiencies were very low because the fundamental wave was a low order mode whereas the harmonic wave was a high order mode resulting in a poor overlap (see chapter 2). Taniuchi and Yamamoto [53] used channel waveguides fabricated using pyrophosphoric acid and demonstrated a conversion efficiency of 1% for 120 mW of power from a GaAs laser via Cerenkov radiation. Sanford and Connors [54] repeated the experiment of Taniuchi and found some inconsistencies in their work. The major fault was in the claimed refractive index change of 0.145. They had only been able to observe a refractive index change of 0.125 in the pyrophosphoric acid proton–exchanged waveguides. Arvidsson et al [55] investigated the effect of annealing the proton–exchanged waveguides on the conversion efficiency in the Cerenkov scheme. It was found that, in general, the effect of annealing was to reduce the conversion efficiency, a result confirmed by Keys et al [56]. Both Sanford and Connors [54] and also Laurell [3] have successfully demonstrated three–wave mixing via Cerenkov radiation by mixing two wavelengths in a channel waveguide. The output at the waveguide end–face consists of three light beams produced by frequency doubling of the two input beams and sum–frequency generation by the mixing of both beams. Such a scheme allows the generation of any arbitrary wavelength where a suitable source is not available for frequency doubling.

Recently, annealed proton–exchanged waveguides have been used in conjunction with periodically domain reversed lithium niobate substrates to demonstrate very efficient quasi phase–matched second harmonic generation. Lim et al [57,58] have used titanium–indiffusion to induce domain reversal. Using a proton–exchanged channel waveguide they have demonstrated very efficient second harmonic generation of both Nd:YAG and dye lasers. Webjorn et al [59,60] have used lithium out–diffusion to fabricate the domain reversed substrates and have successfully demonstrated second harmonic generation of both Nd:YAG and semiconductor lasers.

1.4 New miniature laser sources with proton–exchanged doped lithium niobate

substrates

The addition of dopants to the melt during Czochralski growth is a common procedure. Dopants such as iron have been used to enhance the photorefractive properties of lithium niobate [61]. Such crystals have been widely studied for applications involving holographic data storage/optical memory elements [62]. Another much used dopant is magnesium oxide, MgO. The addition of magnesium oxide to the melt produces a substrate with a reduced susceptibility to photorefractive damage [63]. This is an attractive substrate for use with titanium–indiffused waveguides which would normally suffer optical damage at even moderate power levels [46]. The magnesium oxide is generally added at the concentration level of 4.5% by weight to the melt.

If laser active elements are added to the melt during growth then it is possible to grow crystals which may be used as the gain medium in a laser cavity. Substrates with dopants such as neodymium, erbium have been grown successfully. There are many reasons why such crystals are important, the main ones being that:–

(1) The gain medium is nonlinear, allowing self–frequency doubling of the laser wavelength.

(2) The substrate is electro–optic, allowing the possibility of Q–switching.

(3) Waveguide fabrication is possible, allowing the fabrication of lasers with very low threshold powers due to the high power densities which can be achieved in the waveguide.

(4) Combining all of the above should allow the realisation of a miniature, diode–pumped self–Q–switched, self–frequency doubled laser source.

A significant amount of work has been carried out to demonstrate lasing action in doped lithium niobate. In the 1960's bulk lithium niobate lasers were fabricated using neodymium and erbium doped substrates [64]. The problem of optical damage prevented any serious work on doped lithium niobate as a laser host. Recently, with the advances in crystal growth using magnesium oxide as a co–dopant and by exploiting the superior photorefractive properties of proton–exchanged waveguides, miniature lithium niobate lasers have been fabricated. Lallier et al [65] have fabricated highly efficient diode–pumped neodymium–doped lasers. The pump wavelength was around 820nm, with a lasing

wavelength of 1.08μm. Brinkmann et al [66] have studied erbium–doped substrates for laser applications. Although erbium doped lithium niobate is well known, the authors chose to ion–implant erbium into a previously undoped substrate. After annealing the substrates, a waveguiding region was formed. Using a laser diode as the pump, fluorescence was observed at 1.55μm as expected. There are two major drawbacks with such a laser source:–

(1) The substrate is photorefractive and,

(2) erbium exhibits excited state absorption at a pump wavelength of 820nm.

In order to solve the problem of optical damage either a magnesium oxide doped substrate or a proton–exchanged waveguide region could be used. To prevent excited state absorbtion, pump lasers at about 1.48μm or 0.98μm must be used and, at present, semiconductor lasers at these wavelengths are the subject of intense research. It should be therefore be possible, within the near future, to realise a diode–pumped erbium–doped lithium niobate laser.

1.5 Summary

This chapter has served as an introduction to the work contained in this thesis. A brief outline of second order nonlinear optics was presented and the advantages to be gained by adopting an integrated optics approach were outlined. Following this brief introduction the choice of nonlinear material, i.e. lithium niobate, was justified and some of the properties of this crystal reviewed. The proton–exchange technique for waveguide fabrication was then described. Only proton–exchanged waveguides were used in the work presented in this thesis. Finally, a possible future application of all of the above in the form of a miniature all solid state laser was outlined.

1.6 References

[1]. P.A. Franken, A.E. Hill, C.W. Peters and G. Weinrich, *"Generation of optical harmonics"*, Phys. Rev. Letts, 7, pp.118–120, 1961.

[2]. H. Haus, in *"Nonlinear Optics"*, Proceedings Nato ASI, Glasgow, 1990.

[3]. F. Laurell, Ph. D. Thesis, Royal Institute of Technology, Sweden, 1990.

[4]. Y.R. Shen, *"The principles of nonlinear optics"*, Wiley, New York, 1984.

[5]. R.L. Byer in *"Nonlinear optics"*, Proceedings sixteenth summer school in physics, Eds. P.G. Harper and B.S. Wherret.

[6]. A.A. Ballman, *"Growth of piezo–electric and ferroelectric materials by the Czochralski technique"*, Jnl. Am. Ceram. Soc., 48, p.112, 1965.

[7].S.A. Fedulov, Z.I. Shapiro and P.B. Ladyzhinskii, *"The growth of $LiNbO_3$ $LiTaO_3$ and $NaNbO_3$ by the Czochralski method"*, Sov. Phys. Crst., 10, p.218, 1965.

[8]. K. Nassau, H.J. Levenstein and G.M. Loiacono, *"Ferroelectric lithium niobate 1: Growth, domain structure, dislocations and etching"*, Jnl. Phys. Chem. Solids, 27, p.983, 1966.

[9]. K. Nassau, H.J. Levenstein and G.M. Loiacono, *"Ferroelectric lithium niobate 2: Preparation of domain single crystals"*, Jnl. Phys. Chem. Solids, 27, p.989, 1966.

[10]. S.C. Abrahams, J.M. Reddy and J.L. Bernstein, *"Ferroelectric lithium niobate 3: Single–crystal X–ray diffraction study at 24 °C"*, Jnl. Phys. Chem. Solids, 27, p.997, 1966.

[11]. S.C. Abrahams, W.C. Hamilton and J.M. Reddy, *"Ferroelectric lithium niobate 4: Single–crystal neutron diffraction study at 24 °C"*, Jnl. Phys. Chem. Solids, 27, p.1013, 1966.

[12]. S.C. Abrahams, H.J. Levenstein and J.M. Reddy, *"Ferroelectric lithium niobate 5: Poly–crystal X–ray diffraction study between 24 °Cand 1200 °C"*, Jnl. Phys. Chem. Solids, 27, p.1019, 1966.

[13]. A. Rauber, *"Chemistry and physics of lithium niobate"*, in Current topics in materials science, Vol. 1, Ed. E. Kaldis, North–Holland, 1978.

[14]. R.S. Weis and T.K. Gaylord, *"Lithium niobate: Summary of physical properties and crystal structure"*, Appl. Phys. A, 37, p.191, 1985.

see also "*Properties of lithium niobate*", EMIS Data Review series 5, Institute of Electrical Engineers, INSPEC, 1989.

[15]. J.G. Bergman, A. Ashkin, A.A. Ballman, J.M. Dziedzic, H.J. Levinstein and R.G. Smith, *"Curie temperature, birefringence and phasematching temperature variations in $LiNbO_3$ as a function of melt stoichiometry"*, Appl. Phys. Letts., 12(3), p.92, 1968.

[16].J.E. Midwinter, *"Lithium niobate: The effects of composition on the refractive indices and optical second harmonic generation"*, Jnl. Appl. Phys., 39(7), p.3033, 1968.

[17]. R.C. Miller and W.A. Norland, *"Dependence of second harmonic generation coefficients on $LiNbO_3$ composition"*, Jnl. Apppl. Phys., 42(11), p.4145, 1971.

[18]. J.L. Jackel, C.E. Rice and J.J. Vaselka, *"Proton–exchange for high–index waveguides in $LiNbO_3$"*, Appl. Phys. Letts., 47, p.607, 1982.

[19]. M.L. Shah, *"Optical waveguides in $LiNbO_3$ by ion–exchange technique"*, ibid, 26, p.652, 1975.

[20]. J.L. Jackel, *"High–Δn optical waveguides in $LiNbO_3$: Thallium–lithium ion exchange"*, ibid, 37,p.739, 1980.

see also

J.L. Jackel and C.E. Rice, *"Variation in waveguides formed by immersion of $LiNbO_3$ in $AgNO_3$ and $TlNO_3$: the role of hydrogen"*, ibid, 41, p.508, 1982.

[21]. A. Loni, *"An experimental study of Proton–exchanged lithium niobate waveguides"*, Ph.D. Thesis, University of Glasgow, 1987.

[22]. K. Yamamoto and T. Taniuchi, *"New proton–exchange technique for $LiNbO_3$ waveguide fabrication"*, Technical digest O.F.C. 1987, paper ThU2.

[23]. M. A. Foad, A. Loni, R.W. Keys, J.M. Winfield and R.M. De La Rue, *"Proton–exchanged $LiNbO_3$ optical waveguides made from phosphoric acids: detailed studies and comparisons with guides made with benzoic acid"*, Integrated Optics and Optoelectronics, SPIE Proceedings 1177, paper 05, 1989.

[24]. G. A. Bogert and D. T. Moser, *"Sulfuric acid proton–exchanged channel waveguides fabricated in $LiNbO_3$"*, IEEE Photonics Technology Letters, 2(9), pp.632–633, 1990.

[25]. T. Maciak, *"$LiNbO_3$ optical waveguides obtained by proton–exchange in oleic acid"*, Int. Jnl. Optoelectronics, 5(3), pp.227–234, 1990.

[26]. A. Loni, R.W. Keys, R.M. De La Rue, M.A. Foad and J.M. Winfield, *"Optical characterization of z–cut proton–exchanged $LiNbO_3$ waveguides fabricated using orthophosphoric and pyrophosphoric acid waveguides"*, IEE Proceedings 136, Part J, No. 6, pp.297–300, 1989.

[27]. C.E. Rice, *"The structure and properties of $Li_{1-x}H_xNbO_3$"*, J. Sol. State Chem., 64, pp.188–199,1986.

[28]. A. Loni, R.M. De La Rue and J.M. Winfield *"Proton–exchanged, lithium niobate planar optical waveguides: Chemical and optical properties and room temperature hydrogen–isotopic exchange reactions"*, Jnl. Appl. Phys., 61, p.64, 1987.

[29]. R.G. Wilson, S.W. Novak, J.M. Zavada, A. Loni and R.M. De La Rue, *"SIMS depth profiling of proton–exchanged $LiNbO_3$ waveguides"*, ibid, 66, 1989.

[30]. C.E. Rice and J.L. Jackel, *"Structural changes with composition and temperature in rhombohedral $Li_{1-x}H_xNbO_3$"*, Mat. Res. Bull., 19, p.591, 1984.

[31]. ibid, *"$HNbO_3$ and $HTaO_3$: New cubic perovskites from $LiNbO_3$ and $LiTaO_3$ via ion–exchange"*, Jnl. Solid State Chem., 41, p.308, 1982.

[32]. M. Minakata, K. Kumagai and S. Kawakami, *"Lattice constant changes and electro–optic effects in proton–exchanged $LiNbO_3$ optical waveguides"*, Appl. Phys. Letts., 49, p.992, 1986.

[33]. A. Campari, C. Ferrari, G. Mazzi, C. Summonte, S.M. Al–Shukri, A. Dawar, R.M. De La Rue and A.G.C. Nutt, *"Strain and surface damage induced by proton–exchange in y–cut $LiNbO_3$"*, Jnl. Appl. Phys., 58, p.4521, 1985.

[34]. C. Canali, A. Carnera, G. MeaDella, P. Mazzoldi, S.M. Al–Shukri, A.G.C. Nutt and R.M. De La Rue, *"Structural characterization of proton–exchanged $LiNbO_3$ optical waveguides"*, ibid, 59, p.2643, 1986.

[35]. A. Yi-Yan, *"Index instabilities in proton-exchanged $LiNbO_3$ waveguides"*, Appl. Phys. Letts., 42, p.633, 1985.

[36]. S.M. Al-Shukri, J. Duffy, R.M. De La Rue, M.N. Armenise, C. Canali and A. Carnera, *"Proton-exchanged optical waveguides on lithium niobate: Devices, characterisation and future prospects"*, SPIE vol.-578, Procs. Int. Opt. Cir. Eng. II, 2, 1985.

[37]. K.K. Wong, R.M. De La Rue and S. Wright, *"Electro-optic frequency translator in $LiNbO_3$ fabricated by proton-exchange"*, Opt. Letts., 7, p.546, 1982.

[38]. R.A. Becker, *"A comparison of guided-wave interferometers fabricated on $LiNbO_3$ via titanium-indiffusion and proton-exchange"*, Appl. Phys. Letts., 43, p.131, 1983.

[39]. S. McMeekin and R.M. De La Rue, *"A novel transverse electro-optic waveguide phase modulator realised in titanium-indiffused and proton-exchanged $LiNbO_3$"*, Elec. Letts., 25, p,853, 1989.

[40]. T. Suhara, H. Tazaki and H. Nishihara, *"Measurement of reduction in SHG coefficient of $LiNbO_3$ by proton-exchange"*, ibid, 25, p.1326, 1989.

[41]. R.W. Keys, A. Loni and R.M. De La Rue, *"Measurement of the increase in the SHG coefficient of proton-exchanged $LiNbO_3$ after annealing, using a grating diffraction technique"*, ibid, 26, p.624, 1990.

[42]. K.K. Wong, *"An experimental study of dilute melt proton-exchange waveguides in X- and Z-cut lithium niobate"*, GEC Jnl. Research, 3, p.243, 1985.

[43]. A. Mahapatra, *"Integrated optical ring resonator made by proton-exchage in lithium niobate"*, Appl. Opt., 24, p.2285, 1985.

[44]. M. Papuchon and S. Vatoux, *"Integrated optical polariser on lithium niobate:Ti channel waveguides using proton-exchange"*, Elec. Letts., 19, p.612, 1983.

[45]. J.L. Jackel, A.M. Glass, G.E. Peterson, C.E. Rice, D.H. Olsen and J.J. Vaselka, *"Damage-resistant $LiNbO_3$ waveguides"*, Jnl. Appl. Phys., 55, p.269, 1984.

[46]. R.A. Becker, *"Methods of characterizing the photorefractive susceptibility of $LiNbO_3$ waveguides"*, SPIE Procs. 578, pp.12-18, 1985.

[47]. T. Suhara, *"Proton-exchanged Fresnel lenses in Ti:$LiNbO_3$ waveguides"*, Appl. Opt., 25, p.3379, 1983.

[48]. C. Warren, S. Forouhar, W.S.C. Wang, *"Double ion-exchanged chirp grating lens in lithium niobate waveguides"*, Appl. Phys. Letts., 43, p.424, 1983.

[49]. W. Charczenko, P.S. Weitzman, H. Klotz, M. Serette, J.M. Dunn and A.R. Mickelson, *"Characterization and simulation of proton-exchanged integrated optical modulators with various dielectric buffer layers"*, Jnl. Lightwave Tech., 9, p.92, 1991.

[50]. J.F. Duffy, *"Acousto-optic interactions in lithium niobate*

waveguides",Ph.D. Thesis, University of Glasgow, 1986.

[51] M. Haruna, *"Optical π−arc waveguide interferometer for temperature sensing,* Appl. Opt., 24, p.2483, 1985.

[52]. S. Neveu, J.P. Barety, M. De Micheli, P. Sibillot and D.B. Ostrowsky, *"Phase−matched SHG using the d_{33} coefficient in proton−exchanged guides"*, Paper PD−6, Topical meeting on Integrated and Guided Wave Optics, 24th−26th April, Orlando, Florida, 1984.

[53]. T. Taniuchi and K. Yamamoto, *"Second harmonic generation using proton−exchanged $LiNbO_3$ waveguide"*, Optoelectronics − Devices and Technologies, 2(1), pp.53−58, 1987.

[54]. N. A. Sanford and J. M. Connors, *"Optimisation of the Cerenkov second harmonic generation in proton−exchanged $MgO−LiNbO_3$"*, Jnl. Appl. Phys., 65(4), pp.1429−1437, 1989.

[55]. G. Arvidsson, F. Laurell, B. Jaskorzynska, J. Webjorn, A. Loni, R.W. Keys and R.M. De La Rue, *"Influence of annealing on the conversion efficiency for SHG by Cerenkov radiation from proton−exchanged $LiNbO_3$ waveguides"*, Paper TuA3, Topical meeting on Nonlinear Guided Wave Phenomenon: Physics and Applications, Houston, Texas, Feb. 1989, Opt. Soc. Am.

[56]. R.W. Keys, A. Loni and R.M. De La Rue, *"Characterisation of proton−exchanged waveguides for second harmonic generation using Q−switched Nd:YAG laser pulses"*, IEE Applications of Ultrashort pulses for Optoelectronics, Digest no. 1989/87, May 1989.

[57]. E.J. Lim, M.M. Fejer and R.L Byer, *"SHG of blue and green light in periodically−poled planar $LiNbO_3$ waveguides"*, Technical digest Topical Meeting on Nonlinear Guided wave Phenomena: Physics and Applications, Paper PD3−1, Houston, Texas, 2−4 February 1988.

[58]. E.J. Lim, M.M. Fejer and R.L Byer, *"SHG of green light in periodically−poled planar $LiNbO_3$ waveguides"*, Electronics Letts., 25(3), pp.174−175, 1989.

[59]. J. Webjorn, F. Laurell and G. Arvidsson, *"Periodically domain−inverted lithium niobate channel waveguides for SHG"*, Technical digest Topical Meeting on Nonlinear Guided wave Phenomena: Physics and Applications, Paper THA2−1, Houston, Texas, 2−4 February 1988.

[60]. J. Webjorn, F. Laurell and G. Arvidsson, *"Blue light generated by frequency doubling of laser light in a $LiNbO_3$ channel waveguide"*, IEEE Photonics Tech. Letts., 1(10), pp.316−318, 1989.

[61]. M.G. Clark, F.J. De Salvo, A.M. Glass and G.E. Petersen, *"Electronic structure and optical index damage of iron doped lithium niobate"*, Jnl. Chem. Phys., 59, p.6209, 1973.

[62]. J.J. Amodei and D.L. Staebler, *"Holographic recording in lithium niobate"*, RCA review, 33, p.71, 1972.

[63]. G. Zhong, J. Jian and Wu Zhong−Kang, 11th International Quantum Electronics Conference, IEEE Cat. No. CH 1561−0, p.631, 1980.

[64]. I.P. Kaminov and L.W. Stultz, *"Nd:$LiNbO_3$ Laser"*, IEEE Jnl. Quant.

Elecs., 11, p.306, 1975.

[65]. E. Lallier, J.P. Pochelle, M. Papuchon, M. De Micheli, M.J. Li, Q. He and D.B. Ostrowsky, *"Efficient Nd:MgO:LiNbO$_3$ waveguide laser"*, Elec. Letts., 26, p.927, 1990.

[66]. R. Brinkmann, W. Sohler and H. Suche, *"Continuous-wave erbium-diffused LiNbO$_3$ waveguide laser"*, ibid, 27, p.415, 1991.

CHAPTER 2.

THEORY OF SECOND HARMONIC GENERATION (SHG) IN OPTICAL WAVEGUIDES.

This chapter outlines the theoretical aspects of second order nonlinear optical interactions in an optical waveguide. An expression for the conversion efficiency for SHG in a proton–exchanged optical waveguide is derived based on a simple theoretical model. As an introduction to nonlinear processes in optical waveguides, the theoretical description of phasematched second harmonic generation in optical waveguides is discussed briefly. This is followed by an outline of the theory of SHG in situations where phase–matching is achieved by Cerenkov radiation, with particular reference to proton–exchanged waveguides. In this case the theory is complicated by the inclusion of the radiation field into the equations, which are therefore more difficult to treat mathematically than ones for guided modes alone. Although there are now several published theories of SHG by coupling to Cerenkov radiation in proton–exchanged waveguides, very little had been published when this work was initiated. The recently published theories of Cerenkov SHG are reviewed and the main results outlined and compared.

By formulating the problem in the framework of coupled mode theory, a simple theoretical model has been developed and has been used to predict the conversion efficiency for SHG as a function of waveguide depth and refractive index. A derivation of this calculation will be presented in some detail. The results are in fair agreement with published work based on more rigorous analyses and are also in agreement with measured experimental results. A suitable waveguide design for the optimization of the conversion efficiency for SHG is then given.

2.1 Theory of SHG in optical waveguides.

2.1.1 Conventional phasematching.

For the case of conventional phasematching, where the material birefringence compensates for the phase–mismatch, [1], the theory of SHG is strongly based on that for bulk SHG, [2]. The main difference lies in the electric field distributions of the fundamental and harmonic waves. In bulk SHG, the electric (and magnetic) field distributions can be represented by plane waves or, more realistically, Gaussian field distributions [2]. For SHG in an optical waveguide,the field distributions are determined by the propagating modes of the optical

waveguide structure. It is assumed in this work that the photon densities are high, allowing the use of classical electromagnetic fields.

Assuming a loss–less system, Maxwell's equations are:–

$$\nabla \times E = -\mu\, \partial_t H \tag{2.1}$$

$$\nabla \times H = \partial_t D \tag{2.2}$$

$$\text{where } D = \epsilon_0 E + P \tag{2.3}$$

and ∂_t denotes the derivative with respect to time.

As was discussed in chapter 1, the polarisation is given by a linear and a nonlinear term:–

$$P = P_l + P_{nl} \tag{2.4}$$

The linear (vector) term, P_l, is identically the term used in linear optics and is given by (in the scalar notation):–

$$P_l = \epsilon_0 . \chi^{(1)} . E \tag{2.5}$$

The nonlinear polarisation term, P_{nl}, is given by an equation relating the induced polarisation to the incident electric field via a third rank tensor, $\chi^{(2)}$:–

$$P_{nl} = \epsilon_0 . \chi^{(2)} . E . E \tag{2.6}$$

where $\chi^{(2)}$ is the second order nonlinear polarisation term. For the purpose of this thesis, only the second order terms are important. In component form, the expression for the nonlinear polarisation is given by (in the reduced notation, [3]):–

$$\begin{bmatrix} P_x \\ P_y \\ P_z \end{bmatrix} = \begin{bmatrix} 0 & 0 & 0 & 0 & d_{31} & -d_{22} \\ -d_{22} & d_{22} & 0 & d_{31} & 0 & 0 \\ d_{31} & d_{31} & d_{33} & 0 & 0 & 0 \end{bmatrix} \begin{bmatrix} E_x^2 \\ E_y^2 \\ E_z^2 \\ 2E_yE_z \\ 2E_xE_z \\ 2E_xE_y \end{bmatrix} \tag{2.7}$$

with the nonlinear polarisation tensor written here for the case of $LiNbO_3$ [3]

(see chapter 1).

Assume a waveguide coordinate system which is oriented with the waveguide boundaries normal to the x− axis and with the propagation along the z− direction (Fig. 2.1). Note that these axes are NOT (in general) the crystallographic axes.

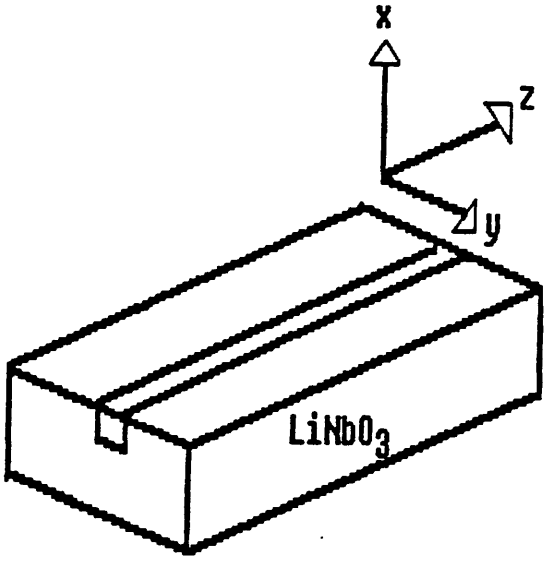

waveguide coordinate system

figure 2.1

For the purposes of this derivation, consider a fundamental frequency electric field with the field direction along the y− axis. Assuming time harmonic electromagnetic fields, Maxwell's equations can be used to derive the wave equation:−

$$\nabla^2 E = -\mu_0.\epsilon_0.\omega^2.E - \mu_0.\omega^2.P_{nl} \qquad (2.8)$$

For the waveguide geometry defined, the nonlinear polarisation term reduces to [4]:−

$$P_{nl} = d_{31}.E_x^2 \qquad (2.9)$$

where E_x is the fundamental requency electric field along the y−axis. For waveguide SHG (in a non−resonant cavity configuration) it can be assumed that the conversion efficiency is low enough so that the fundamental beam remains almost completely undepleted (although the equations can also be solved in the case of high conversion efficiency). For an interaction length L, Eq. 8 can be solved in the framework of coupled mode theory to give the expression for the conversion efficiency [4]:−

$$\eta = C.\text{sinc}^2(\Delta k.L/2).I \qquad (2.10)$$

where C is given by:−

$$C = 2.\frac{\omega^2}{n_\omega^2 n_{2\omega} c^3 \epsilon_0}.d_{eff}^2.L^2.P_\omega \qquad (2.11)$$

and I, known as the overlap integral is given by:−

$$I\ (m^{-1}) = \int (E_{2\omega}).(E_\omega)^2.dxdy \qquad (2.12)$$

$E_{2\omega}$ and E_ω are the electric field distributions at the second harmonic and fundamental frequencies respectively, normalised as defined in chapter one (Eq. 1.14b). For waveguide SHG, the electric field distributions at the harmonic and fundamental frequencies are determined by the waveguide structure. That is, they are described mathematically by the solutions to Maxwell's equations for the waveguide structure − the so−called waveguide modes. The β_ω and $\beta_{2\omega}$ factors represent the effective refractive indices of the fundamental and harmonic waves. The $\text{sinc}^2(\Delta kL/2)$ term describes the effect of the phase−mismatch, Δk. When $\Delta k = 0$, the interaction is said to be phasematched. It is important to arrange that $\Delta k = 0$ so that the conversion efficiency can be maximised. In a waveguide geometry, several techniques can be used to arrange for phasematched SHG. These techniques will be outlined in a subsequent section.

From inspection of Eq. 10 it can be seen that the harmonic power generated is proportional to the square of the fundamental guided power in the waveguide and also to the square of the interaction (waveguide) length. The overlap integral is an important concept in waveguide nonlinear optics. The overlap integral describes the spatial overlap of the interacting waveguide modes at the fundamental and harmonic wavelengths [4]. As the modal field distributions are strongly dependent on the wavelength of light and the refractive index profile, it is important to arrange for the maximum spatial overlap of the interacting modes in order to

optimise the conversion efficiency.

2.2 Phasematching Techniques.

For waveguide SHG there are several techniques by which phasematching can be arranged. In bulk SHG, only birefringent nonlinear materials normally allow the phasematching condition to be met. The various techniques of phasematching will briefly be described.

2.2.1 Birefringence.

In optically birefringent materials the fundamental mode (of a given polarisation state) can be phasematched to a harmonic wave of orthogonal polarisation [1]. This is achieved by either variation of the fundamental wavelength [5], by temperature tuning of the birefringence [6], or, for planar slab waveguides, by angle tuning the direction of propagation of the fundamental beam [7]. For the case of $LiNbO_3$ waveguides, typically only titanium–indiffused waveguides can be used for birefringence phasematching, since proton–exchanged waveguides allow only a single state of polarisation to be propagated (depending on the crystal cut), [8]. Fig. 2.2 shows the arrangement for SHG in a titanium–indiffused waveguide. Typical phasematching temperatures for titanium–indiffused waveguides are in the range $-10\,^{o}C$ to $80\,^{o}C$ [4] depending on the substrate used, e.g. undoped or MgO–doped, and on the fundamental wavelength.

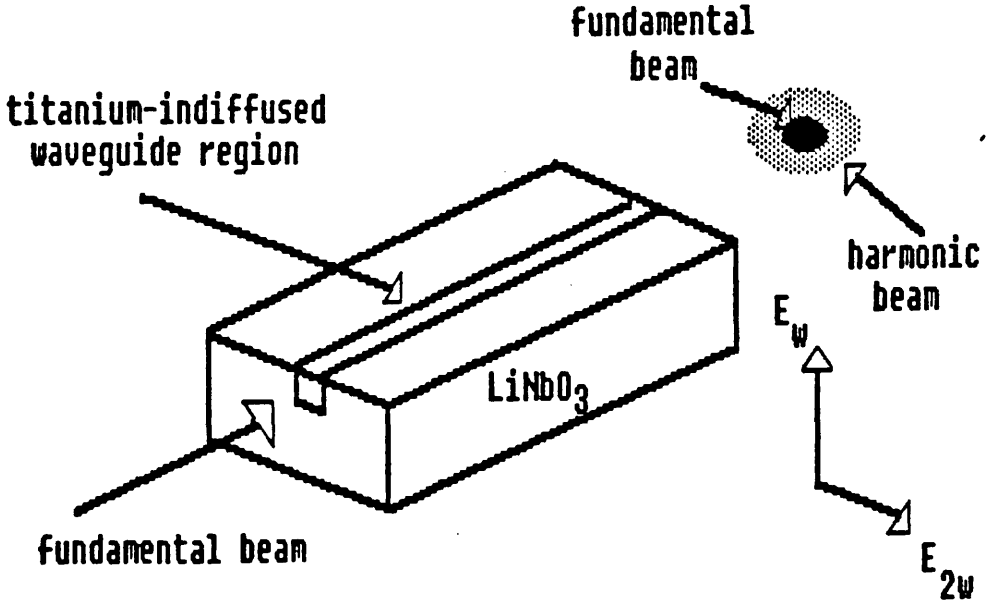

figure 2.2 second harmonic generation in a titanium-indiffused waveguide

2.2.2 Modal Dispersion.

In a multimode optical waveguide, phasematching can take place between a low order waveguide mode at the fundamental wavelength and a higher order waveguide mode at the harmonic wavelength [9]. This implies that phasematched SHG can take place without the need for a birefringent substrate. However, in this case, the overlap integral is typically so small that the conversion efficiency is generally very low [1]. For titanium–indiffused waveguides, a single mode waveguide at the fundamental waveguide will generally be multimoded at the harmonic wavelength. By temperature tuning the birefringence it is often possible to phasematch separately to each of the individual waveguide modes at the harmonic wavelength [6].

2.2.3 Grating Structures.

If the wavevector mismatch is given by $\Delta k = k_{2\omega} - 2k_{\omega}$ then the phasematched condition $k_{2\omega} - 2k_{\omega} - \Delta k = 0$ may be satisfied by using a grating structure of wavevector $K = \Delta k$. The grating wavevector, K, is defined by $K = 2\pi/\Lambda$, where Λ is the wavelength of the grating structure. Such a grating structure can be derived from a periodic modulation of the linear refractive index, or by a periodic modulation of the nonlinear coefficient, or both [9]. It is more efficient to modulate the nonlinear coefficient, as a modulation of the refractive index leads to high scattering losses. Grating phasematched SHG is an especially useful approach for SHG in crystals which cannot be phasematched by normal means but which are nevertheless highly nonlinear [10].

2.3.1 Theory of Cerenkov SHG in proton–exchanged waveguides.

As noted previously, conventional phasematching via the waveguide birefringence is impossible in "conventional" proton–exchanged waveguides. This is a consequence of the proton–exchange process which allows only a single polarisation state to be guided. By using a buried proton–exchanged waveguide, where both of the refractive indices are increased, birefringent phasematching may be possible. To date the author is not aware of any published experimental results for SHG in buried proton–exchanged waveguides. Phasematching via the Cerenkov effect is one particulary convenient method of frequency doubling efficiently [11]. As there are an infinite number of allowed radiation modes for any waveguide structure [12] the Cerenkov effect can provide phasematching of any fundamental wavelength. It is therefore particularly suited to phasematching of semiconductor

lasers operating in the 800nm wavelength range where conventional phasematchimg is non– trivial.

The physical basis of the "Cerenkov" effect is as follows. The input optical field generates a nonlinear polarisation field proportional to the square of the input field. This nonlinear polarisation field is bound to the fundamental field and as such must travel at the same phase velocity. If the refractive index of the substrate region at 2ω is greater than the effective refractive index of the fundamental guided mode (and hence the nonlinear polarisation field), second harmonic light will be radiated into the substrate (Fig. 2.3).

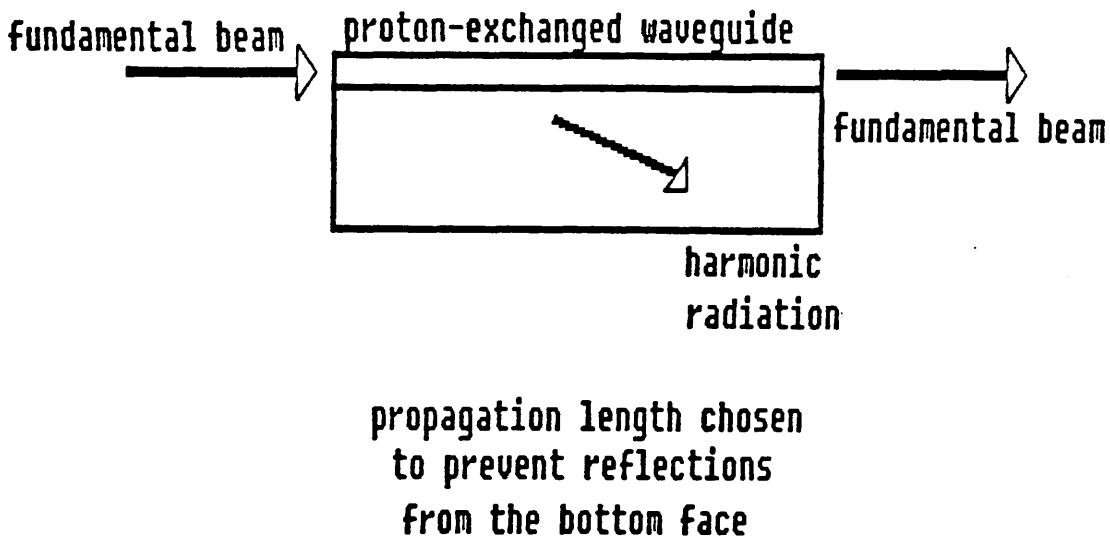

figure 2.3 second harmonic generation in a proton-exchanged waveguide by Cerenkov radiation

Formally, the condition for Cerenkov radiation can be derived as follows. Consider a waveguide with substrate refractive index n_s and superstrate refractive index n_c. The guided modes will propagate with an effective index N_{eff} which obeys:–

$$n_s^{\omega},\ n_c^{\omega} < N_{eff} \qquad (2.13)$$

Normal dispersion implies that $n_s^{2\omega} > n_s^{\omega}$. Thus:–

$$n_s^{\omega} < N_{eff} < n_s^{2\omega} \qquad (2.14)$$

but also $n_c^{2\omega} < N_{eff} < n_s^{2\omega}$ (2.15)

This is the condition for substrate radiation modes (as opposed to cover radiation modes).

The phase velocity of the nonlinear polarisation wave is given by:—

$$V_{nl} = 2.\omega/(k_{2\omega}.N_{eff}) \quad (2.16)$$

and the phase velocity of a free wave at the same wavelength propagating in the substrate is:—

$$V_{2\omega} = 2.\omega/(k_{2\omega}.n_s^{2\omega}) \quad (2.17)$$

It can be seen from Eqs. 2.15, 2.16 and 2.17 that $V_{nl} > V_{2\omega}$ and, under the conditions of Eq. 2.15, the nonlinear polarisation field is a source of Cerenkov radiation. Phasematching implies that the component of momentum along the direction of propagation is conserved, i.e. $2\beta_\omega = \beta_{2\omega}$, which gives:—

$$N_{eff} = n_s^{2\omega}.\cos\theta \quad (2.18)$$

This phasematching condition (conservation of wavevector along the direction of propagation) implies that the harmonic wave is radiated uniformly into a cone whose semi—angle is given by Eq. 2.18. For a wave propagating at an angle θ to the optic axis in a lithium niobate waveguide, the refractive index of the substrate which the wave "sees" is given by, [13]:—

$$n_s^{2\omega} = \frac{n_o^{2\omega}.n_e^{2\omega}}{\{(n_o^{2\omega}.\cos\theta)^2 + (n_e^{2\omega}.\sin\theta)^2\}^{0.5}} \quad (2.19)$$

where n_o and n_e are the ordinary and extraordinary refractive indices of lithium niobate. Combining Eqs. 2.18 and 2.19 gives an expression for the angle at which the radiation is emitted into the substrate (the "Cerenkov" angle):—

$$\theta = \frac{\tan^{-1}\{n_o^{2\omega}.((n_e^{2\omega})^2 - N_{eff}^2)^{0.5}\}}{n_e^{2\omega}.N_{eff}} \quad (2.20)$$

As n_o and n_e are properties of the crystal, the Cerenkov angle can be varied simply by varying the effective index of the guided mode, i.e. by varying the waveguide fabrication conditions. Measurement of the Cerenkov angle has been used to characterise waveguides as an alternative to more traditional methods such as prism coupling [14] and is an especially powerful technique for stripe

waveguides. Cerenkov SHG has been observed in many types of waveguide other than proton–exchanged waveguides, for example in optical fibres [15], ZnS films on ZnO substrate [16] and in MNA/glass waveguides [17].

Cerenkov SHG can be treated in the theoretical framework of coupled mode theory. The main problem with this approach occurs when the orthogonality relations are invoked. The resulting overlap integral is now between a guided mode at the fundamental wavelength and a radiation mode at the harmonic wavelength. The difficulty in this approach lies in the normalisation of the radiation mode, [12]. For waveguides with a step–like refractive index profile it is possible to normalise the radiation modes but, for waveguides with an arbitrary refractive index profile, the radiation modes are not easy to compute and even more difficult to normalise [12]. This makes modelling of Cerenkov SHG in annealed proton–exchanged waveguides very difficult.

In order to model Cerenkov SHG, several alternative theories have been derived. Tien et al [16], who were the first to report on Cerenkov SHG, modelled the effect in terms of antenna theory using expressions derived from waveguide theory. Their calculation is complicated and the final expressions do not lend themselves to a simple insight into the problem.

Li et al [18, 19] and Buritskii et al [20] have also treated the problem in terms of an antenna theory. Li et al have obtained a simple expression relating the conversion efficiency for SHG in a step–index proton–exchanged waveguide to the waveguide parameters and have used this expression to model the conversion efficiency as a function of waveguide depth and waveguide refractive index. The results which they have obtained are in good agreement with experimental results and are also consistent with results obtained using other theoretical treatments. The theory of Buritskii et al is similar to that of Tien and apparently gives results which are in close agreement with experimental results. The waveguide modelled in the work of Buritskii et al was a titanium–indiffused waveguide and to the knowledge of the author no results have been published by then for proton–exchanged waveguides.

The beam propagation method is a sophisticated computational technique which has long been used in the analysis of waveguide problems [21]. Using the beam propagation approach Fujiwara et al [22] have obtained results which agree very well with the published results of Taniuchi and Yamamoto [11]. This approach also allows the Cerenkov angles and far–field radiation pattern of the harmonic

waves to be calculated.

By working in the framework of the effective index method, it is possible to construct Maxwell's equations in component form and solve the equations in a self–consistent manner. Sanford et al [23] and Hayata et al [24] have used this approach to solve the problem of Cerenkov SHG. In both cases, the analyses are, algebraically, very complicated but the resulting equations model very well the dependence of SHG conversion efficiency on the waveguide parameters.

2.3.2 Main features of the published results.

Although the conversion efficiency for SHG by Cerenkov radiation has been calculated using several different mathematical techniques, the results are generally consistent with each other in terms of the dependence of conversion efficiency on the waveguide parameters. The main results of these theories will be pointed out, as any new theory must be in agreement with established results.

In all cases, the waveguide depth for maximum conversion efficiency is close to the cut–off depth for the lowest order waveguide mode at the fundamental wavelength. This implies that the shorter the fundamental wavelength, the shallower the waveguide must be in order to maximise the conversion efficiency. The shape of the conversion efficiency versus waveguide depth curve is generally the same in each case. The conversion efficiency starts off low and quickly rises to a maximum. It then falls off, but increases again to reach a lower secondary peak before falling off again. An example of such a graph is shown in Fig 2.4.

2.3.3 A simplified model of Cerenkov SHG based on coupled mode theory.

In order to calculate results from theories such as those based on direct solutions of Maxwell's equations, antenna theory or the beam propagation method on a computer, relatively sophisticated mathematical algorithms have to be implemented. However, by adopting the coupled mode theory approach commonly used in waveguide problems, a mathematically simple and computationally more straightforward solution to the problem can be derived. The difficulty in this approach lies in the modelling of the field of the harmonic radiation mode. As has been stated, it is very difficult to normalise the modal field expressions for an arbitrary refractive index profile, so this type of approach can lead to inaccuracies in the calculation of the conversion efficiency. However, the radiation modes of a step index waveguide have been calculated [24] and, by using a

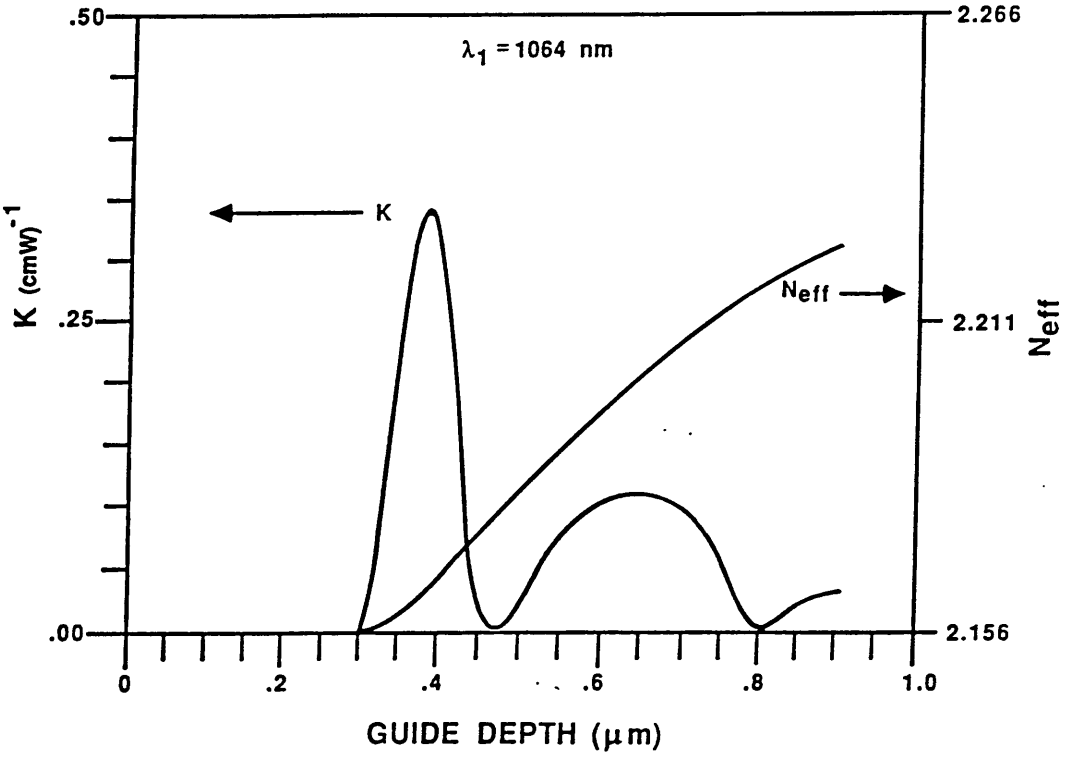

figure 2.4 theoretical plot of conversion efficiency (in arbitrary units) versus waveguide depth for Cerenkov SHG (after [23])

coupled mode theory approach, a prediction of the dependence of conversion efficiency on waveguide depth can be made. A calculation of the absolute conversion efficiency is not required from this theory. It is only required that the theory predicts the shape of the conversion efficiency versus waveguide depth curve in order to allow comparison with experimental results. If it can be assumed that for gentle annealing, i.e. short times, the refractive index profile of proton–exchanged waveguides does not deviate much from a step index profile, the effect of annealing the waveguide on the conversion efficiency can also be modelled. In this case the waveguide refractive index may be reduced, but the refractive index is still step–like. This will only be valid for small changes in the refractive index.

Marcuse has used such a coupled mode theory approach to model the electro–optic coupling between a guided mode and a radiation mode in an electro–optic cut–off modulator. The coupled mode theory of Cerenkov radiation closely follows the analysis of Marcuse.

In an electro–optic cut–off modulator, a guided mode of a waveguide is coupled to an unguided radiation mode via an applied electric field [25]. The application of the electric field alters the refractive index of the waveguide region via the electro–optic effect [26]. If the applied field is large enough, the refractive index of the waveguide region can be reduced to such an extent that it can no longer support even one guided modes at that wavelength. A radiation mode can propagate however, and the guided mode is then coupled to one of these modes. The angle at which the radiation mode is emitted into the substrate region is given by a phasematching condition analogous to that of Cerenkov radiation. This similarity in behaviour between the electro–optic cut–off modulator and Cerenkov SHG allowed the author to construct a model for Cerenkov SHG in a framework entirely equivalent to that used to model the electro–optic modulator. The author is grateful to Dr. A.K. Ghatak of the Indian Institute of Technology for valuable discussions on certain aspects of the model.

In order to calculate the conversion efficiency for SHG, a coupling constant is calculated for the coupling of the fundamental waveguide mode to the harmonic radiation mode. This coupling coefficient can then be used to estimate the power exchanged between the two modes and, hence, the conversion efficiency for SHG.

2.3.4 Derivation of the coupling coefficient.

An outline of the calculation of the coupling coefficient will be given. As the calculation is rather involved, a detailed derivation will not be given but can be found in a paper by Marcuse [27] or in a standard textbook on waveguide analysis [12].

The starting point is in Maxwell's equations (Eqs. 2.1, 2.2). The electric and magnetic fields are expressed in terms of longitudinal and transverse components. Using these expressions the normal modes of the waveguide can de derived. By invoking the orthogonality relations and expressing the electric and magnetic fields as a superposition of guided and radiation modes, an expression for the coupling coefficient is derived. The expression is complicated but can be simplified, given the assumption that the anisotropy of the medium is small (a reasonable approximation for lithium niobate).

The coupling coefficient is given by

$$K = (\omega/4.j.P).\int_{\pm\infty}(E_\mu)^*.(\epsilon - \epsilon').E_\nu.dx \qquad (2.21)$$

where ω is related to the fundamental frequency, E_μ and E_ν are the electric field distributions for the harmonic wave and fundamental wave respectively, * denotes the complex conjugate and P is the power carried by the fundamental wave. The term $(\epsilon - \epsilon')$ represents the difference between the dielectric tensor of the actual waveguide structure (including nonlinear effects) and the ideal waveguide structure (linear effects only) whose modes are E_ν. The subscript on the integral sign indicates the limits of the integration.

2.3.5 Calculation of the conversion efficiency

From Eq. 2.21, the coupling coefficient can be rewritten in terms of the fundamental and harmonic waveguide modes as:–

$$K = (\omega/4.j.P).\int_{\pm\infty}(E_{2\omega})^*.(\epsilon - \epsilon').E_\omega.dx \qquad (2.22)$$

where P is the power per unit width. (Alternatively the electric fields could be expressed in two dimensions and the integral taken with respect to dx.dy). The term $(\epsilon - \epsilon')$ can be calculated from the continuity of the electric displacement vector D, as defined below.

The waveguide structure is defined in Fig. 2.1. The refractive indices of the

cladding, the waveguide and the substrate are defined as n_c, n_f and n_s respectively. For the linear waveguide the D vector is given by:–

$$D = \epsilon_0.E + P = \epsilon_0.E.(1 + \chi^{(1)}) \qquad (2.23)$$

This gives for ϵ':–

$$\epsilon' = \epsilon_0(1 + \chi^{(1)}) \qquad (2.24)$$

For the case of a waveguide with a nonlinearity, D is given, (to second order), by:–

$$D = \epsilon_0.E + \epsilon_0.\chi^{(1)}.E + \epsilon_0.d_{33}.E.E$$

$$= \epsilon_0.E.(1 + \chi^{(1)} + d_{33}.E) \qquad (2.25)$$

Similarly, it can be seen that ϵ can be reduced to:–

$$\epsilon = \epsilon_0(1 + \chi^{(1)} + d_{33}.E) \qquad (2.26)$$

Thus, from the continuity of D:–

$$\epsilon - \epsilon' = \epsilon_0.d_{33}.E \qquad (2.27)$$

The coupling coefficient Eq. 2.22 becomes:–

$$K = (\omega/4.j.P).\int_{\pm\infty}(E_{2\omega})^*.\epsilon_0.d_{33}.(E_\omega)^2.dx \qquad (2.28)$$

Assuming d_{33} is not a function of the co–ordinate x and using normalised field distributions (P = 1 mW m^{-1}), Eq. 2.28 becomes:–

$$K = (\omega.\epsilon_0.d_{33}/4.j).\int_{\pm\infty}(E_{2\omega})^*.E_\omega^2.dx \qquad (2.29)$$

The coupling efficiency is best expressed in terms of the attenuation coefficient α of the guided mode. Neglecting propagation losses, the attenuation is caused by power loss from the guided mode E_ω to the radiation mode $E_{2\omega}$. The power attenuation is given by the formula:–

$$2.\alpha.L = 2.\pi.(\beta_\omega/k_s^{2\omega}).|K|^2 \qquad (2.30)$$

where β_ω is the propagation constant of the guided fundamental mode and $k_s{}^{2\omega}$ is the propagation constant for the harmonic wave in the substrate. The total power attenuated is given by:-

$$\Delta P/P = 2.\alpha.L \qquad (2.31)$$

where ΔP is the power transferred to the harmonic mode at 2ω and $P = P_\omega{}^2$. Thus:-

$$P_{2\omega}/P_\omega{}^2 = 2.\pi.(\beta_\omega/k_s{}^{2\omega}).|K|^2.L \qquad (2.32)$$

$$= C^2.\{\int_{h,+\infty} E_{2\omega}.E_\omega{}^2.dx + \int_{0,h} E_{2\omega}.E_\omega{}^2 dx +$$

$$\int_{0,-\infty} E_{2\omega}.E_\omega{}^2.dx\}^2 \qquad (2.33)$$

In the above Eq. 2.33 the integral of Eq. 2.29 over the limits $\pm\infty$ has been reduced to three separate integrals. The three terms represent the overlap integral in the superstrate, the waveguide and the substrate regions respectively. It was assumed in this work that the d_{33} coefficient is the same in both the waveguide and substrate regions. Later work, see chapter 5, aimed at measuring the d_{33} coefficient has shown this to be an invalid assumption. It will be shown in chapter 5 that the d_{33} coefficient in the proton-exchanged waveguide region is, for typical processing conditions, significantly lower than the d_{33} coefficient of the substrate region. The effect of a reduced d_{33} in the waveguide region is to introduce an additional factor, f, into the second of the overlap integrals. However, since only the relative shape of the conversion efficiency curve is required, this additional factor has a relatively small effect on the final results.

The electric field distributions must be derived for the particular waveguide geometry used. For proton-exchanged waveguides in z-cut lithium niobate only TM modes can be supported. The magnetic field distributions for the fundamental waveguide mode are given by [28]:-

$$Hy = H_c{}^\omega.\exp[-\gamma_c{}^\omega.(x-h)];\ h < x \qquad (2.34a)$$

$$= H_f{}^\omega.\cos[k_f{}^\omega.x - \varphi_s];\ 0 < x < h \qquad (2.34b)$$

$$= H_s{}^\omega.\exp[\gamma_s{}^\omega.x];\ h < 0 \qquad (2.34c)$$

and for the harmonic radiation mode, they are given by:–

$$H_y = H_c^{2\omega}.\exp[-\gamma_c^{2\omega}.(x-h)];\ h < x \qquad (2.34d)$$

$$= H_f^{2\omega}.\cos[k_f^{2\omega}.(x-h) + \varphi_c^{2\omega}];\ 0 < x < h \qquad (2.34e)$$

$$= H_s^{2\omega}.\cos[k_s^{2\omega}.x + \varphi^{2\omega}];\ h < 0 \qquad (2.34f)$$

From the boundary conditions

$$\tan \varphi_s^{\omega} = (n_f^{\omega}/n_s^{\omega})^2.\gamma_s^{\omega}/k_f^{\omega} \qquad (2.35a)$$

$$\tan \varphi_c^{\omega} = (n_f^{\omega}/n_c^{\omega})^2.\gamma_c^{\omega}/k_f^{\omega} \qquad (2.35b)$$

$$\tan \varphi_c^{2\omega} = (n_f^{2\omega}/n_c^{2\omega})^2.\gamma_c^{2\omega}/k_f^{2\omega} \qquad (2.35c)$$

$$[k_s/(n_s^{2\omega})^2].\tan \varphi_c = [k_f/(n_f^{2\omega})^2].\tan(\varphi_c - k_f^{2\omega}.h) \qquad (2.35d)$$

For the purposes of this analysis both the exponential terms describing the wavevector ($e^{j\beta z}$) and the time dependence ($e^{j\omega t}$) of the fields can be dropped from the analysis.

Using the expression for the TM guided and radiation modes of a waveguide with a step–like refractive index profile, the electric field component, E_x, of the TM mode is calculated via Maxwell's equations and substituted into Eq. 2.30. The conversion efficiency can then be calculated for a step–index waveguide of any depth and refractive index difference and substrate index.

Using this formalism, the conversion efficiency has been calculated as a function of waveguide depth for z–cut proton–exchanged waveguides. Rather than assume a value for the refractive index difference, the value used in the calculations was that which has been experimentally measured for such waveguides. Fig. 2.5 shows a typical graph of conversion efficiency as a function of waveguide depth for the case of a proton–exchanged waveguide fabricated using neat benzoic acid at a temperature of 235 ^{0}C.

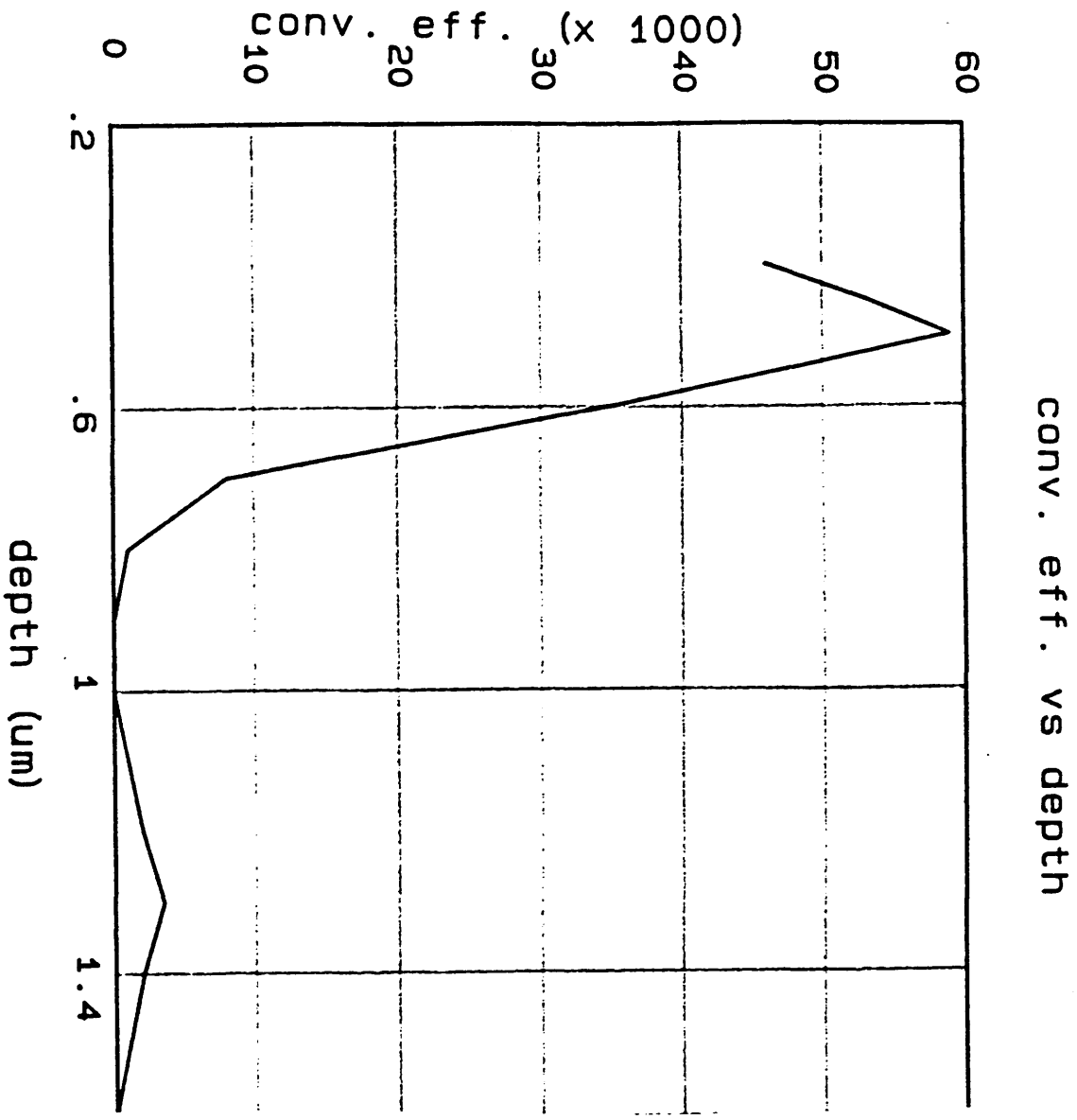

figure 2.5 calculated conversion efficiency (arbitrary units) versus waveguide depth using eqns. 2.33 - 2.35

It can be seen from Fig. 2.5 that the conversion efficiency peaks at a waveguide depth of 0.48μm, close to the cut−off depth of 0.4μm for a proton−exchanged waveguide with fabrication conditions typically as above. This figure compares well with the other published result for the conversion efficiency as a function of waveguide depth (see, for example, Fig 2.4). There is a flat region in the figure which is not seen in any other published result, where the increase in the conversion efficiency towards the secondary peak tends to occur directly after the minimum in conversion efficiency separating the two peaks. However, given the relative simplicity of the model and the difficulties in calculating the overlap integral accurately, the results obtained from the analysis provide useful insight.

The theory was then used to calculate the effect on the conversion efficiency as the refractive index difference between the waveguide and substrate was decreased.

Although the refractive index profile used was step–like throughout, this is a good first approximation to the case of annealing a waveguide. Fig. 2.6 shows a graph of conversion efficiency as a function of the refractive index difference between the waveguide region and the substrate for various refractive index differences. It can be seen that the effect of lowering the refractive index difference is to reduce the conversion efficiency. This result also agrees with experimental results.

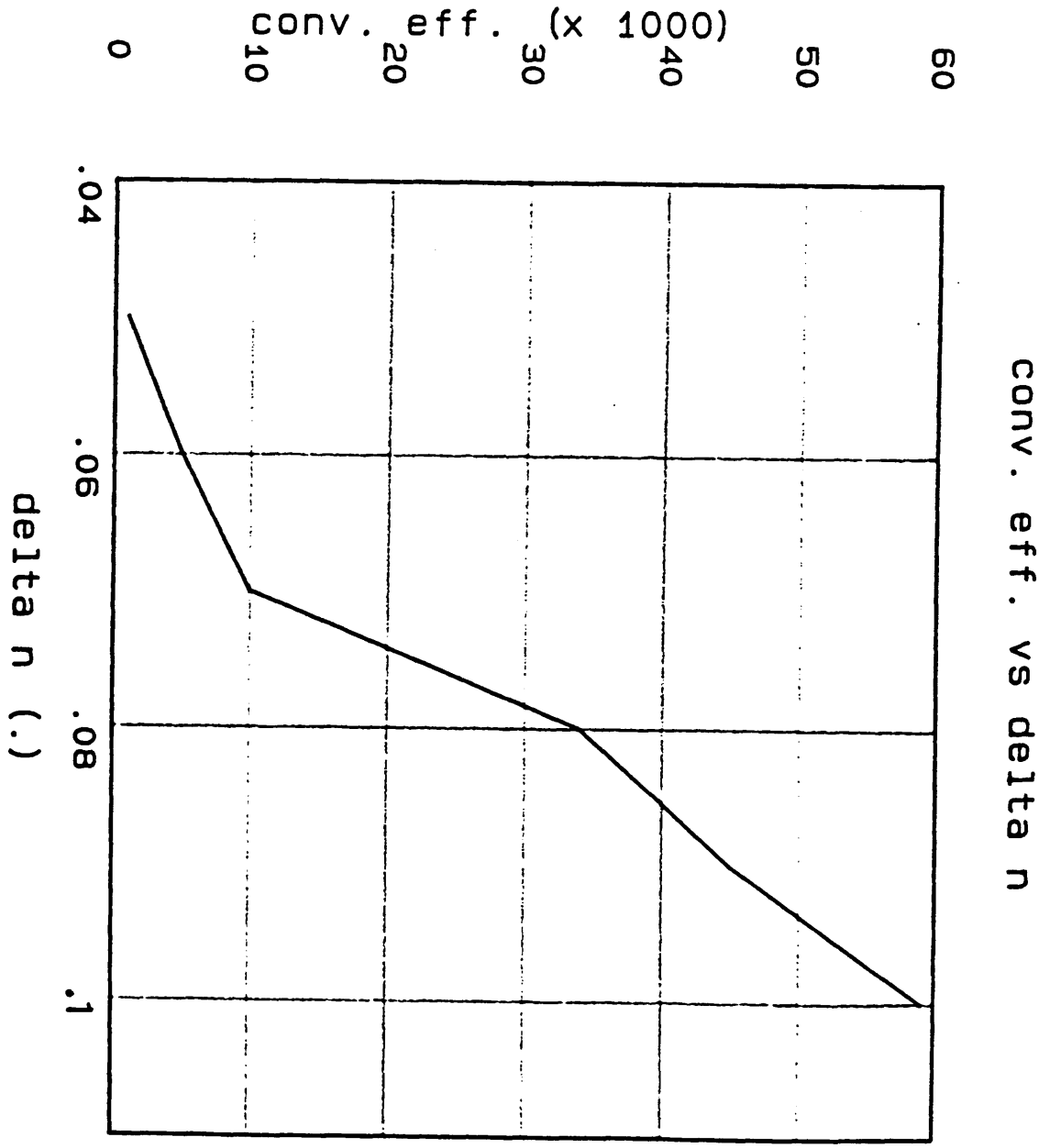

figure 2.6 variation of conversion efficiency (arbitrary units) with index difference (all other parameters equal)

The reduction in conversion efficiency is due to several factors. As the refractive index decreases so does the overlap integral. The power density (power/mode spot size) in the waveguide also decreases because of the increase in the mode spot size of the fundamental guided wave. The decrease in the power density and the increase in the mode spot size can easily be modelled and are shown in Fig. 2.7. In order to be more accurate in the modelling of annealed waveguides, it would be desirable to insert the changes in the refractive index profile as annealing progressed into the model. This approach would, however, make it very difficult to calculate the radiation modes, because the step index model would no longer be applicable. Although the model is crude, it has predicted quite well the dependence of conversion efficiency on waveguide depth and has shown, within limits, that the primary effect of annealing is to reduce the conversion efficiency for SHG. In order to model more accurately the effect of annealing, a more sophisticated theoretical model would be required, but such work is outside the scope of this thesis.

2.4 Conclusions.

A model for SHG in proton–exchanged waveguides via the Cerenkov effect has been presented. The model is based on a coupled mode theory of the interaction of a guided mode and a radiation mode. Whilst the model is relatively simple, it allows a prediction of the relationship between the conversion effiency for SHG and the waveguide depth. Assuming a step–refractive index profile for both the model waveguide and a proton–exchanged waveguide, the calculated results are in broad agreement with experimental results. Using this model the effect of annealing the waveguide has been modelled. It has been found that the effect of annealing the waveguide is to reduce the conversion efficiency for SHG, a result expected from experimental results. Although the theory is not rigorous it nevertheless is in fair agreement with other, more rigorous, theoretical treatments. By using more rigorous mathematical techniques to calculate the effective index of the guided mode at the fundamental wavelength and also to calculate the overlap integral more accurately, it should be possible to extend the theory and to obtain a better agreement with published results.

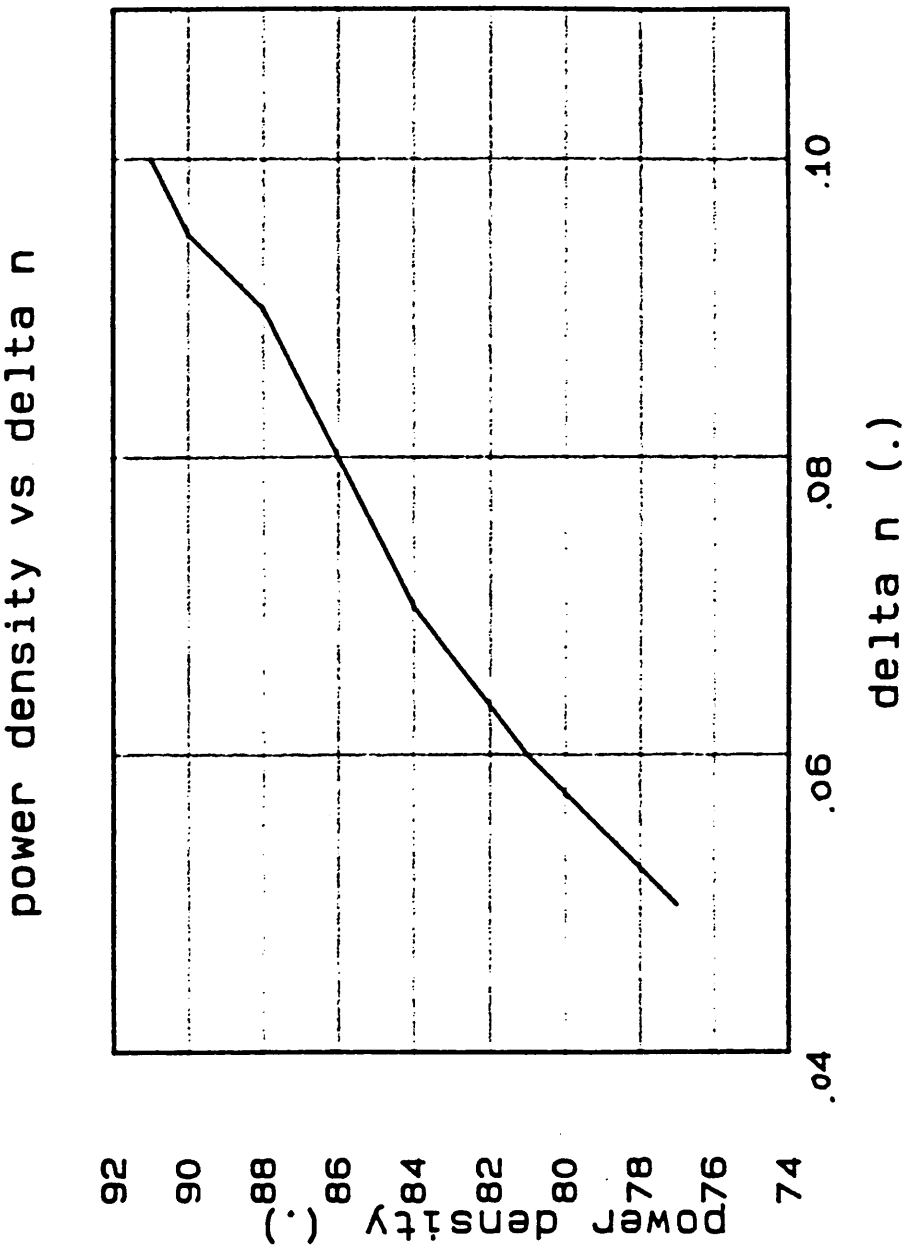

figure 2.7 variation of power density with index difference (all other parameters equal)

2.5 References.

[1]. W. Sohler in "*New Directions in Guided Wave and Coherent Optics*" Eds. D.B. Ostrowsky and E. Spitz, NATO ASI series no. 79.

[2]. Y.R. Shen, "*The Principles of Nonlinear Optics*", Wiley, New York, 1984.

[3]. R.L. Byer in "*Nonlinear Optics*" Proceedings of the Sixteenth Summer School in Physics, Eds. P.G. Harper and B.S. Wherret.

[4]. F. Laurell, Ph. D. Thesis, Royal Institute of Technology, Stockholm, 1990.

[5]. M. De Micheli, "*Nonlinear effects in TIPE–$LiNbO_3$ waveguides for optical communications*", J. Opt. Commun., 4, pp.25.31, 1983.

[6]. F. Laurell and G. Arvidsson, "*Frequency doubling in Ti:MgO:$LiNbO_3$ channel waveguides*", J. Opt. Soc. Am. B, 5, pp.292–299, 1988.

[7]. G.I. Stegeman and C.T. Seaton, "*nonlinear integrated optics*", J. Appl. Phys., 58, pp.R57–R78, 1985.

[8]. A. Loni, Ph. D. thesis, University of Glasgow, 1986.

[9]. B. Jaskorzynska, G, Arvidsson, F. Laurell, "*Periodic structures for phase–matching in SHG in titanium $LiNbO_3$ waveguides*", Proceedings Integrated Optical Circuit Engineering III, SPIE Volume 651, 1986.

[10]. N. Bloembergen and A.J. Sievers, "*Nonlinear optical properties of periodical laminar structures*",Appl. Phys. Letts, 17(11), pp.483–485, 1970.

[11]. T. Taniuchi and K. Yamamoto, "*Second harmonic generation using proton–exchanged $LiNbO_3$ waveguide*", Optoelectronics – Devices and Technologies, 2, pp.53–58,1987.

[12]. D. Marcuse, "*Optical Waveguide Theory*", Academic Press,

[13]. T. Taniuchi and K. Yamamoto, "*Second harmonic generation with GaAs laser diode in proton–exchanged $LiNbO_3$ waveguide*", Technical Digest E.C.O.C, pp.171–174, 1986.

[14]. P.K. Tien and R. Ulrich, J. Opt. Soc Am., 60, p.1325, 1970.

[15]. K.I. White and B.K. Nayar, "*Second harmonic generation in nonlinear fibre waveguides: efficient designs using radiation modes*", ibid., 5(2), pp.317–324, 1989.

[16]. P.K. Tien, "*Light waves in thin films and integrated optics*", Appl. Opt., 10, pp.2395–2413, 1971.

[17]. T. Taniuchi, unpublished.

[18]. M. De Micheli and D.B. Ostrowsky, "*Nonlinear integrated optics*", Physics World, pp.56–60, 1990.

[19]. M.J. Li, M. De Micheli and D.B. Ostrowsky, "*Cerenkov configuration second harmonic generation*", Paper THB15–1, Technical Digest Nonlinear Guided Wave Phenomenon: Physics and Applications, Santa Fe, New Mexico, 1989.

[20] K. S. Buritskii, *"Cerenkov second harmonic generation of semiconductor laser radiation (λ = 1.3 μm) in Ti:LiNbO$_3$ waveguide"*, Paper THB10−1, ibid.

[21]. J. V Roey, J. Van der Donk and P.E. Lagasse, *"The beam propagation method"*, J. Opt. Soc. Am., 71, pp.803, 1981.

[22]. T. Fujiwara, M. Izutsu, H. Murata, Y. Tanabe and T. Sueta, *"BPM analysis of SHG in form of Cerenkov radiation"*, Paper WBB4−1, Technical Digest Nonlinear Guided Wave Phenomenon: Physics and Applications, Santa Fe, New Mexico, 1989.

[23]. N.A. sanford and J.M. Connors, *"Optimization of the Cerenkov sum−frequency generation in proton−exchanged Mg:LiNbO$_3$ channel waveguides"*, J. Appl. Phys., 65, pp.1429−1437, 1989.

[24]. K. Hayata, T. Sugarawa and M. Koshiba, *"Modal analysis of the second harmonic electro−magnetic field generated by the Cerenkov effect in optical waveguides"*, IEEE J. Quant. Elec., 26, pp.123−134, 1990.

[25]. D. Marcuse, *"Electrooptic coupling between TE and TM modes in anisotropic slabs"*, ibid, 11, pp.759−767, 1975.

[26]. J.M. Hammer in *"Integrated Optics"*, Ed. T. Tamir, Springer Verlag, Berlin, 1975.

[27]. D. Marcuse, *"Coupled−mode theory for anisotropic waveguides"*, Bell System Technical Journal, 54, pp.985−995, 1975.

[28]. T. Tamir in *"Integrated Optics"*, Ed. T. Tamir, Springer Verlag, Berlin, 1975.

CHAPTER 3

EXPERIMENTAL INVESTIGATIONS OF SECOND HARMONIC GENERATION (SHG) IN PROTON–EXCHANGED WAVEGUIDES.

3.1.1 Introduction

This chapter deals with the experimental investigation of Cerenkov SHG in proton–exchanged optical waveguides. Planar waveguides were initially used to investigate the dependence of second harmonic generation conversion efficiency on the waveguide fabrication time. The effect of annealing the waveguides was then investigated. This work was carried out with a Q–switched Nd:YAG laser. Second harmonic generation was also investigated in stripe waveguides, using both a c.w. Nd:YAG laser and a semiconductor laser. The results from this experimental work have been compared with the theoretical results of the previous chapter. In general, the results for conversion efficiency are in reasonably good agreement with the theoretical model.

3.1.2 Review of published work

Cerenkov second harmonic generation in proton–exchaged waveguides was first demonstrated using channel waveguides by Taniuchi and Yamamoto [1]. The waveguides were fabricated by either immersion or by spin–coating in pyrophosphoric acid using tantalum as a mask (chapter 4 contains more details of the fabrication process). With a channel waveguide of dimensions (in mm) of 0.4 x 2.5 x 12 they were able to generate 0.2 mW of harmonic light at 0.42 μm from 20 mW of fundamental power at 0.84 μm from a GaAs laser, a conversion efficiency of 1%. By refining the waveguide design to increase the conversion efficiency they were able to generate up to 1.05 mW of harmonic power with a fundamental power of 120 mW [2]. The waveguide dimensions were 0.4 x 2 x 6 mm.

By using MgO–doped lithium niobate and pyrophosphoric acid waveguides Tohmon et al [3] were able to frequency double a laser operating at 0.78 μm to generate harmonic light in the ultra–violet spectral region. In order to achieve high efficiency the authors used the laser in a gain–switched mode to take advantage of the high peak powers available. The fundamental pulses had a duration of 21.5 ps with a trailing edge. The harmonic pulses had a duration of 19.3 ps with a much reduced trailing edge. Using a waveguide with of dimensions

0.33 x 1.4 x 18 mm the authors were able to produce 1.35 mW of peak harmonic power from 600 mW of peak fundamental power, a conversion efficiency of 0.2%.

Sanford and Connors [4] have investigated both second harmonic generation and sum-frequency generation in proton-exchanged waveguides fabricated in MgO-doped lithium niobate. In the second harmonic generation experiments they used both a Nd:YAG laser (1.064 μm) and a semiconductor laser (0.833 μm) and for the sum-frequency generation they coupled in both the semiconductor laser and light at 1.3 μm. For a fundamental wavelength of 1.064 μm and power of 0.57 mW they were able to generate 3.1 nW of harmonic power. They found however that, in disagreement with the work of Taniuchi et al, when using powers greater than 2 mW at 0.833 μm optical damage became a problem. Since Taniuchi et al do not state explicitly that they are using a pulsed source at the fundamental wavelength then it must be assumed that they are coupling into the waveguide c.w. powers well above the threshold at which optical damage might be expected. It would therefore seem unlikely that no optical damage will occur at these high c.w. powers.

In another experiment Li et al [5] have used a multimode planar proton-exchanged waveguide to generate harmonic radiation from a Nd:YAG laser. Interestingly, they used x-cut lithium niobate and fabricated a waveguide of depth 4.4 μm which supported 5 modes. Only four of these modes produced a harmonic wave, the refractive index of the lowest order mode being greater than the substrate index, thus not satisfying the conditions for Cerenkov radiation. The maximum conversion efficiency measured was 0.25% for the fourth order mode. The Nd:YAG laser was operated in a pulsed mode but details of the pulse power levels were not given.

3.2.1 Experimental SHG of a Nd:YAG laser

For the initial second harmonic generation studies, planar waveguides were used because they were easy to fabricate and input coupling could be achieved by means of prisms. A Nd:YAG laser was used as the fundamental pump source to investigate the dependence of SHG on the waveguide fabrication conditions.

There were two important reasons for use of the Nd:YAG laser in a Q-switched mode. Firstly, the conversion efficiency for second harmonic generation is proportional to the peak power density of the fundamental wave (see chapter 2),

thus increasing the conversion efficiency for second harmonic generation by a factor given by the ratio of the peak pulse power to the average power of the fundamental wave. Secondly, lithium niobate is a photo-refractive material and may suffer optical damage at even moderate average optical power levels [6]. If optical damage occurs the output beam is reduced in intensity and in extreme cases can be cut-off completely [6]. The photo-refractive effect is dependent on the average optical power so that, for Q-switched pulses with a low repetition rate, the photo-refractive effect is not a problem. By using Q-switched pulses, high conversion efficiencies can be achieved while the average power is low enough to prevent optical damage.

In our experiments a Q-switched pulse length of 200 ns was used at a repetition rate of 1.25 kHz. The increase in the conversion efficiency relative to the c.w. case should then be:-

$$P_p \; / \; P_{ave} = T \; / \; \tau_p = 4000 \qquad (3.1)$$

where T is the period of the pulses and τ_p is the pulse-width of the individual pulses.

In all cases the average power in the waveguide was kept at, or below, 1 mW. At these power levels no optical damage was observed.

3.2.2 Measurement of the Cerenkov angle in planar waveguides

The Cerenkov angle was defined in chapter 2 as the angle at which the harmonic wave is emitted into the substrate. From Eq. 2.19, the Cerenkov angle is given by:-

$$\theta = \frac{\tan^{-1}\{n_o{}^{2\omega}.[(n_e{}^{2\omega})^2 - N_{eff}{}^2)^{0.5}]\}}{N_{eff}.n_e{}^{2\omega}} \qquad (3.2)$$

where the definitions are as given in chapter 2. The ordinary and extra-ordinary refractive indices of lithium niobate were calculated using the Sellmeier relations [7]. At a wavelength of 0.532 μm, these refractive indices are:-

$n_o = 2.323$

$n_e = 2.234$

Measurements of the refractive indices at wavelengths of 1.064 μm, 0.6328 μm and 0.532 μm were in close agreement with the calculated values. Substituting these figures into Eq. 3.2 and rearranging gives an expression for the Cerenkov angle:–

$$\theta = \tan^{-1} \{(1.04/N_{eff}).\sqrt{(4.99 - N_{eff}^2)}\} \qquad (3.3)$$

The Cerenkov angle was measured by placing a screen at a fixed distance perpendicular to the polished end face of the waveguide. By simple geometry, the Cerenkov angle could be deduced. This angle was then substituted into the Snell's law equation to give the Cerenkov angle in the substrate. The effective index of the fundamental guided mode was calculated using the prism–coupling technique.

A series of proton–exchanged waveguides was fabricated in 1% dilute melt benzoic acid at an acid temperature of 235 °C, with fabrication times in the range 1–4 hrs. Fig. 3.1 shows the relationship between the measured (θ_{meas}) and calculated (θ_{calc}) Cerenkov angles. As can be seen, the calculated and measured Cerenkov angles are in close agreement. Figs. 3.2 and 3.3 illustrate SHG in a planar waveguide and a typical Cerenkov far–field radiation pattern respectively.

3.2.3 Conversion efficiency for SHG in planar waveguides

The aim of this section of the work was to investigate the effect of the waveguide fabrication conditions on the conversion efficiency for SHG. By fabricating waveguides with a range of depths, the dependence of conversion efficiency on waveguide depth could be investigated experimentally. The effect of annealing was investigated and compared to the unannealed case.

3.2.4 Conversion efficiency versus waveguide depth

It is difficult to estimate the depth of a the guiding region of a single mode planar waveguide of unknown refractive index profile. An accurate estimate of waveguide depth can usually only be achieved for a waveguide which supports four or more modes. This allows the waveguide depth to be estimated using an IWKB fit, which is appropriate for a general refractive index profile (see, for example, [8]). When a single mode step index waveguide is used, the waveguide depth can be estimated by measuring the effective index of the guided mode and substituting this value, together with the substrate refractive index and the refractive index of the waveguide into the dispersion relation for the waveguide.

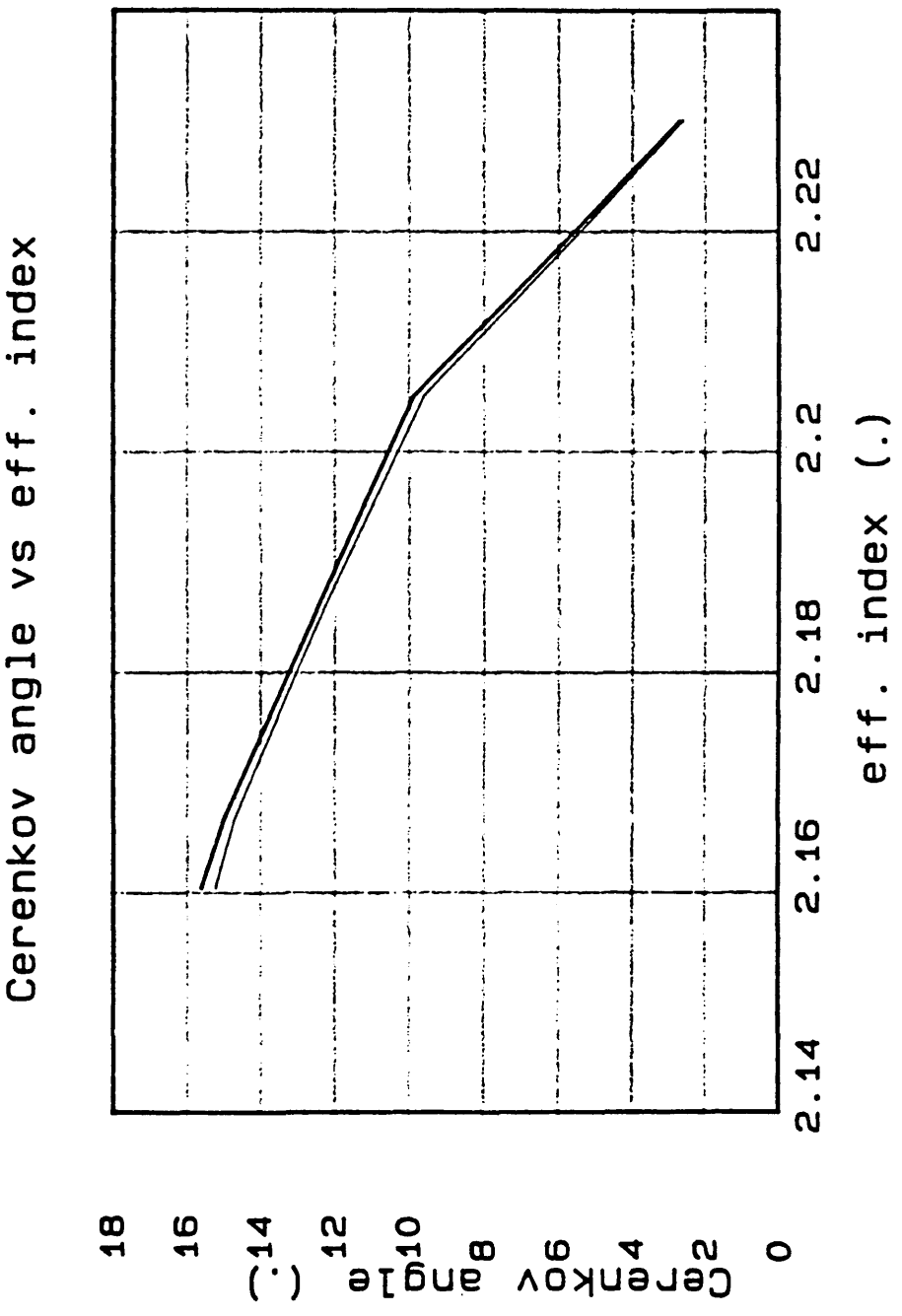

figure 3.1 Cerenkov angle in substrate as a function of the effective index of the fundamental wave at 1.06 um

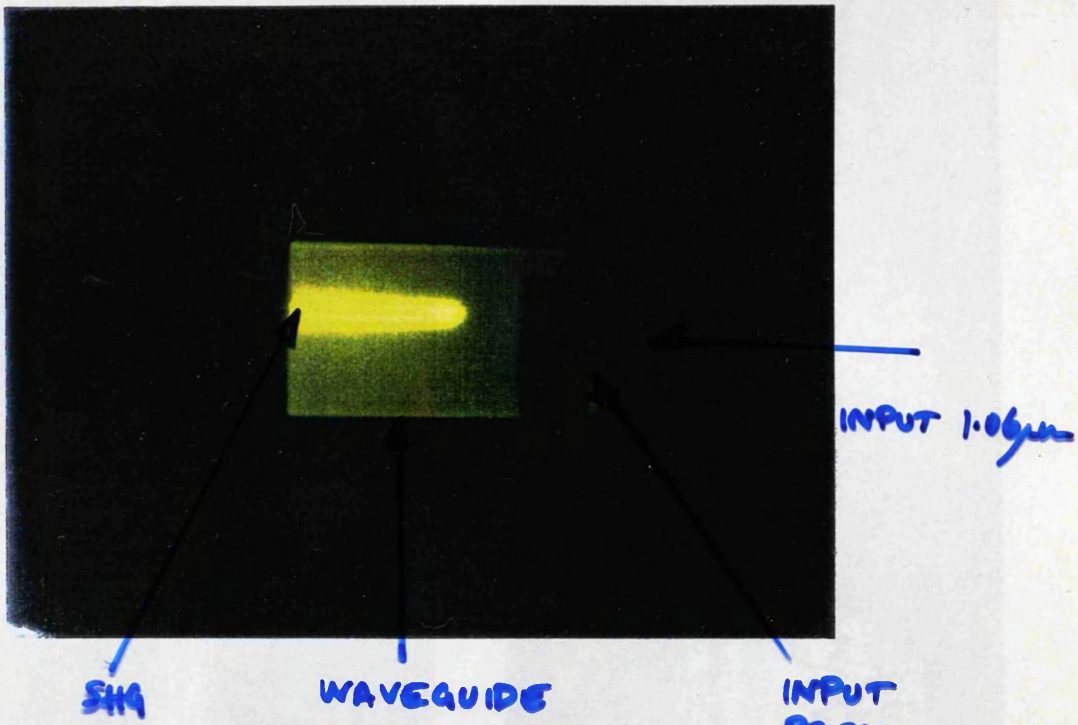

figure 3.2

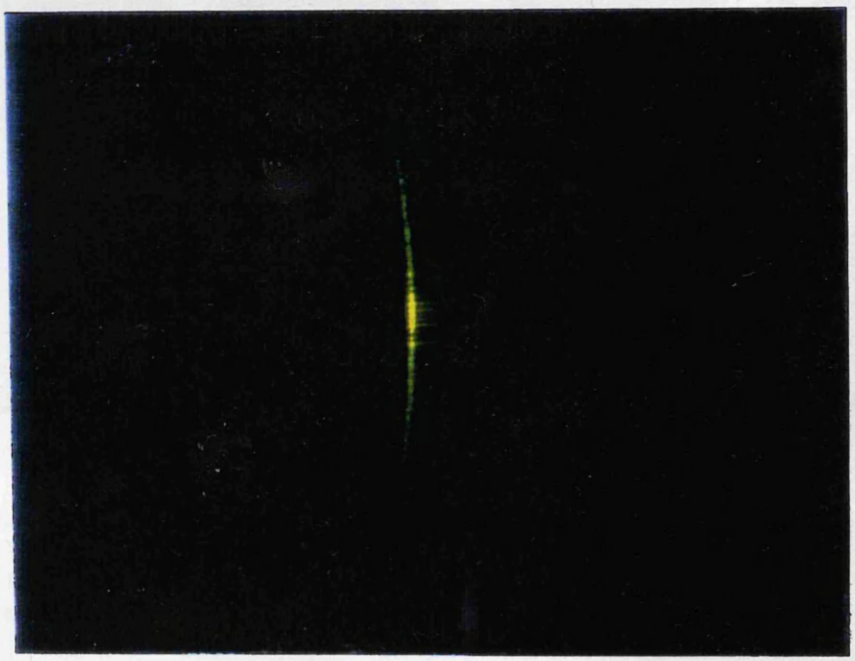

figure 3.3

FAR FIELD CERENKOV PATTERN.

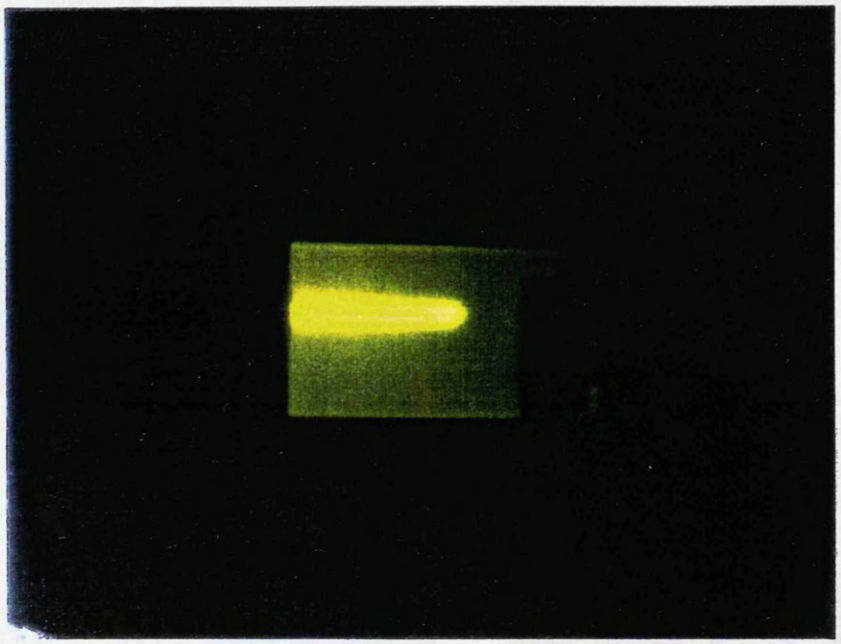

figure 3.2

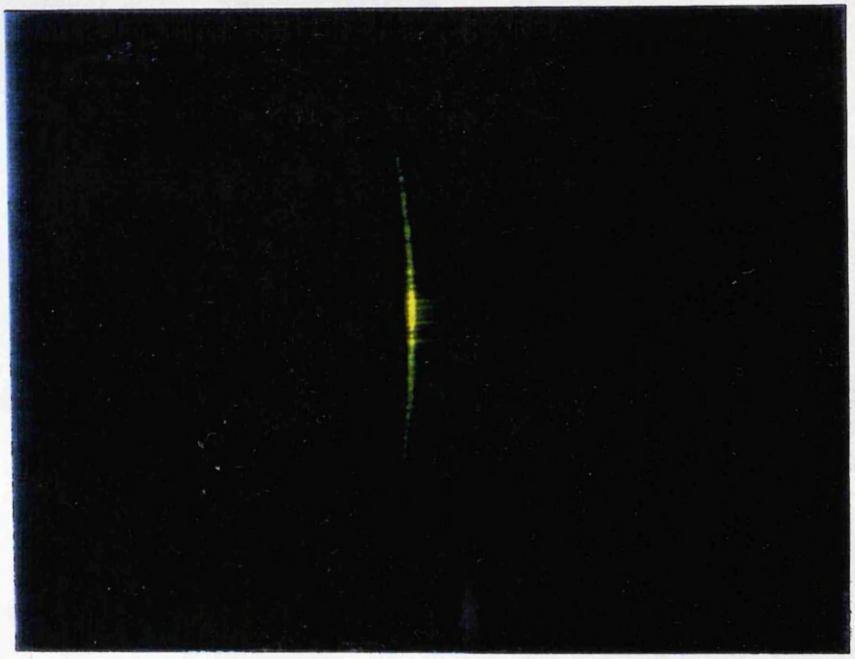

figure 3.3

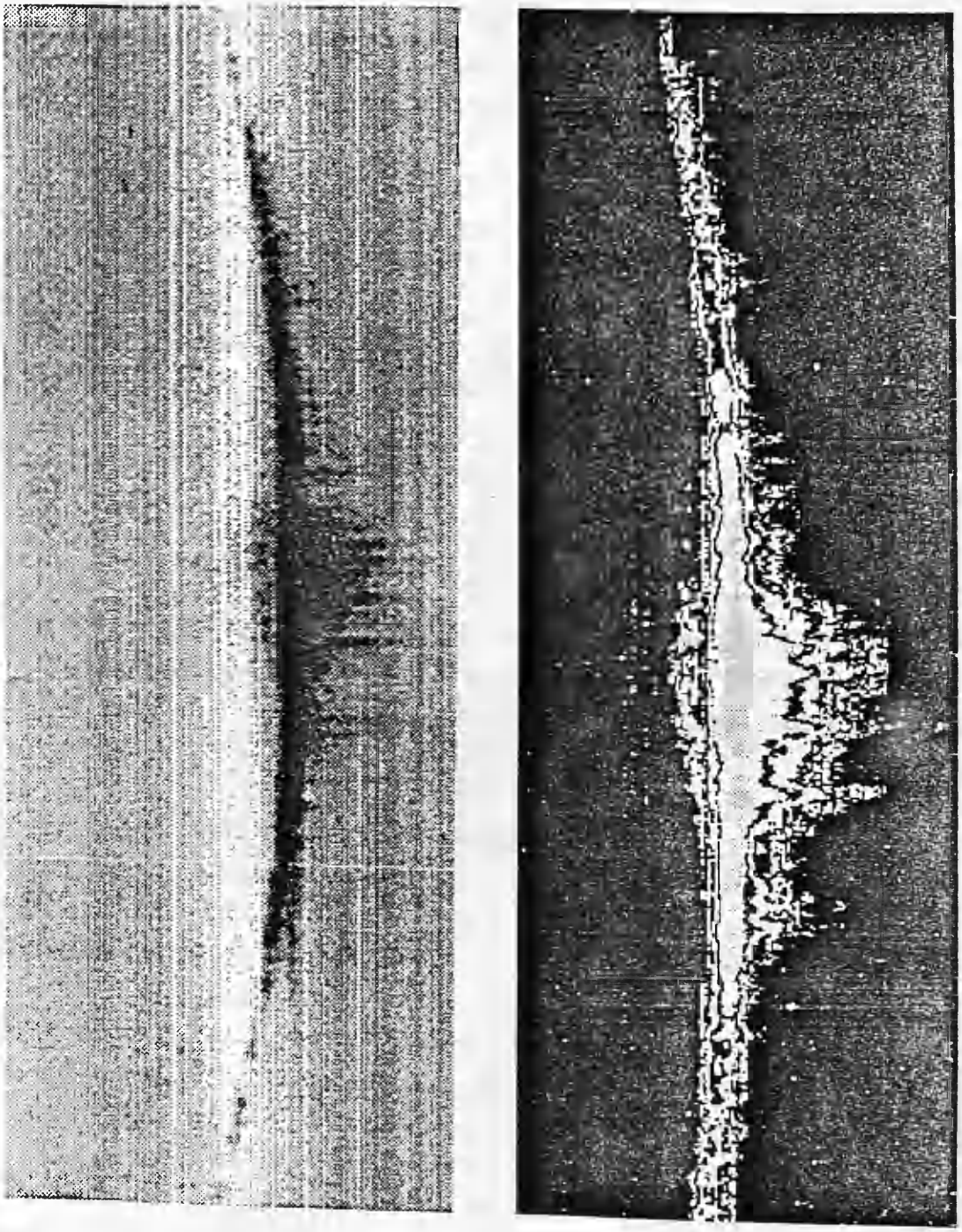

Computer-enhanced images of the far-field SHG radiation pattern. I am grateful to Professor J. Barker, Department of Electronics and Electrical Engineering, for these pictures.

The refractive index of the waveguide layer has to be known accurately in order to achieve a reasonably accurate estimate. A second method is to carry out multi–wavelength measurements of the effective index of a single mode waveguide and solve the dispersion relation in a self–consistent manner to estimate the waveguide depth.

A third, but less accurate, method of estimating the waveguide depth is to use the waveguide fabrication time and the diffusion coefficient for proton–exchange. The diffusion coefficient can be measured accurately (to at least two decimal places) and is derived from a knowledge of the waveguide depth calculated from an IWKB fit to the measured effective indices of the guided modes. From a knowledge of the diffusion coefficient and the waveguide fabrication time the waveguide depth, d, can be estimated using the formula:–

$$d^2 = 4.D(T).t \qquad (3.4)$$

where D(T) is the diffusion coefficient for an acid temperature of T K and t is the exchange time in hours. This is a standard result from the theory of diffusion and still applies in the case of a limited source with an Arrhenius–type behaviour [9].

In the present work the waveguide depths were estimated by the diffusion constant method. A series of nine waveguides was fabricated in *neat* melt benzoic acid at 235 °C for exchange times between 8 min and 70 min. These waveguides were single–moded at $\lambda = 1.064$ μm. Using the same acid melt conditions, a second series of waveguides was made for longer exchange times (up to 6 hours). The latter waveguides were multi–moded (> 4 modes) at $\lambda = 0.6328$ μm. The effective indices of the guided modes at $\lambda = 0.6328$ μm were measured and, by substituting these indices into an IWKB analysis, the depth of the waveguide was estimated. By plotting out a graph of depth squared (d^2) versus exchange time (t), a value for the diffusion constant for proton–exchange under the above conditions was estimated. This value of diffusion coefficient was then used to estimate the depths of the first set of waveguides, knowing the exchange time used for the waveguide fabrication. The depths estimated by this method were in agreement with the depths estimated by measuring the effective index of the guided modes and substituting this value of effective index into the waveguide dispersion relation to find the waveguide depth.

Using the Nd:YAG laser in the Q–switched mode with the same parameters (T,

τ_p) as above (see Eq. 3.1), the conversion efficiency for second harmonic generation was measured for each of the waveguides in the series. The interaction length in each case was 3mm. This interaction length was chosen so that there could be no reflections from the bottom face of the substrate (see Fig. 3.4). The fundamental power was measured using a calibrated germanium detector and the harmonic power was measured using a calibrated silicon detector (with an appropriate filter to remove any stray fundamental power). The output powers were measured at the polished exit face of the waveguide. It was assumed that the power (fundamental or harmonic) in the waveguide was the same as that measured at the exit face (after accounting for Fresnel losses), equivalent to assuming that the waveguide propagation losses are negligible. For the interaction lengths used in this work, this is a valid assumption since the losses will be of the order of 0.3 dB, based on estimated propagation losses of 1 dB/cm. Fig. 3.5 shows the experimental arrangement used to measure the conversion efficiency.

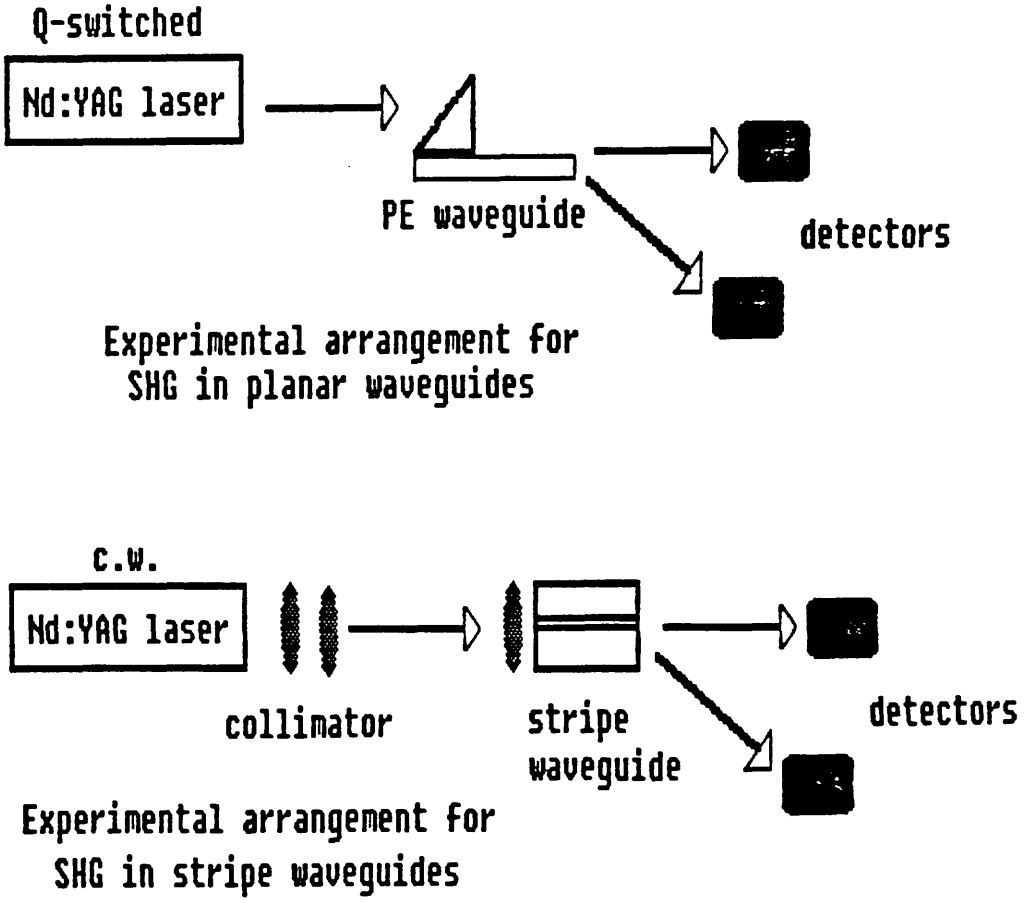

figure 3.5

In all the waveguides investigated, the fundamental beam waist in the waveguide was different in each case. In this work the beam waist was defined by the full–width half maximum intensity of the zeroth order waveguide mode of the fundamental wave. The differences in waveguide depths, beam waist and input coupling efficiency meant that the fundamental power density was not the same in each waveguide. In order to allow a valid comparison of conversion efficiency for each waveguide, it was necessary to calculate the conversion efficiency for the case of an equivalent fundamental power in each waveguide. This was equivalent to normalizing the measured conversion efficiency to a fixed input power.

The normalization procedure adopted throughout this work was as follows. The measured conversion efficiency was calculated as:–

$$\eta = \langle P^{2\omega} \rangle \; / \; \langle P^{\omega} \rangle \qquad (3.5)$$

where $\langle P \rangle$ denotes the mean value of the power at ω or 2ω. For waveguide second harmonic generation, 1 W of fundamental power is an unrealistically high power on which to base the normalization of the conversion efficiency. Instead, the measured conversion efficiencies were normalized to 1 mW of fundamental power (typical of the average fundamental power levels used in the experiments). A figure of 1 mW for the fundamental power was also used in the theoretical calculations. As was mentioned above, the measured fundamental beam waist was different for each waveguide, a typical value of the fundamental beam waist, measured by scanning the near field of the output beam with a pinhole, being in the range 0.5 mm to 3.8 mm. For comparison, all the measured conversion efficiencies were normalised to a beam waist of 1 mm. This allowed a comparison to be made between the measured conversion efficiency for each waveguide and the shape of the theoretical curve for conversion efficiency. At this stage only a qualitative comparison could be made. Without more exact estimates of the waveguide depths a quantitative comparison cannot be made. A final normalization was carried out by taking the maximum value of the normalized conversion efficiencies and equating it to unity. The remaining normalized conversion efficiences were then scaled with respect to unity.

Fig. 3.6 shows a graph of normalized conversion efficiency, as defined above, versus the waveguide depth. Comparing Fig. 3.6 with Fig. 2.5 of chapter 2, it can be seen that there is a reasonable agreement between the theoretical conversion efficiency curve and the experimental curve. In proton–exchanged waveguides the refractive index is only quasi–steplike and this will introduce an

error between the theory and experimental curves.

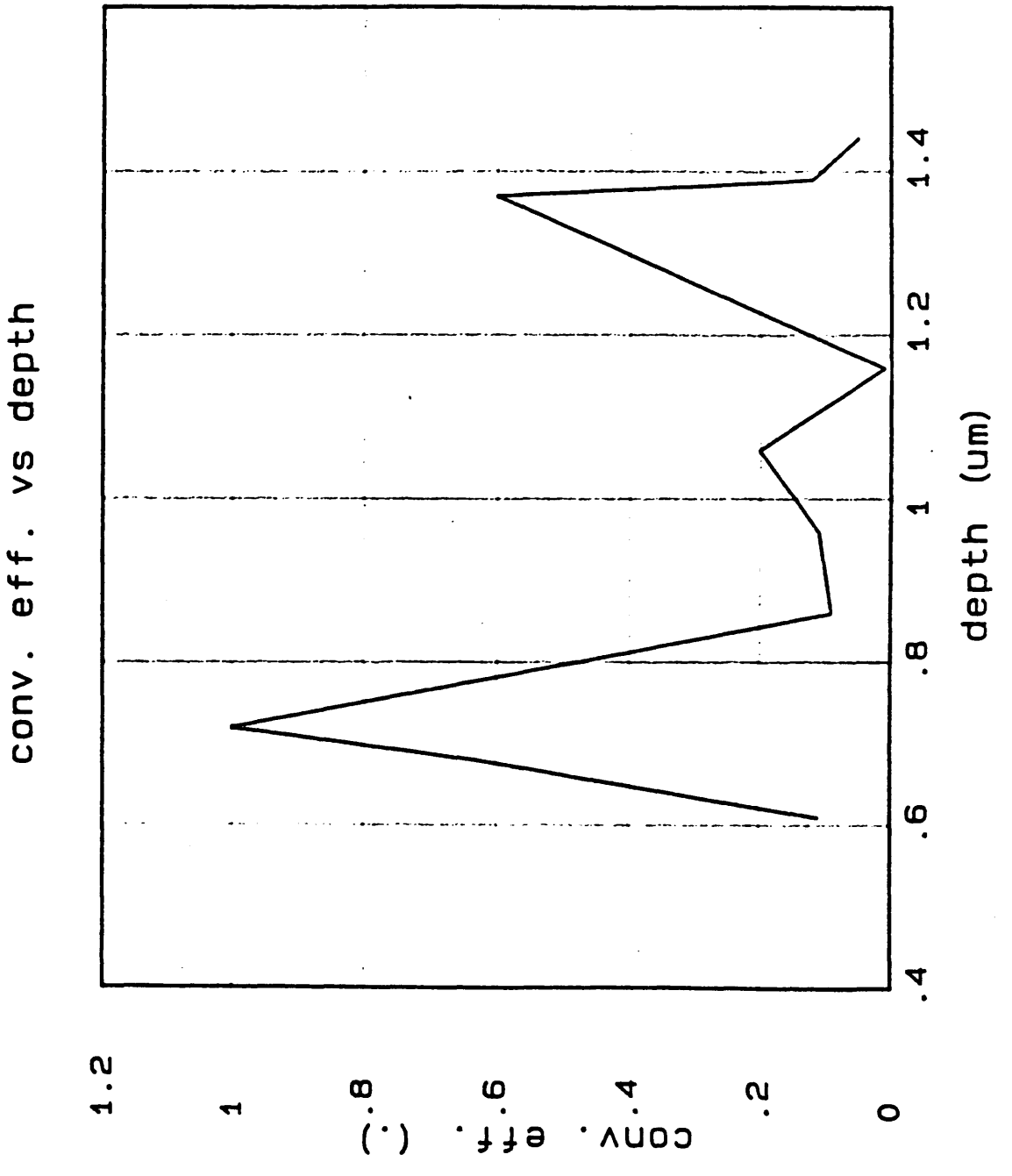

figure 3.6 measured normalised conversion efficiency (% /mW/mm) as a function of unannealed waveguide depth

Using the waveguide depths estimated from the "measured" diffusion coefficient, the conversion efficiency "peaks" at a waveguide depth of approximately 0.7 μm with a value of 1% mW^{-1}. The measured average fundamental power was 0.38 mW and the measured average harmonic power was 4 μW. The corresponding peak powers were 1.54 W and 1 mW respectively. The actual, i.e. un-normalized, fundamental power densities in the waveguide were 31 Wcm^{-2} (average) and 0.12 $MWcm^{-2}$ (peak) for a measured fundamental beam waist of 1.6 mm.

3.2.5 Effect of annealing on the conversion efficiency

Suhara et al [10] have shown that the d_{33} nonlinear coefficient is reduced by a factor of approximately 2 in proton-exchanged lithium niobate. It has also been shown by the author [11] (see also chapter 5) that annealing of proton-exchanged regions leads to a partial restoration of the d_{33} coefficient in the waveguide region. The initial reduction is not unexpected. The nonlinear and electro-optic coefficients of lithium niobate are closely related material parameters. It has been shown by Minakata et al [12], Loni et al [13] and more recently by McMeekin and De La Rue [14], that the proton-exchange process leads to a reduction in the electro-optic coefficients. The reduction in the d_{33} coefficient and the electro-optic coefficients will be discussed in more detail in chapter 5.

Loni et al [13] have shown that low loss waveguides with a substantially restored electro-optic coefficient can be fabricated by annealing for 20mins at 275 °C followed by 15mins at 375 °C. The annealing took place in an atmosphere of flowing wet oxygen. On the assumption that the nonlinear coefficient might behave in a similar fashion to the electro-optic coefficient, the above fabrication procedure was adopted by the author in order to investigate the effect of annealing on the nonlinear conversion efficiency. The same waveguides as used previously were used throughout the following work. The first annealing stage was carried out in two 10min stages. After each annealing stage the conversion efficiency and the fundamental beam waist were re-measured for each waveguide. Fig. 3.7 shows the normalized conversion efficiency as a function of waveguide depth for the first two (10 min.) annealing stages. In this case the normalization is still with respect to the maximum value of conversion efficiency obtained using the un-annealed waveguides (i.e. the same waveguide as in the previous section). The waveguide depths were assumed to be unchanged after the annealing stage. As the annealing is for only a short period, this should be a valid approximation.

After the third annealing stage the conversion efficiency in each case had fallen by an order of magnitude, and these results are not plotted in the figure.

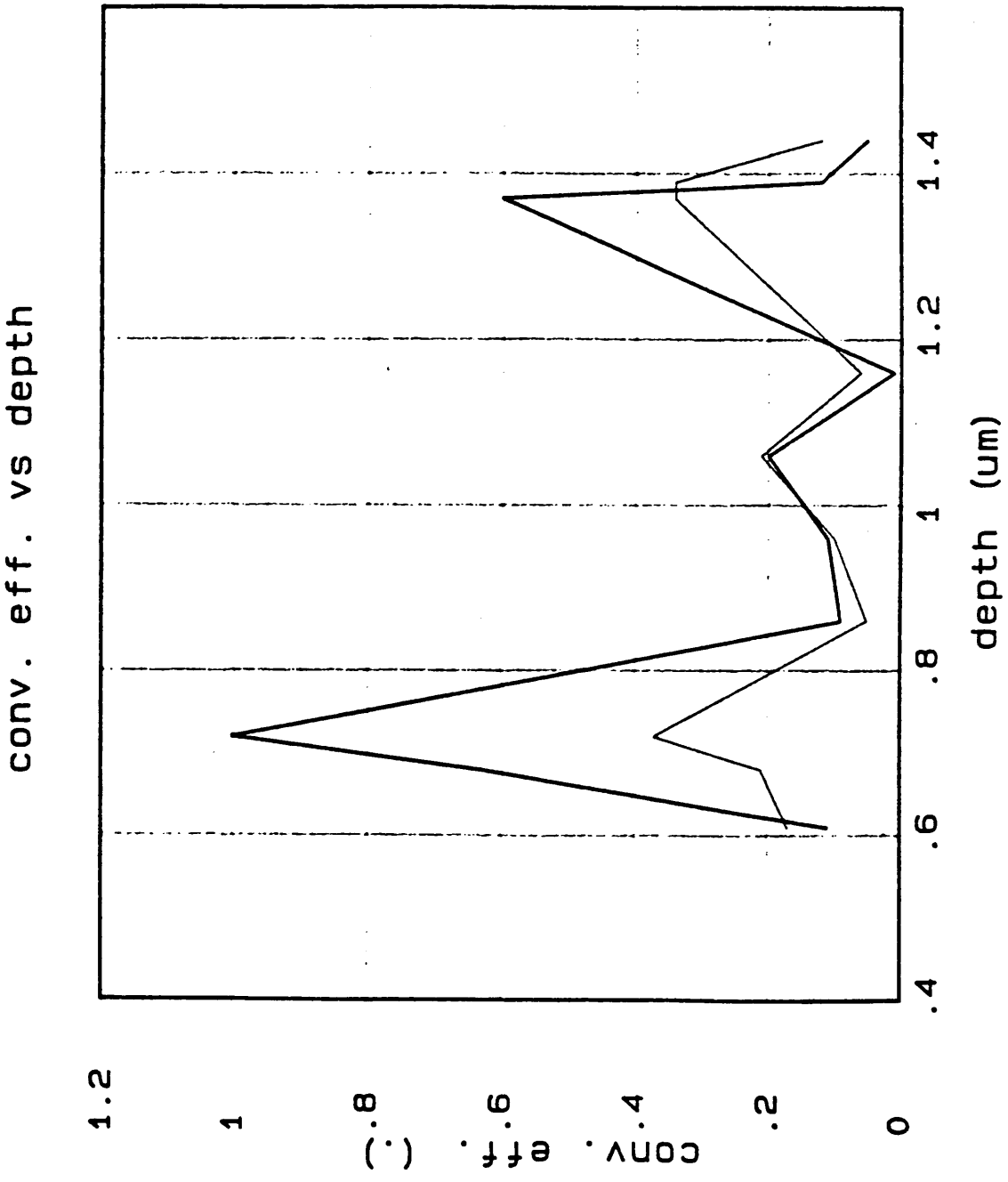

figure 3.7 measured normalised conversion efficiency (% /mW/mm) as a function of waveguide depth after 10 mins. annealing at 275^{0}C (unannealed curve also shown)

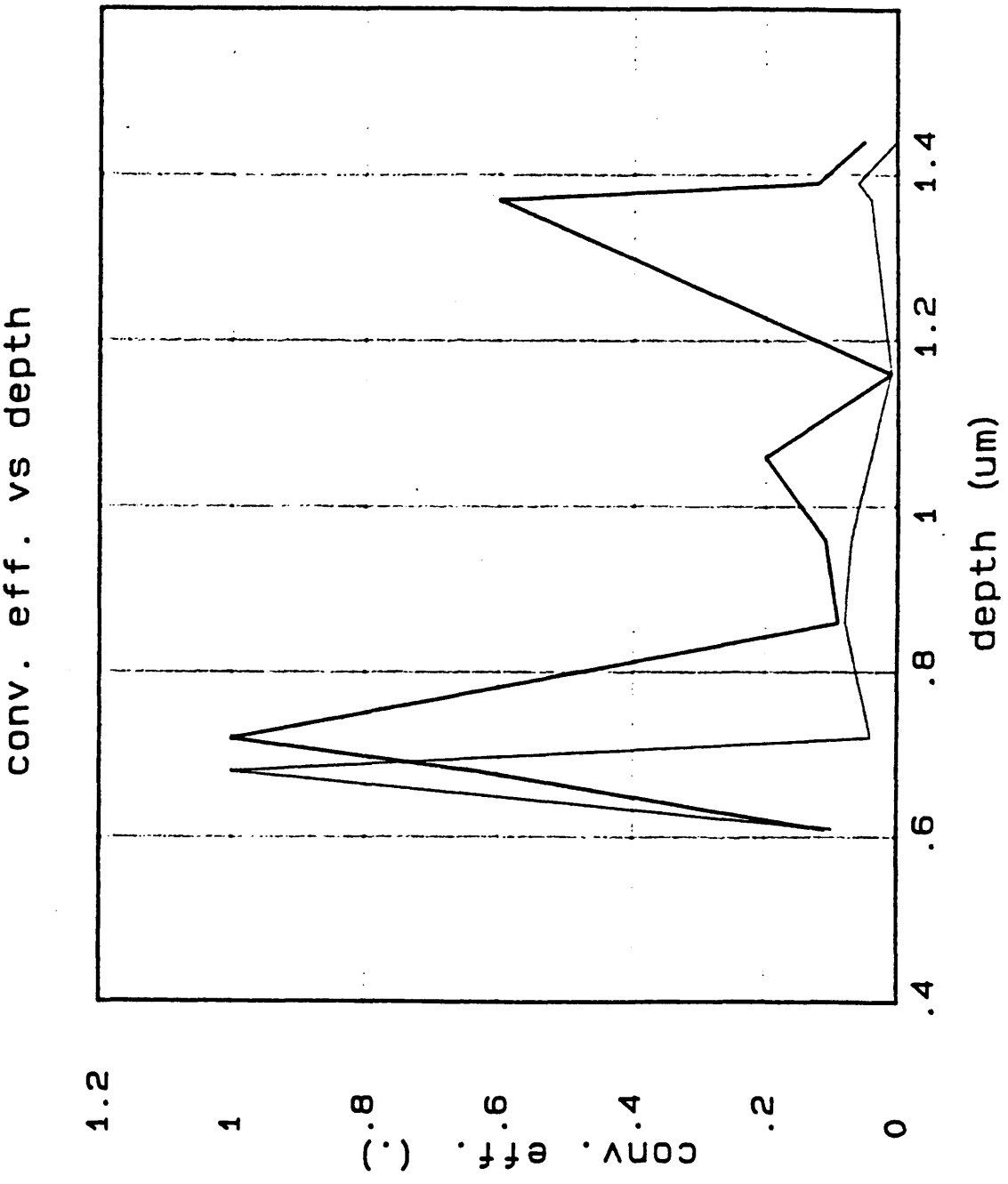

figure 3.7(b) measured normalised conversion efficiency (% /mW/mm) as a function of waveguide depth after 20 mins. annealing at 275^0C (unannealed curve also shown)

On inspection of Figs. 3.6 and 3.7, it can be seen that the general trend is towards a reduction in the conversion efficiency after annealing the waveguides, although in some cases there is a slight increase. For example, after annealing for 20min, in one case the conversion efficiency increased to the same level as the highest value measured before annealing.

In order to understand the effect of annealing on the conversion efficiency it is important to consider the annealing process in detail. There are several inter-related parameters which determine the effect of annealing on the conversion efficiency. From the theoretical model, annealing leads to a reduction in the conversion efficiency. However, the model did not take account of any change in the depth of the waveguide or changes in the intrinsic nonlinearity of the waveguide region.

Annealing the waveguides may produce the following changes;

(1) An increase in the waveguide depth and a reduction in the refractive index of the proton-exchanged region.

(2) A change in the magnitude of the overlap integral between the fundamental and harmonic waves.

(3) An increase in the d_{33} nonlinear coefficient of the waveguide region.

(4) A reduction in the propagation losses.

An increase in the waveguide depth could lead to either an increase or a decrease in the conversion efficiency. Whether the conversion efficiency is increased or decreased depends on the initial waveguide depth. If, for example the waveguide depth were initially less than 0.7 μm (i.e. below the peak in figure 8 of chapter 2) then increasing the depth would be expected to lead to an increase in the conversion efficiency. When the depth had risen above 0.7 μm the conversion efficiency would begin to be reduced. All of this assumes that there is no change in the effective index of the guided mode on annealing and that there is no change in the nonlinear d_{33} coefficient of the waveguide region. However, the effective index is expected to be reduced on annealing and, from theory, this would lead to a change in the phase-matching condition, which will manifest itself as a change in the Cerenkov angle.

Figure 3.8 illustrates the measured change in the Cerenkov angle as a function of annealing time for various annealing temperatures.

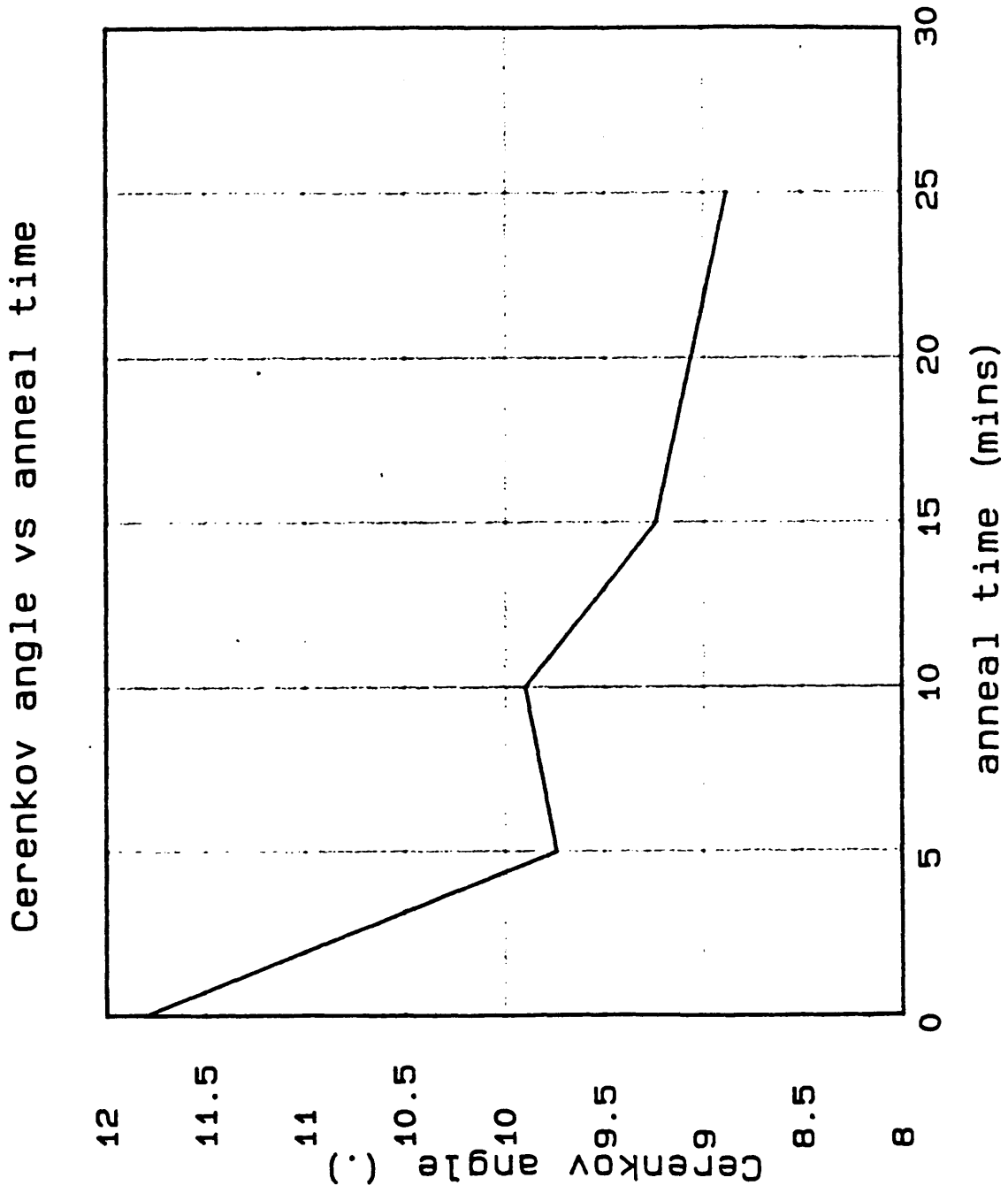

figure 3.8 Reduction of Cerenkov angle as a funtion of annealing time (at 275^{0}C)

Clearly, the combined effects of increasing the waveguide depth and a lowering of the effective index make it difficult to predict the effect of annealing on the conversion efficiency. In order to model properly the effects of annealing, the exact refractive index profiles, the waveguide depth and the profile of the nonlinearity distribution would be required. A lowering of the waveguide refractive index (and hence effective index) also leads to a reduction in the power density of the guided mode. This will also give a reduction in the conversion efficiency via Eq. 2.33.

It was seen in chapter 2 that, on the assumption that the waveguide depth remained constant, the refractive index profile remained a step function and that there was no reduction in d_{33} due to proton–exchange, the effect of reducing the refractive index of the waveguide region (equivalent to reducing the effective index for a waveguide of a given depth) was to reduce the overlap integral. The reduction in the overlap integral reduces the conversion efficiency via Eq. 2.33.

The partial restoration of the d_{33} nonlinear coefficient by annealing could have either a positive or a negative effect on the conversion efficiency. This is because the overlap integral has two contributions, one from the substrate region and the other from the waveguide region. These contributions can be written as:–

$$I = d'_{33}.\int(\text{waveguide}) + d_{33}\int(\text{substrate}) \qquad (3.10)$$

where d'_{33} and d_{33} are the waveguide and substrate nonlinearities respectively and $\int(.....)$ is the overlap integral in the appropriate region, as defined in chapter 2.

The overlap integral for a given region can be either positive or negative, depending on the electric field distributions in the waveguide and substrate regions. Consider the case where the overlap integral is positive in the substrate but negative in the waveguide. On annealing the waveguide, d'_{33} will be partially restored [11]. Assume to a first approximation that the overlap integrals are unchanged on annealing. Under these conditions the combined overlap integral of Eq. 3.10 will be reduced, thus reducing the conversion efficiency. If, on the other hand, the contributions to the overlap integral are both positive then annealing will increase the overlap integral of Eq. 3.10, thus increasing the conversion efficiency.

The effect of reduced propagation losses is to increase the conversion efficiency

[15]. For the waveguides used, the propagation losses are small and, given the mild annealing conditions, are not expected to be reduced significantly by the annealing process. Therefore no significant increase in the conversion efficiencies is expected.

These arguments present no single, clear, explanation of the effect of annealing on the conversion efficiency. However, the important points can be summarised as follows;

(1) Annealing reduces the waveguide refractive index, which in turn leads to a reduction in the conversion efficiency via the overlap integral.

(2) Annealing leads to a reduction in the power density, which in turn will reduce the conversion efficiency.

(3) The restoration of the nonlinearity in the waveguide region can lead to either an increase or a decrease in the conversion efficiency.

3.3.1 SHG in stripe waveguides

The use of stripe, or channel, waveguide structures for SHG offers the potential of obtaining conversion efficiencies which are much higher than those measured for planar waveguides because of the higher power densities which can readily be realized in stripe waveguides. As a consequence of the increased power density within the waveguide, efficient SHG of even moderate power levels of light from c.w. semiconductor laser diodes becomes possible. With stripe waveguides, there exists the possibility of generating light of a chosen wavelength by the process of three-wave mixing. Using two lasers of different frequencies (the pump and signal), an idler wave is produced at either the difference or sum frequency. In proton-exchanged waveguides, three-wave mixing is automatically phase-matched for Cerenkov generation. This has been experimentally demonstrated by Sanford et al [4] in proton-exchanged waveguides. Three-wave mixing has also been carried out in titanium-indiffused waveguides by Laurell et al [16].

Experimental work has been carried out by the author to investigate SHG of both c.w. Nd:YAG laser and c.w. semiconductor diode laser radiation in stripe waveguides. As for the case of planar waveguides, the guided fundamental wave in a stripe waveguide can produce second harmonic generation by Cerenkov radiation.

3.3.2 SHG of c.w. Nd:YAG laser radiation

The waveguides used were fabricated in neat melt benzoic acid at 235 °C for a range of exchange times between 10 min and 70 min. The waveguide stripe widths were between 3 μm and 7 μm in 1 μm steps. The waveguides were defined by standard photolithographical techniques with aluminium as the masking layer. Typically, the waveguides were 5 mm long. Input coupling was achieved via end-fire coupling with x40 microscope objectives. The fundamental and harmonic powers were measured using calibrated germanium and silicon detectors and the power measurements were again taken at the exit face of the waveguide.

For the Nd:YAG laser, coupling losses were high due to mode-mismatch and care was taken to optimize the input coupling efficiency and so minimise these losses. The total loss was estimated to be 6 dB, approximately 3.5 dB being due to lens and waveguide end-face reflection losses, and approximately 2.5 dB being due to waveguide propagation losses and input coupling modal mismatch. The total throughput fundamental (c.w.) power levels measured were typically only 1 to 2 mW, with the corresponding harmonic power levels up to a maximum of 0.7 μW. Fig. 3.9 shows the normalised conversion efficiency as a function of the square root of the exchange time for waveguide fabrication in a series of 7 μm wide stripes. In this case the normalization need only be carried out with respect to the fundamental power as the stripe widths are equal in each case. As expected there is a specific depth at which the maximum in the conversion efficiency occurs. For these particular conditions, the maximum conversion efficiency measured was 2.4% mW^{-1} for a fundamental power of 1.6 mW in the waveguide, with a corresponding harmonic power of 65 nW. Assuming that the diffusion coefficient for the proton-exchange process is essentially the same for fabrication of both the 7 μm stripes and for planar waveguides, the waveguide depth was estimated as 0.7 μm. The power density in the waveguide was then estimated as 0.03 $MWcm^{-2}$, which is comparable to the peak power density of the Q-switched pulses used for the planar waveguide experiments (c.f. section 3.2.4).

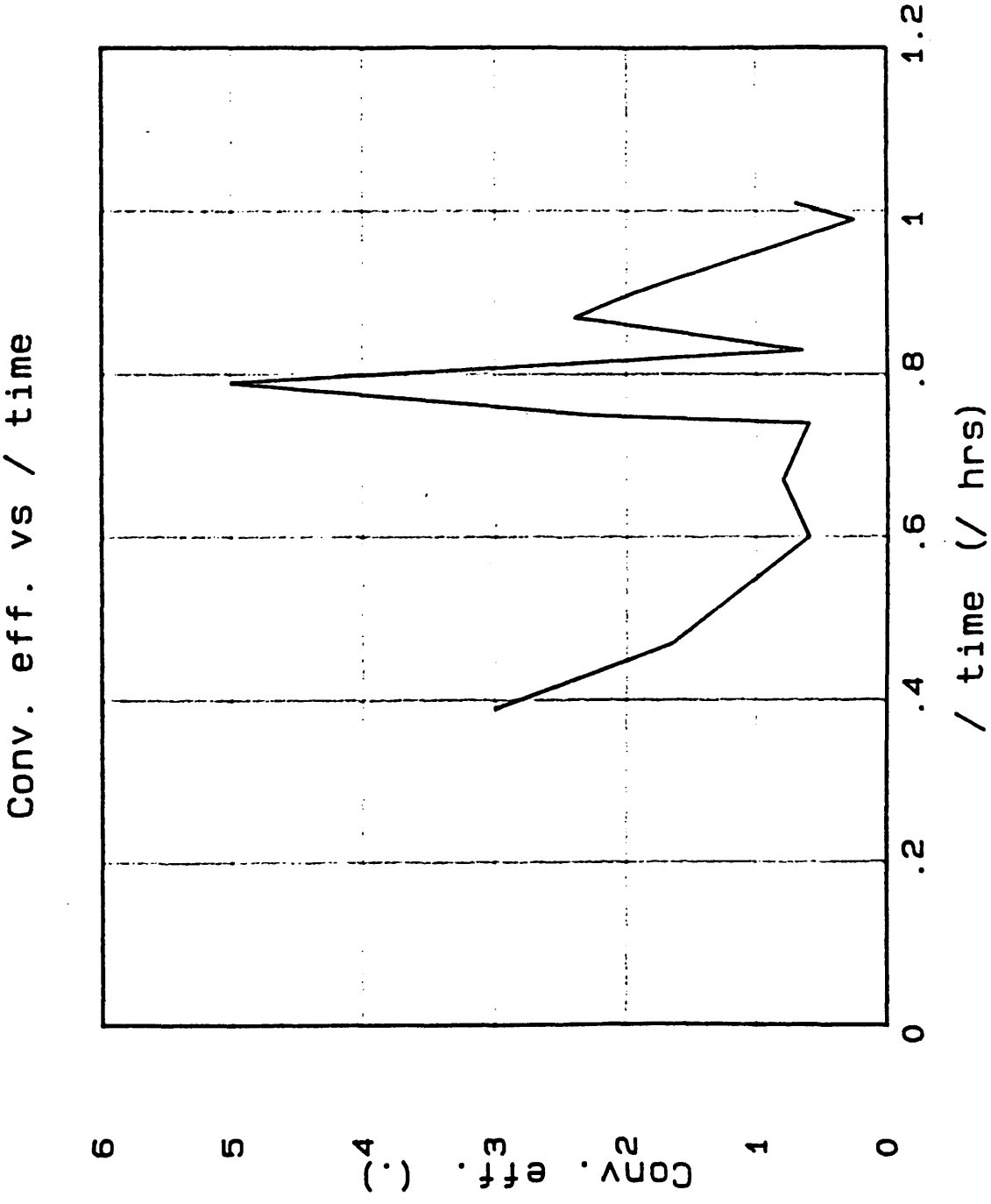

figure 3.9 normalised conversion efficiency (% /mW/mm) as a function of the square root of the exchange time for 7 um wide stripe guides

The conversion efficiency for second harmonic generation is expected to be proportional to the power density in the waveguide. For waveguides of similar depth, this implies that the conversion efficiency is inversely proportional to the stripe width. This dependence was investigated by measuring the conversion efficiency as a function of stripe width for waveguides with nominally the same depth. The waveguide widths were 4, 5, 6, and 7 μm. Care was taken to optimise the input coupling in each case. Fig. 3.10 shows the normalised conversion efficiency as a function of stripe width. It can be seen that the relationship is inverse as expected.

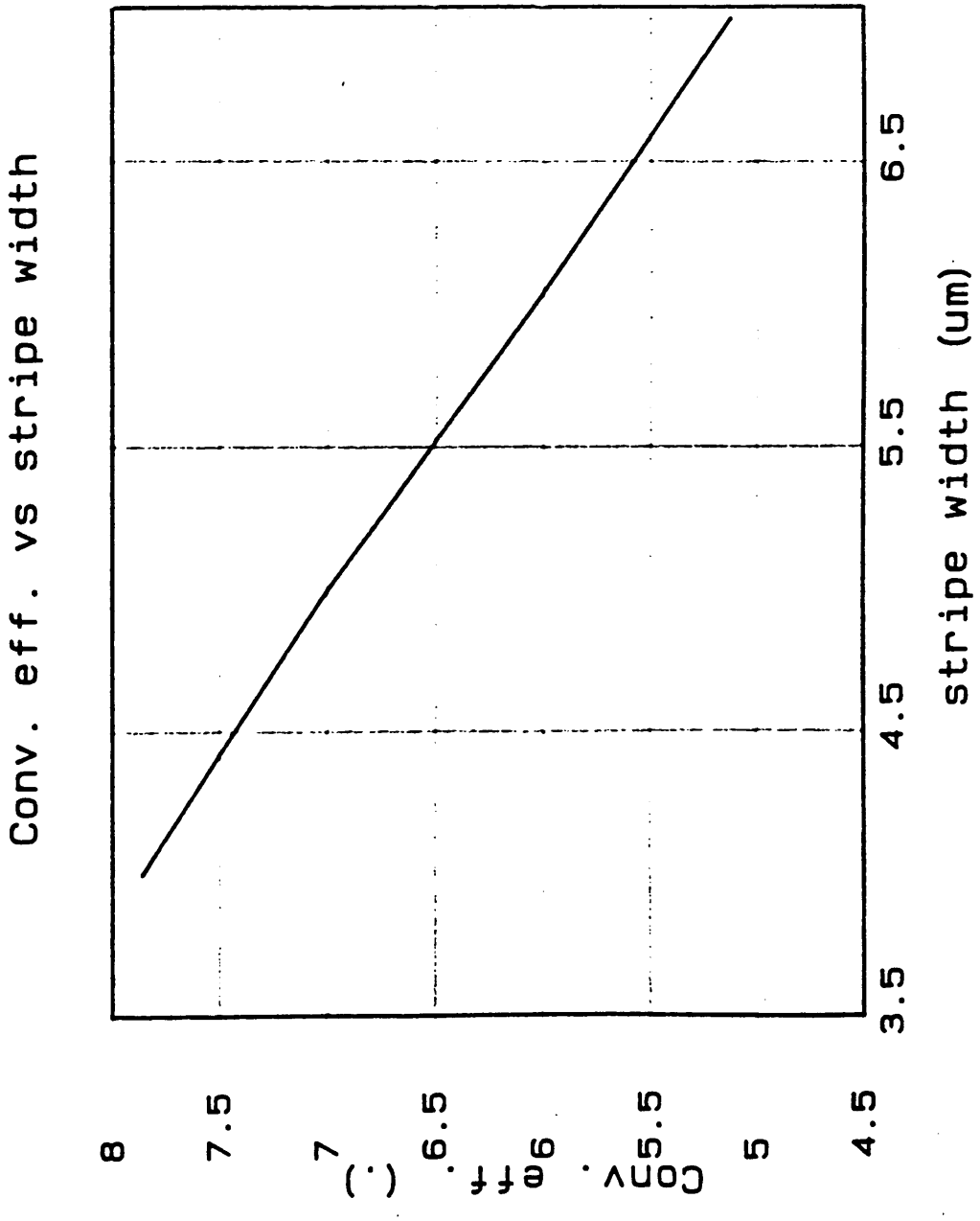

figure 3.10 normalised conversion efficiency (% /mW/mm) as a function of the stripe width

In all of the work on stripe waveguides, despite the relatively high power densities within the waveguide, no photorefractive damage was observed. Fig. 3.11 shows a typical far-field radiation patterns of Cerenkov second harmonic generation of a Nd:YAG laser in a stripe waveguide.

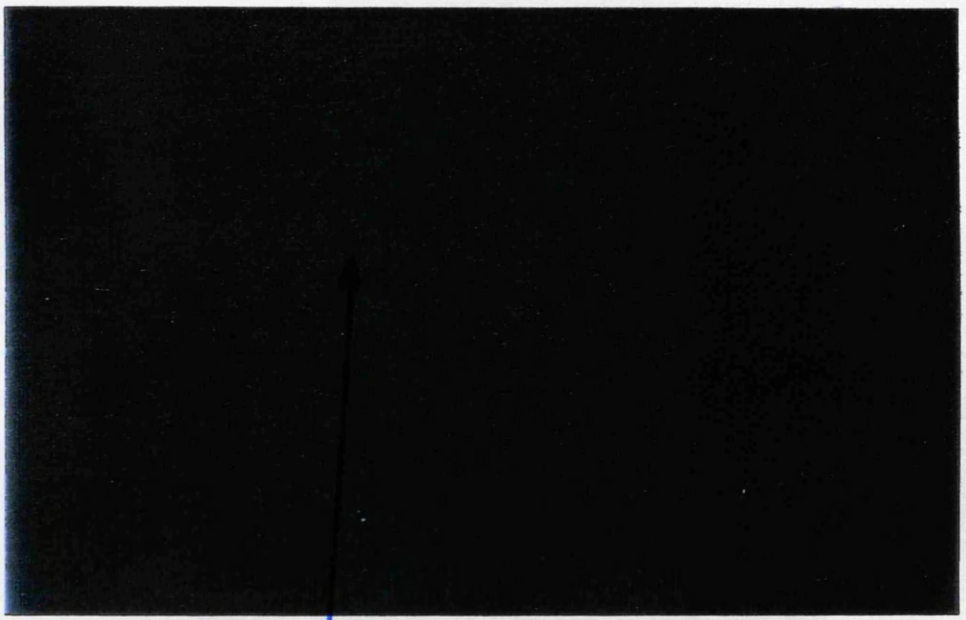

figure 3.11

SHG CERENKOV RING

SEE FOLLOWING PAGE

In all of the work on stripe waveguides, despite the relatively high power densities within the waveguide, no photorefractive damage was observed. Fig. 3.11 shows a typical far-field radiation patterns of Cerenkov second harmonic generation of a Nd:YAG laser in a stripe waveguide.

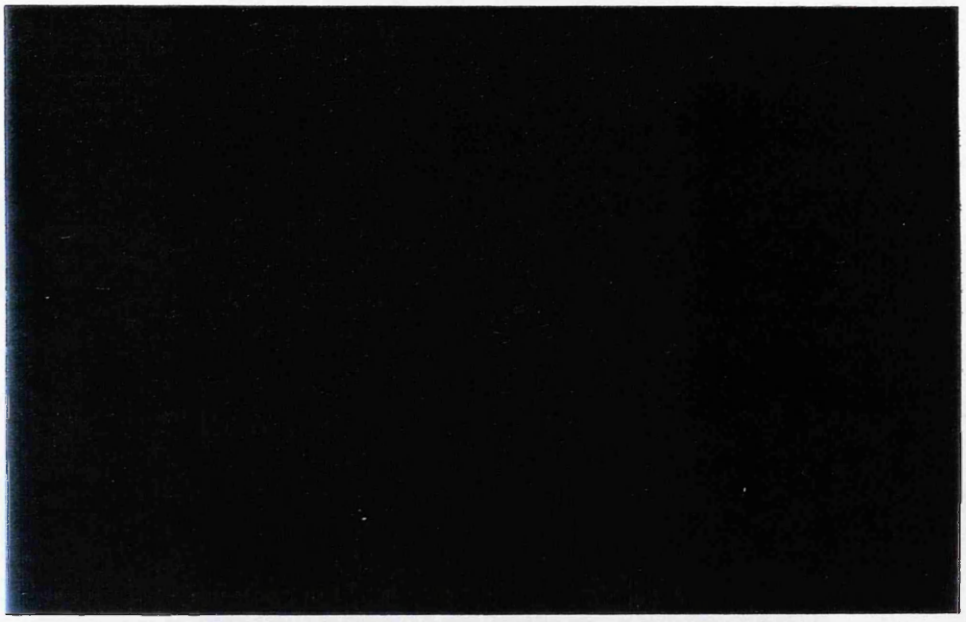

figure 3.11

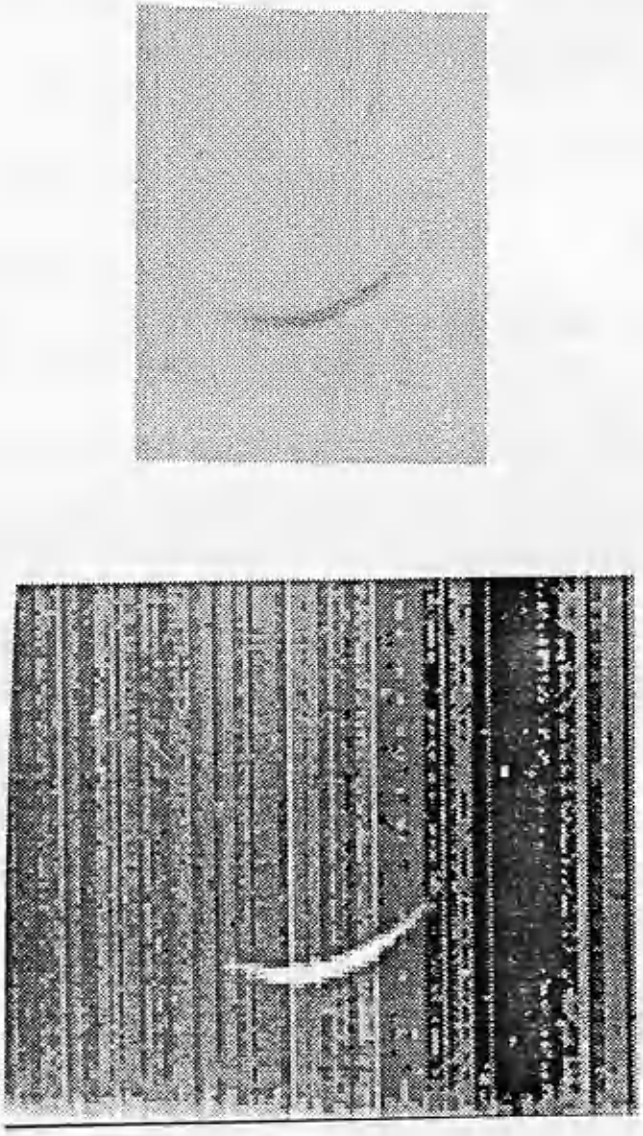

Computer-enhanced images of the far-field SHG radiation pattern from a proton-exchanged stripe waveguide. This shows the crescent shape of the radiation pattern and is an enhancement of figure 3.11.

3.3.3 SHG of c.w. semiconductor laser radiation

SHG of semiconductor laser radiation was also investigated. The waveguides in this study were fabricated in neat melt benzoic acid at 200 °C for exchange times between 75 min and 140 min. The output light from the semiconductor laser was collimated with a x40 microscope objective. Using a x50 microscope objective lens the light was coupled into waveguides with stripe widths between 2 μm and 20 μm. Again the guides were typically 5 mm long. The total loss was around 10dB with approximately 3.5 dB due to reflection losses at the waveguide end face and lens throughput losses, and approximately 6 dB mode–mismatch and propagation losses. The higher mode–mismatch losses in this case are due to the elliptical radiation pattern from the laser diode.

The semiconductor laser used was a Sharp LT015 model capable of a maximum output power of 40 mW. This laser operated on a single longitudinal mode at a wavelength of 838 nm. The high losses kept the total throughput power to 1 to 3 mW at the waveguide output. For an exchange time of 75 min a maximum conversion efficiency of 2.78% mW^{-1} was measured with the 20 μm stripe, based on the output power levels. This corresponded to 200 μW of fundamental power with 0.875 μW of harmonic power being generated. It should be noted that these waveguides were transversely multi–moded at this wavelength. The measured harmonic power is the sum of the harmonic power over all of the waveguide modes. Figs. 3.12 and 3.13 illustrate the Cerenkov ring pattern generated by a semiconductor diode laser in a stripe waveguide. The multiple "rings" are due to the multi–mode nature of the waveguide. Consequently the phase–matching angle will be slightly different for each waveguide mode. The second set of rings are due to reflections of the harmonic radiation from the polished bottom face of the substrate.

The high conversion efficiencies measured indicate the potential for a practical semiconductor pumped frequency doubled light source. By reducing the coupling losses and mode–mismatch losses higher conversion efficiencies could be obtained. The mode–mismatch losses may be reduced by reshaping the semiconductor laser beam (from elliptical to circular) using, for example, an anamorphic prism pair. Another way of increasing the conversion efficiency would be to coat the waveguide end faces with dielectric mirrors to form a resonant cavity at the fundamental wavelength. This would confine the fundamental radiation within the cavity and enhance the conversion efficiency. Sohler et al [15] have estimated that a resonant cavity could increase the conversion efficiency by an order of

magnitude. The beam quality of the harmonic radiation could be a problem for many practical device applications, and it would be necessary to reshape the beam. A possible solution to this problem could be the fabrication of a holographic lens on the rear face of the substrate to reshape the beam.

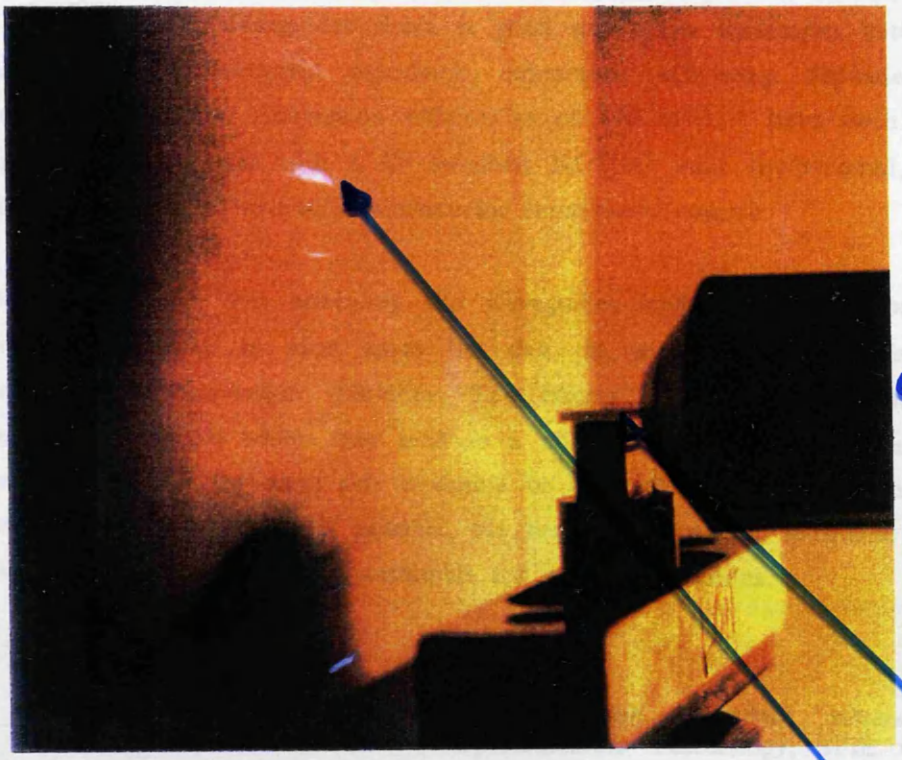

figure 3.12

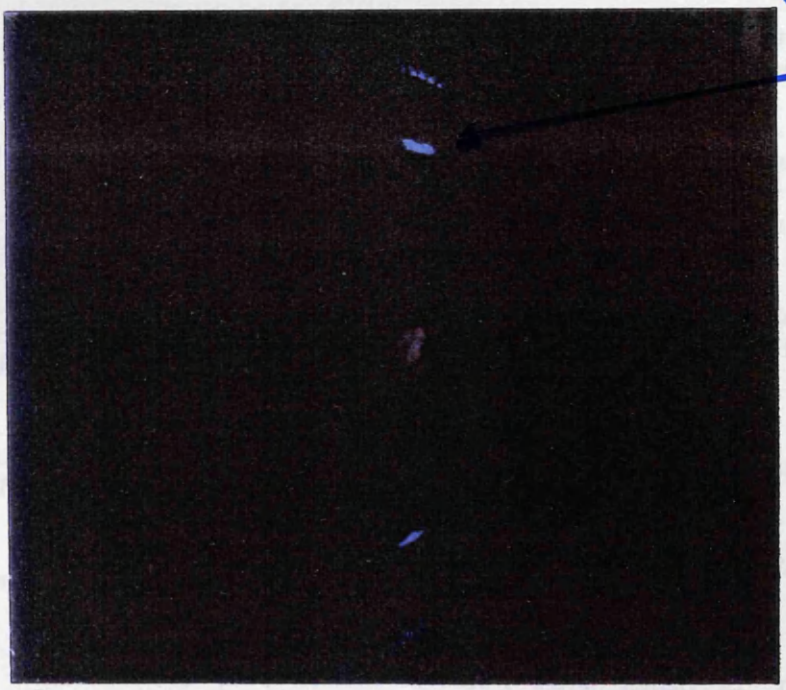

figure 3.13

magnitude. The beam quality of the harmonic radiation could be a problem for many practical device applications, and it would be necessary to reshape the beam. A possible solution to this problem could be the fabrication of a holographic lens on the rear face of the substrate to reshape the beam.

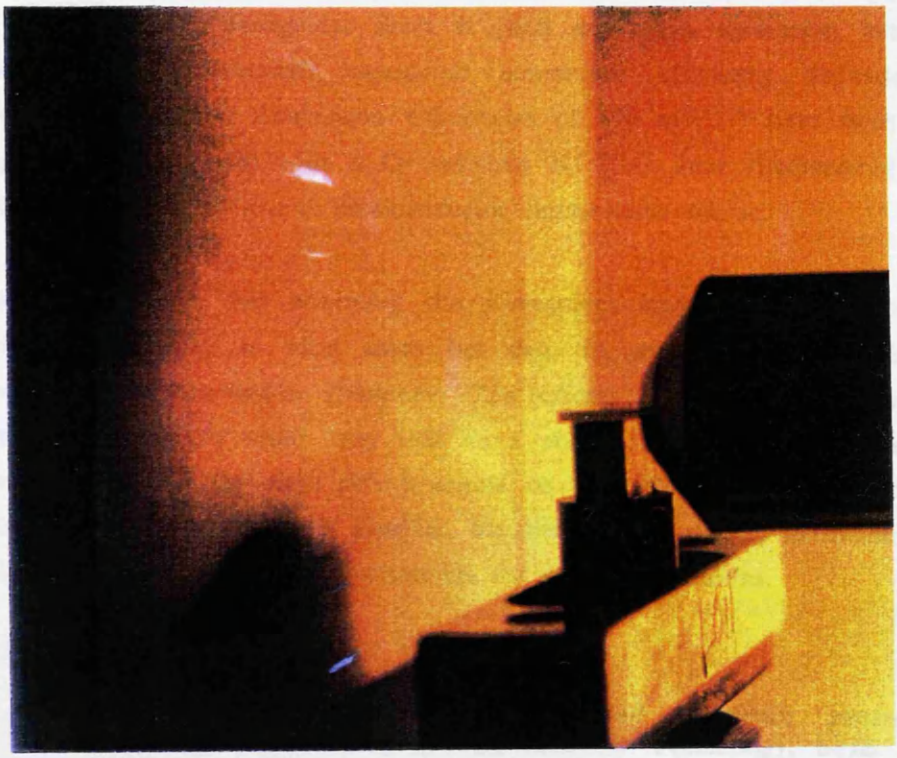

figure 3.12

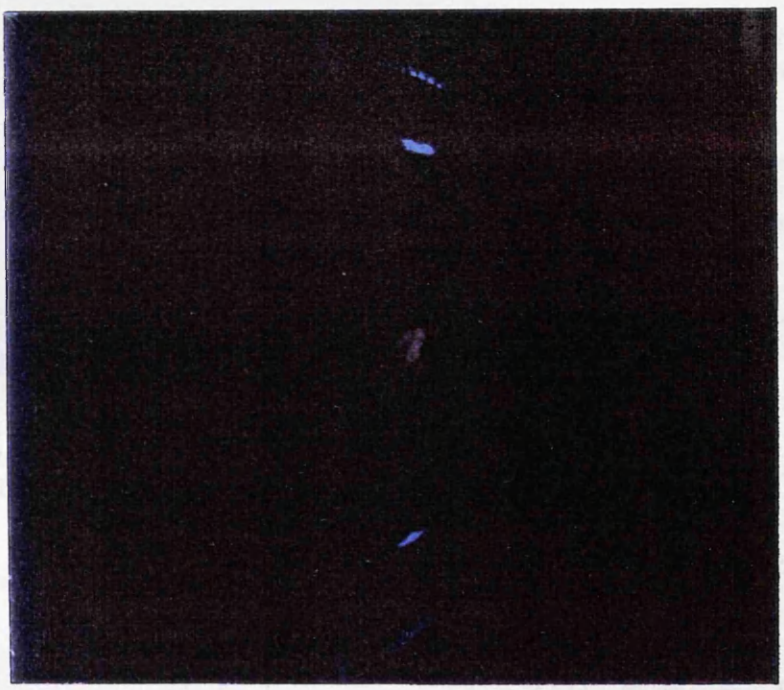

figure 3.13

3.4 Conclusions

Proton–exchanged waveguides have been used to produce efficiently frequency–doubled radiation from a Nd:YAG laser and a semiconductor laser. For the case of planar waveguides there is good qualitative agreement between the measured and theoretically calculated conversion efficiency dependences on waveguide parameters. Conversion efficiencies of 1% mW^{-1} have been obtained using planar waveguides with a Q–switched Nd:YAG laser fundamental, and up to 2.8% mW^{-1} with a c.w. semiconductor fundamental source.

It has been found that annealing the waveguides leads to a reduction in the conversion efficiency in most cases but can, in some cases, give rise to an increase in the conversion efficiency. The effects of annealing on the various waveguide parameters which may lead to a change in conversion efficiency have been discussed. On the debit side it should be pointed out that, although efficient second harmonic generation is possible, the beam shape of the harmonic radiation at the output was found to be unsuitable for many applications.

3.5 References

[1]. T. Taniuchi and K. Yamamoto, *"Second harmonic generation in proton–exchanged guides"*, Advanced Optoelectronic Technology, SPIE vol. 864, pp.36–41, 1987.

[2]. T. Taniuchi and K. Yamamoto, *"Second harmonic generation usind proton–exchanged $LiNbO_3$ waveguide"*, Optoelectronics– Devices and Technologies, 2, pp.53–58, 1987.

[3]. G. Tohmon, J. Ohya, K. Yamamoto and T. Taniuchi, *"Generation of ultra–violet picosecond pulses by fequency–doubling of laser diode in proton–exchanged $MgO–LiNbO_3$ waveguide"*, IEEE Photonics Tech. Letts., 2, pp.629–631, 1990.

[4]. N.A. Sanford and J.M. Connors, *"Optimization of the Cerenkov sum–frequency generation in proton–exchanged $Mg:LiNbO_3$ channel waveguides"*, J. Appl. Phys., 65, pp.1429–1437, 1989.

[5]. M.J. Li, M. De Micheli, Q. He and D.B. Ostrowsky, *"Cerenkov configuration second harmonic generation in proton–exchanged lithium niobate guides"*, IEEE J. Quat. Elecs., 26, pp.1384–1393, 1990.

[6]. J.J. Jackel, A.M. Glass, C.E. Rice and D. Holman, *"Damage resistant $LiNbO_3$ waveguides"*, J. Appl. Phys., 55, pp.269–272, 1983.

[7]. M.V. Hobden and J. Warner, *"The temperature dependence of of the refractive indices of of pure lithium niobate"*, Phys. Letts., 22, pp.243–245, 1966.

[8]. J. Finak, H. Jerominek, Z. Opilski and K. Wotjala, *"Planar diffusion glass*

waveguides obtained by immersion in molten planar KNO_3", Optica Acta XII, pp.11–17, 1982.

[9]. J. Crank, *"The Mathematics of Diffusion"*, Clarendon Press, Oxford, 1975.

[10]. T. Suhara, H. Tazaki and H. Nishihara, *"Measurement of the reduction in SHG coefficient of $LiNbO_3$ by proton–exchanging"*, Elec. Letts., 25, pp.1326–1328, 1989.

[11]. R.W. Keys, A. Loni and R.M. De La Rue, *"Measurement of the increase in the SHG coefficient of proton–exchanged $LiNbO_3$ after annealing using a grating diffraction technique"*, ibid., 26, pp.624–626, 1990.

[12]. M. Minikata, K. Kumagai and S. Kawakami, *"Lattice constant changes and electro–optic effects in proton–exchanged $LiNbO_3$ optical waveguides"*, Appl. Phys. Letts., 49, pp.992–994,1986.

[1]. A. Loni, R.M. De La Rue and J.M. Winfield, *"very low loss proton–exchanged $LiNbO_3$ waveguides with a substantially restored electro–optic effect"*, Technical Digest: Topical Meeting on Integrated and Guided Wave Optics, Santa Fe, New Mexico, OSA, 1988.

[14]. S. McMeekin and R.M. De La Rue, *"Novel transverse electro–optic waveguide phase modulator realised in titanium–indiffused and proton–exchanged $LiNbO_3$"*, Elec. Letts., 25, pp.853–854, 1989.

[15]. R. Regener and W. Sohler, *"Efficient second harmonic generation in $Ti:LiNbO_3$ channel waveguide resonators"*, J. Opt. Soc. Am. (B)., 5, pp.267–277, 1988.

[16]. F. Laurell, Ph. D. thesis, Royal Instsitute of Technology, Sweden, 1990.

CHAPTER 4

SHG IN PROTON-EXCHANGED WAVEGUIDES FABRICATED USING BENZOIC AND PYROPHOSPHORIC ACIDS: A COMPARISON.

4.1 Introduction

The aim of the work presented in this chapter was to compare the conversion efficiencies for second harmonic generation in proton-exchanged waveguides fabricated using both benzoic acid and pyrophosphoric acid. It has been reported [1] that proton-exchanged waveguides fabricated with "phosphoric" acid exhibit a higher refractive index ($\Delta n \simeq 0.145$ @ 0.6328 μm) than those fabricated with benzoic acid ($\Delta n \simeq 0.126$ @ 0.6328 μm). If this is the case then a higher conversion efficiency for harmonic generation might be expected because of the tighter mode confinement and, therefore, increased power density within the waveguide. The results presented in this chapter show, that, whilst the refractive index increase is slightly larger for phosphoric acid waveguides, the difference found by the author is not as large at that claimed in [1] and that the efficiency of second harmonic generation in phosphoric acid waveguides is only slightly larger.

Also reported is a comparison between second harmonic generation in MgO-doped lithium niobate, in which the photorefractive sensitivity can be up to one hundred times less than undoped lithium niobate [2]. Although optical damage effects are also reduced by using proton-exchanged waveguides, optical damage may become an important consideration if the conversion efficiencies are increased by alternative phase-matching techniques (such as quasi-phasematching) which lead to high power harmonic generation. The results of a study into second harmonic generation using proton-exchanged MgO-lithium niobate waveguides are presented. Both benzoic and pyrophosphoric acids were used to fabricate the waveguides.

4.2.1 Proton-exchange using Pyrophosphoric acid

Although benzoic acid is now routinely used as the protonic source for waveguide fabrication, other acids such as oleic acid [3] and sulphuric acid [4,5] have been used. In all cases, the resulting waveguide properties are reported to be similar to those of benzoic acid waveguides. However, as mentioned above, it has been reported [1, 6-8] that waveguides fabricated using phosphoric acids exhibit a

larger refractive index increase and much lower propagation losses than waveguides fabricated using benzoic acid. Before making a brief review of the published work on phosphoric acid waveguides some background on the chemistry of phosphoric acids is presented.

4.2.2 Chemistry of Phosphoric acids

It is well known that there are a number of forms of phosphoric acid, the most common of which are orthophosphoric acid, H_3PO_4, and pyrophosphoric acid, $H_4P_2O_7$. Both of these acids have been used to fabricate optical waveguides. Orthophosphoric acid can be prepared by reacting pyrophosphoric acid with water according to the reaction:–

$$H_4P_2O_7 + H_2O \text{ ---> } 2H_3PO_4$$

Pyrophosphoric acid (as used in this work) is a colourless crystalline solid at room temperature which melts at 54.3 °C. In this work only pyrophosphoric acid was used as the protonic source. As pyrophosphoric acid is a solid at room temperature, it was first necessary to liquefy it. This was easily achieved by gently heating an appropriate amount of solid above 55 °C and allowing it to cool down. As it cools it remains a clear, highly viscous liquid. Because the acid is deliquescent, the acid used for proton–exchange is almost certainly a mixture of phosphoric acid species, the major constituent possibly being pyrophosphoric acid. From a practical device point of view what is of crucial importance is that fabrication of the waveguides is reproducible. That is, if one starts with nominally pyrophosphoric acid to fabricate waveguides and is given certain conditions, other waveguides fabricated under the same conditions using (nominally) the same acid material should have the same properties.

4.2.3 Review of published work

As stated in the introduction, Yamamoto and Taniuchi [1] were the first to report the fabrication of proton–exchanged waveguides using phosphoric acids. Using orthophosphoric acid at temperatures between 150 °C and 280 °C and for diffusion times between 5 min. and 6 hours, waveguides were fabricated on z–cut substrates, but not on x– or y–cut substrates. Using prism coupling, they estimated that the effective diffusion coefficient was 0.33 $\mu m^2/hr$, and therefore similar to that of benzoic acid. However, the temperature at which this value is measured was not given. As stated previously, the measured refractive index step

was quoted as 0.145 @ 0.6328 μm. Using stripe waveguides and a cut–back technique, they measured the propagation loss to be as low as 0.9 dB/cm.

A second technique pioneered by Yamamoto and Taniuchi was that of spin–coating [6]. In this process the pyrophosphoric acid is first melted and a small amount coated onto the surface of the substrate using a spinner. No further details of the coating process are given. The substrates were then heated in an oven at 230 °C. The resulting waveguides exhibited properties very similar to those fabricated by immersion in orthophosphoric acid.

The surface–coating technique was also used by Goto and Yip [7]. Waveguides were fabricated in a vertical furnace at a temperature of 200 °C and had a refractive index increase of 0.131 @ 0.6328 μm and an estimated propagation loss of 0.25 dB/cm. The diffusion coefficient was estimated to be 0.113 μm^2/hr, which is greater than their measured value for benzoic acid (0.081 μm^2/hr).

In another study, Pun et al [8] fabricated waveguides by immersion in pyrophosphoric acid. They used acid temperatures between 190 °C and 250 °C and exchange times between 15 min and 22.5 hrs. The refractive index step was found to be 0.145 and the waveguide losses were said to be less than 1 dB/cm. Although they quote no figures, they claim that the diffusion coefficient is greater than that for benzoic acid. This conclusion presumably holds for each temperature at which the waveguide fabriaction was carried out. It was also stated that waveguides could not be fabricated on either x– or y–cut substrates, in agreement with Yamamoto [1].

In a paper primarily dealing with second harmonic generation in proton–exchanged waveguides, Sanford and Connors [9] have measured the refractive index difference of pyrophosphoric acid waveguides as being 0.132. The *stripe* waveguides of this work were fabricated in z–cut MgO doped lithium niobate. The diffusion coefficient was measured as 0.19 μm^2/hr. However, when planar waveguides were fabricated, the diffusion coefficient was measured as 0.33 μm^2/hr, in agreement with [1]. The discrepancy in these two values is attributed to over–etching of the tantalum mask somehow having an effect on the lithium niobate surface. The agreement of the diffusion coefficients measured by Yamamoto et al and Sanford et al is confusing. Yamamoto and Taniuchi [1] quote their results for proton–exchange in congruent lithium niobate, whereas the work of Sanford and Connors used MgO–doped lithium niobate. The fact that Sanford and Connors measure the same diffusion coefficient is strange because it

is well known that the diffusion constant for proton–exchange into MgO–doped substrates is much less than that for proton–exchange into congruent lithium niobate [10,11] (see fig. 4.2).

In a comprehensive study involving optical characterisation, infra–red and atomic absorbtion spectroscopy, Foad et al [12] could observe no significant differences in the properties of waveguides fabricated using either ortho– or pyrophosphoric acids. Two sets (of seven samples) of waveguides were fabricated at 210 °C using othophosphoric acid and pyrophosphoric acid. Waveguides fabricated with orthophosphoric acid showed a maximum refractive index change of 0.132 whilst waveguides fabricated using pyrophosphoric acid showed a 0.134 index step. The diffusion coefficients were the same for both acids (0.23 μm^2/hr), and were almost equivalent to the diffusion coefficient of benzoic acid at the same temperature (0.25 μm^2/hr). Based on the results of this work the authors postulated that, for proton–exchange, it is the temperature and the exchange time of the reaction which are the parameters of prime importance, not the acidity of the medium. Confirming this, the work also reported the fabrication of waveguides on x–cut substrates for short exchange times (up to 1.5 hr).

Loni et al [13] have carried out a comparative study of waveguides fabricated by surface coating and immersion. The surface coating was carried out by two methods. In the first, approximately 0.1 ml of pyrophosphoric acid was coated onto the surface using a syringe whilst in the second, the pyrophosphoric acid was deposited onto the substrate and then spun at 460 rpm for 40 s to leave a thin coating of acid on the surface. After *spin* coating, the surface coatings were visibly non–uniform, an effect attributed to surface tension. Waveguides were also formed by immersion used orthophosphoric acid at a temperature of 210 °C as the protonic source. In all three cases the resulting waveguides had step index profiles with an index increase of around 0.134. After fabrication some of the waveguides supported only 3 or 4 modes. A step–index fit to the data calculated a refractive index differences of 0.134 whilst an inverse WKB fit could give a calculated maximum refractive index difference of up to 0.165. It is possible that the high refractive index difference found by some researchers is an artefact of the curve fitting routine to the measured effective indices if too few modes are involved.

The estimated diffusion coefficients for the surface coating techniques were lower than the diffusion coefficients when using benzoic acid immersion. However, the diffusion coefficients for immersion were practically the same for orthophosphoric and benzoic acids as expected. Table 4.1 lists all the measured diffusion

coefficients. The waveguide losses for phosphoric acid were estimated to be 2–3 dB/cm, i.e. similar to those found when using benzoic acid.

Table 4.1

Diffusion coefficients for various phosphoric acid proton–exchange processes

Fabrication technique	Acid temperature	Measured coefficient (μm^2/hr)	Benzoic acid coefficient (μm^2/hr) *
Surface coating	220 °C	0.22	0.39
Spin coating	235 °C	0.54	0.74
Immersion	210 °C	0.23	0.25

* By immersion in benzoic acid.

It is obvious that there is wide disagreement in the published data regarding proton–exchange using phosphoric acids. It does seem generally agreed that orthophosphoric and pyrophosphoric acids are essentially equivalent in terms of the properties of the resulting waveguides. It also seems agreed that, under the same experimental conditions for the immersion process, the diffusion coefficients of phosphoric and benzoic acids are essentially equal. What is not agreed on is the refractive index increase. For the purposes of the work reported in the rest of this chapter, it has been assumed that the refractive index step is 0.134, as measured by Foad et al [12] and Loni et al [13].

One comparison which has not been made is the possibility of fabricating proton–exchanged waveguides by spin– or surface–coating using benzoic acid. No experiments were carried out by the author to investigate the possibility of fabricating waveguides by such a technique, and, to the author's knowledge there have been no papers published to date describing such a process.

4.3.1 Magnesium Oxide doped lithium niobate

It was reported by Zhong et al [2] that lithium niobate doped with greater than 4.6% atomic weight of magnesium oxide added to the melt had the ability to withstand optical intensities of about 100 times as great as congruent lithium niobate, a figure which has subsequently been confirmed by other researchers [14]. Consequently, MgO–doped lithium niobate is now available commercially.

The material is made by adding a given amount of MgO to the melt during crystal growth. The resulting material has refractive indices which are different from congruent material, the indices being:–

$n_o = 2.2897$

$n_e = 2.1940$

c.f. for congruent lithium niobate

$n_o = 2.323$

$n_e = 2.234$

Proton–exchange using MgO–doped substrates has been reported by several authors. Both Jackel [10] and Digonnet et al [11] have independently characterized proton–exchanged waveguides in x– and y–cut lithium niobate doped with 5% MgO. Loni et al [15] have characterized z–cut lithium niobate doped with 4.5% MgO. The resulting waveguides have similar refractive index profiles and index increases to waveguides fabricated in undoped material. However, the diffusion coefficients, pre–exponential factors and activation energies are very different in the two cases. Waveguides fabricated in MgO–doped lithium niobate have a higher activation energy and consequently lower diffusion coefficients [15]. An infra–red absorption spectroscopy study [15] of proton–exchange in both MgO–doped and congruent lithium niobate has indicated that the OH environment in the two materials may be different. However, it appears that there is little difference (in terms of the refractive index profiles) between waveguides formed by proton–exchange in either MgO–doped or congruent lithium niobate.

The higher power handling capability of MgO–lithium niobate is interesting from a nonlinear optics viewpoint. It means that it may be possible to realise much higher efficiencies for second harmonic generation because the optical damage threshold has been increased. The differences in the refractive indices of the two substrates imply that the phasematching conditions will also be different. For conventional birefringence phasematching, the phasematching temperature is below 0°C [16]. For MgO–lithium niobate the phasematching temperature is much closer to room temperature [17]. For Cerenkov second harmonic generation the

differences in the refractive indices are not so significant. The main difference is a change in the Cerenkov angle and there is also a slight difference in the shape of the efficiency versus waveguide depth and in the position of the maximum conversion efficiency (see 4.4.1).

4.4.1 A comparison between pyrophosphoric and benzoic acid waveguides for second harmonic generation

In this section, experimental work to measure the second harmonic generation efficiency on planar proton–exchanged waveguides will be described. Four sets of waveguides were fabricated:–

(1) congruent lithium niobate, benzoic acid,

(2) congruent lithium niobate, pyrophosphoric acid,

(3) MgO–lithium niobate, benzoic acid,

(4) MgO–lithium niobate, pyrophosphoric acid.

The pyrophosphoric acid waveguides were fabricated by immersion. In all cases, as in the work of the previous chapter, the waveguides were fabricated at an acid temperature of 235 °C. Before any of the above waveguides were fabricated a check was made to see if the diffusion coefficients for benzoic and pyrophosphoric acids were indeed equal. Although the temperature of the acid for this work was 210 °C, it can be seen from Fig. 4.1 that the coefficients for the two acids are equal (to within the limits of experimental error). It can also be seen that the diffusion coefficient for proton–exchange into MgO–lithium niobate is less than that for congruent lithium niobate (Fig. 4.2).

Using the theory developed in chapter 2, the efficiency for second harmonic generation was calculated for each of the four cases. In general, the results were in agreement with chapter two and the following conclusions could be drawn:–

(1) Waveguides made in pyrophosphoric acid, with a slightly higher waveguide refractive index, give more efficient harmonic generation. From the model, at the optimum waveguide depth, a relative increase of around 18% over benzoic acid waveguides may be expected, see Fig. 4.3. The dependence of conversion efficiency on waveguide depth is generally the same as for benzoic acid

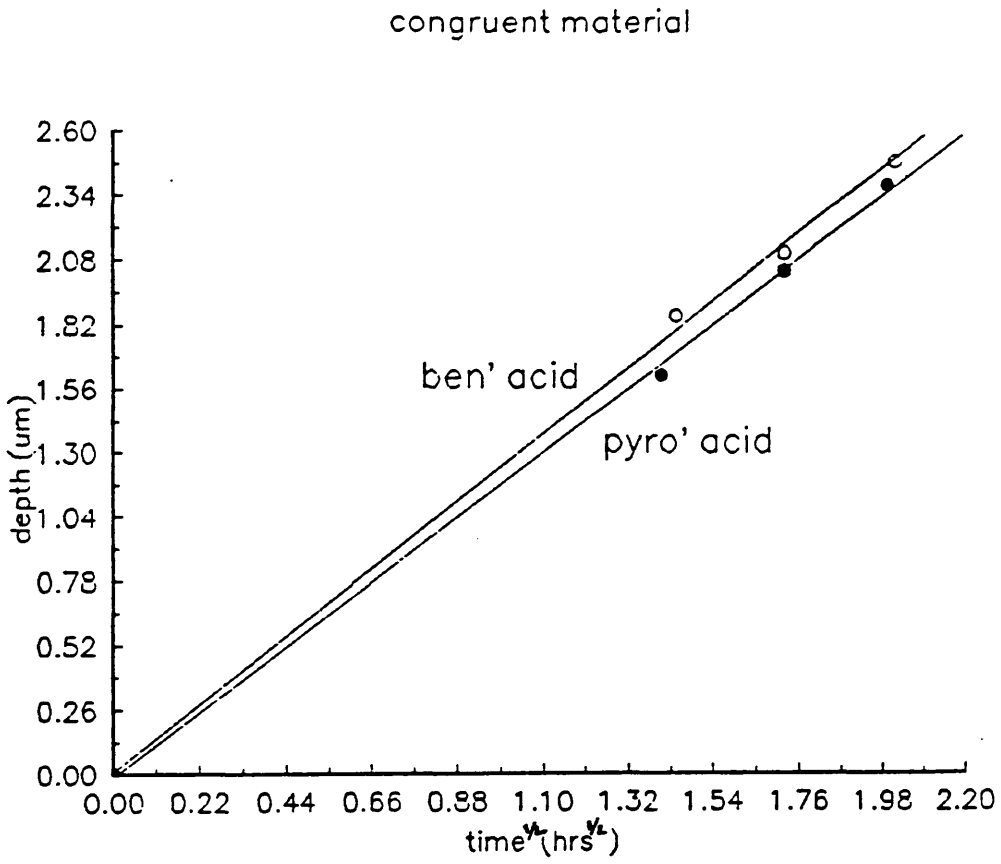

figure 4.1

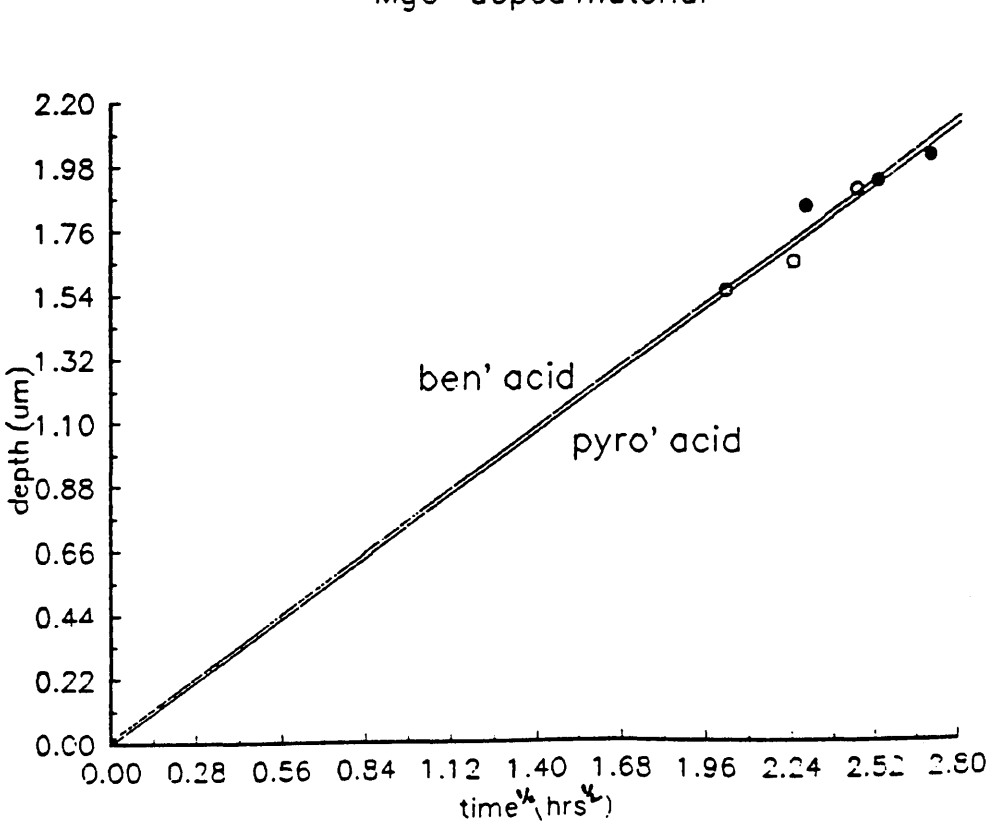

figure 4.2

waveguides, see Fig. 4.4.

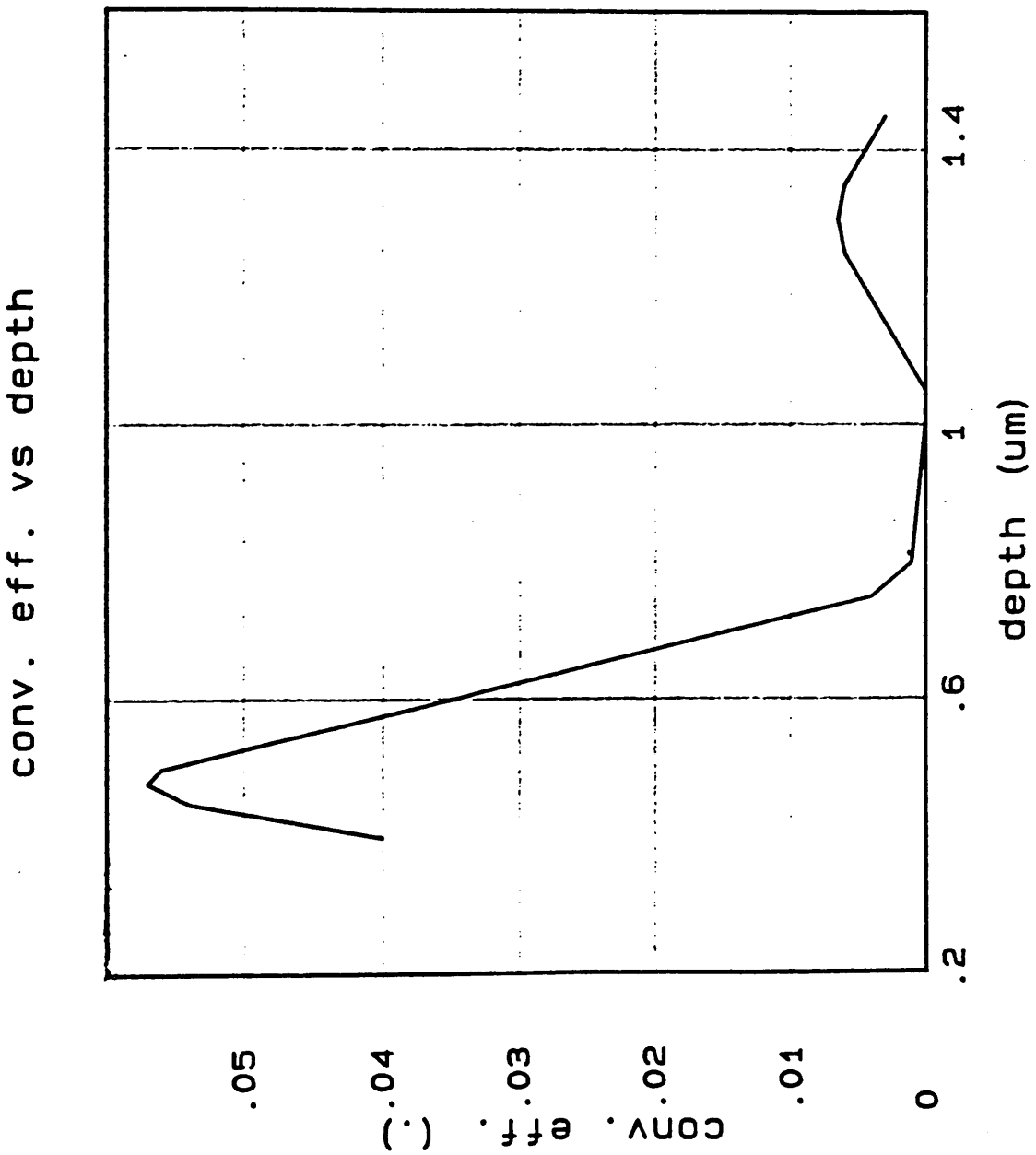

figure 4.3 theoretical plot of conversion efficiency in congruent material using pyrophosphoric acid

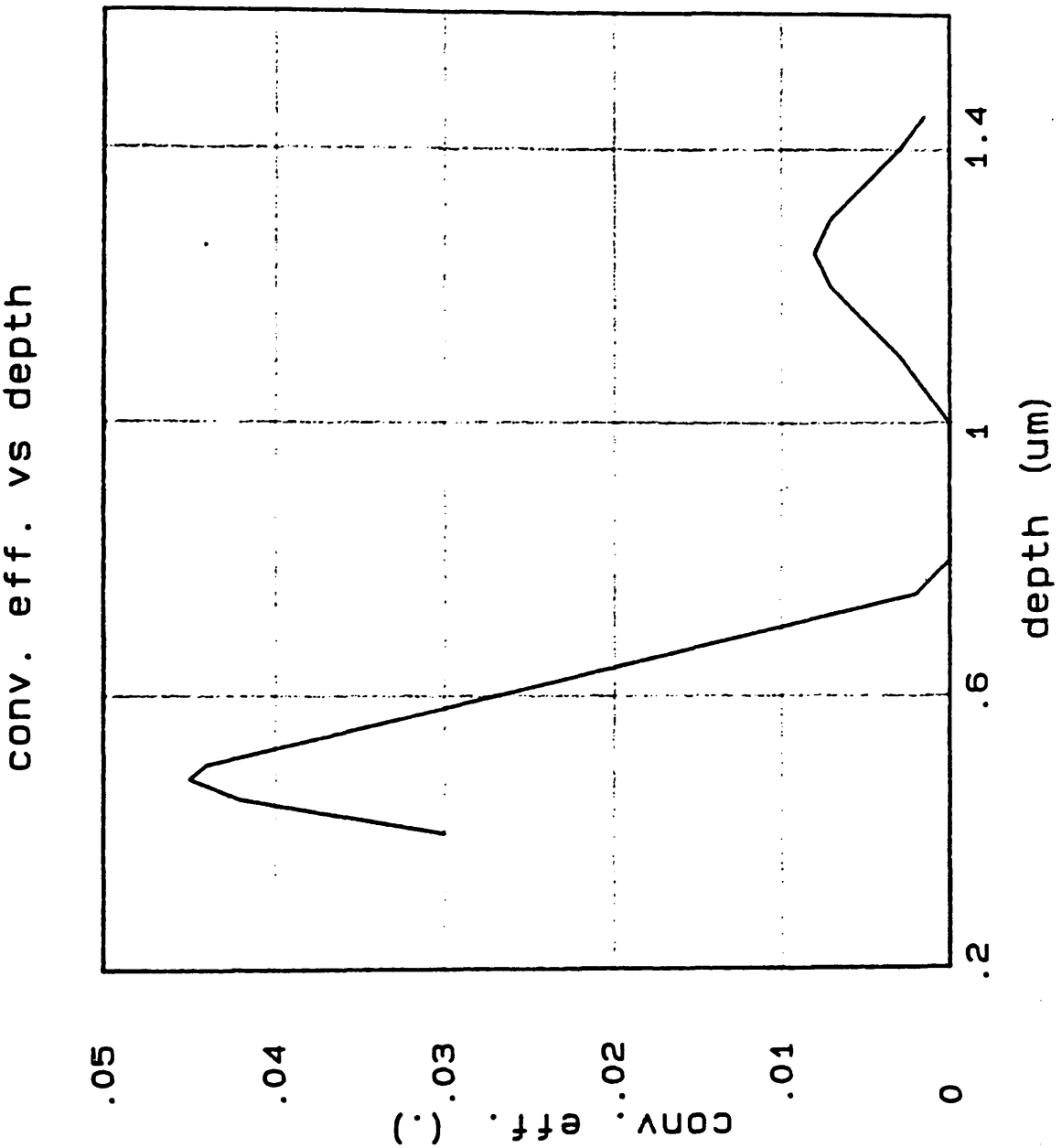

figure 4.4 theoretical plot of conversion efficiency in congruent material using benzoic acid

(2) Second harmonic generation in MgO– lithium niobate is no more efficient than in congruent material and, in some cases may be lower. This can be seen from Fig. 4.5 which is plotted for the case of a pyrophosphoric acid waveguide in MgO– lithium niobate. On inspection of Fig. 4.5 and comparing it with Fig. 4.3 it can be seen that the main peak is shifted slightly to smaller waveguide depths and that the peak conversion efficiency is only slightly higher for MgO– lithium niobate, but the differences are not likely to be significant in any practical device.

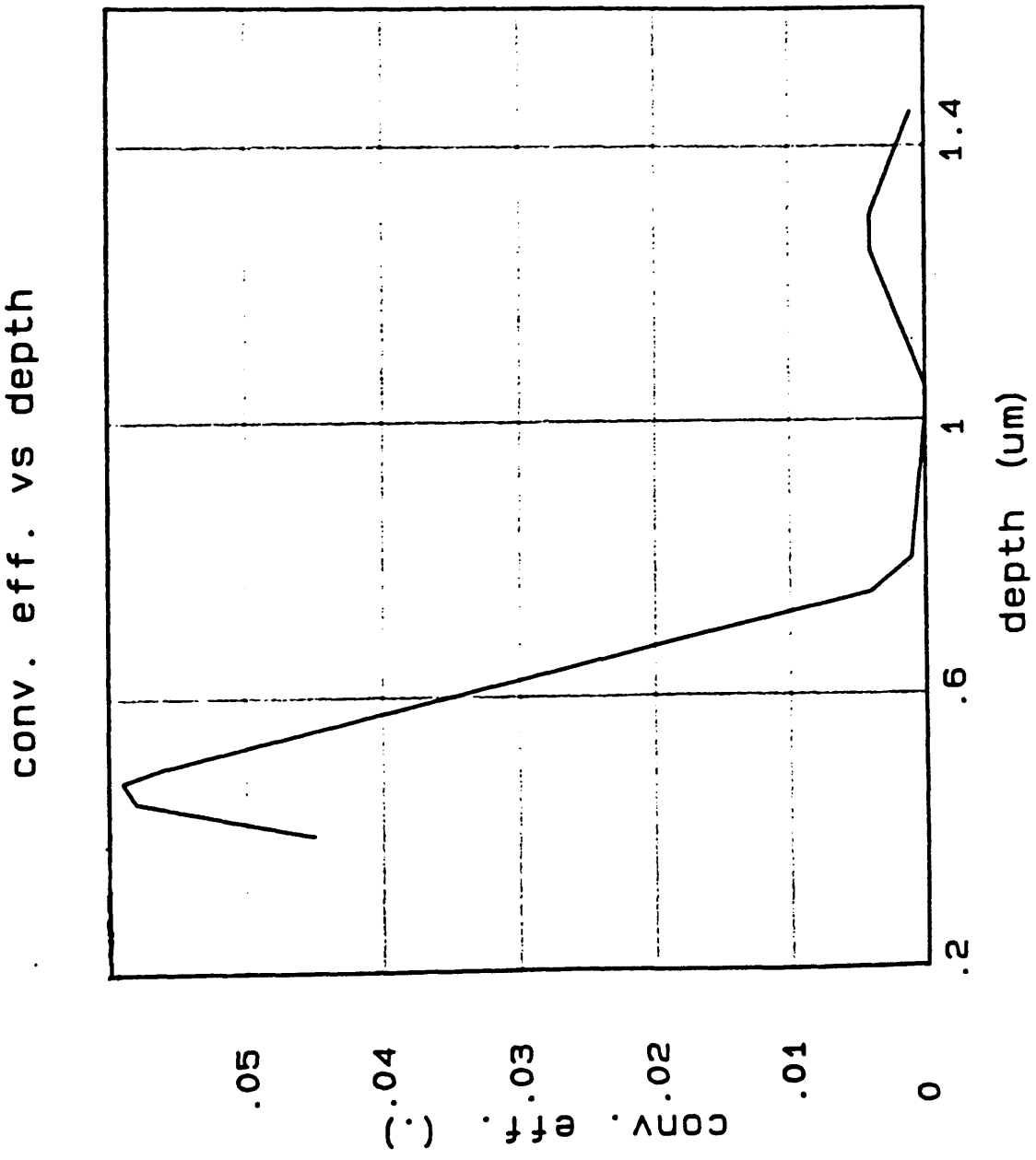

figure 4.5 theoretical plot of conversion efficiency in MgO-doped material using pyrophosphoric acid

For this calculation it was assumed that the nonlinear coefficients of MgO– lithium niobate are the same as those of congruent material and the refractive index difference is still the same. To the knowledge of the author, there have been no definitive measurements of the nonlinear d_{33} coefficient of MgO– lithium niobate, although there is some evidence to suggest that the nonlinear d_{31} coefficient may be lower than that of congruent lithium niobate [18]. However, this was based on a measurement of non–congruent MgO– lithium niobate.

4.4.2 Brief review of experimental method and normalization procedure

Before discussing the comparison of second harmonic generation in benzoic and phosphoric acid waveguides the experimental method will quickly be reviewed and details of the normalisation procedure re–iterated.

Second harmonic generation was carried out with a Q–switched Nd:YAG laser as the fundamental source. The wavelength was 1.064 μm and the Q–switched pulses were 200 ns long with a repetition rate of 1.25 kHz. The experimental arrangement is shown in Fig. 4.6.

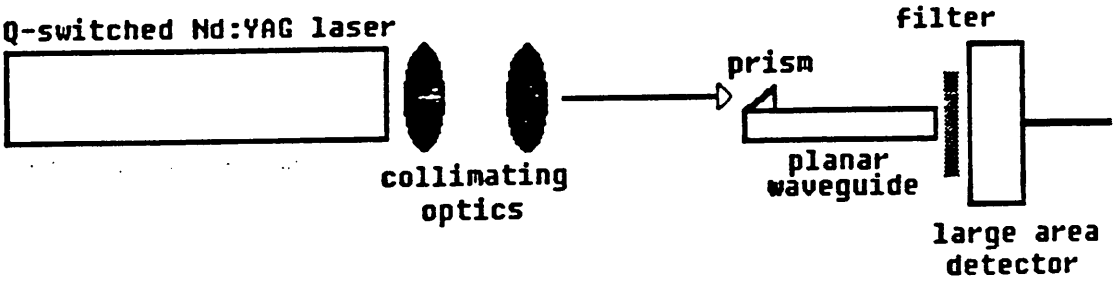

figure 4.6 experimental set up for measurement of the conversion efficiency

The normalised conversion efficiency was defined as the conversion efficiency which would be achieved with a fundamental power (in the waveguide) of 1 mW with a beam waist of 1 mm. That is, the measured fundamental powers are scaled to a level of 1 mW and the measured fundamental beam waists are scaled to a width of 1 mm.

4.4.3 Second harmonic generation in congruent material

Two sets of waveguides were fabricated for this experiment, one set for each of the two acids. The exchange times for the reaction were the same for each of the acids and, in both cases, the acid temperature used was 235 °C. Using the same experimental arrangement as described in the previous chapter (and re-iterated in 4.4.2), the conversion efficiency for harmonic generation was measured for each waveguide. Again, the beam waists were measured and the normalised conversion efficiencies calculated. Figs. 4.7 and 4.8 show the dependence of conversion efficiency with waveguide depth (plotted as the effective index of the guided fundamental mode) for the benzoic acid and pyrophosphoric acid waveguides respectively. It can be seen from these figures that the two curves are very similar (as expected from the theoretical curves). The maximum normalised conversion efficiencies for harmonic generation for both acids are listed in table 4.2. It can be seen that for the pyrophosphoric acid waveguide the normalised conversion efficiency is 16% greater than that of benzoic acid, which is remarkably close to the 18% predicted from the simple theory of chapter 2. The results are also in general agreement with those of the previous chapter.

Table 4.2

Acid used	substrate	conversion efficiency (normalised) (%/mW.mm)
Benzoic	congruent	4.3
Pyro'	congruent	5.1

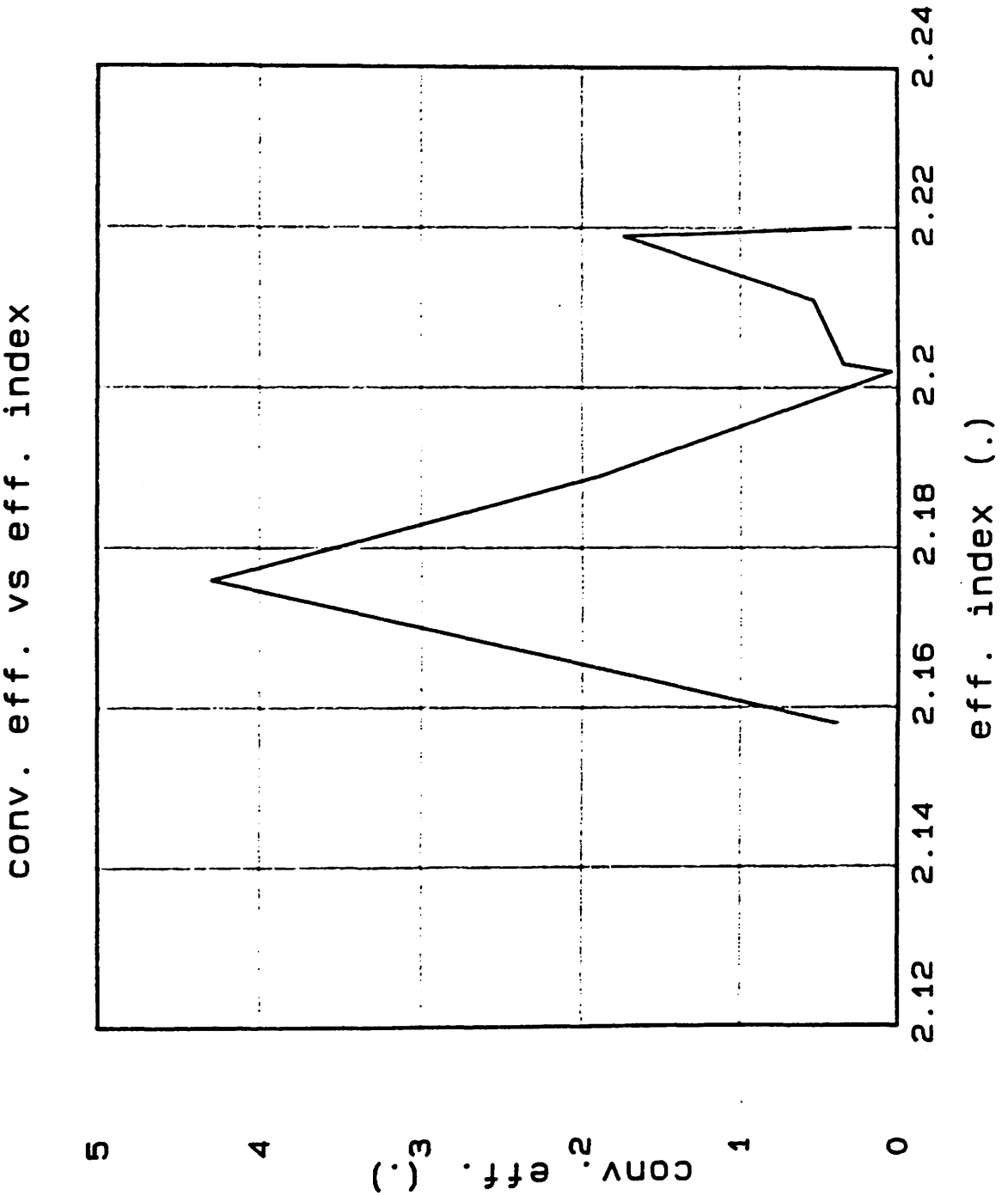

figure 4.7 experimental plot of conversion efficiency for waveguides fabricated using benzoic acid with a congruent substrate

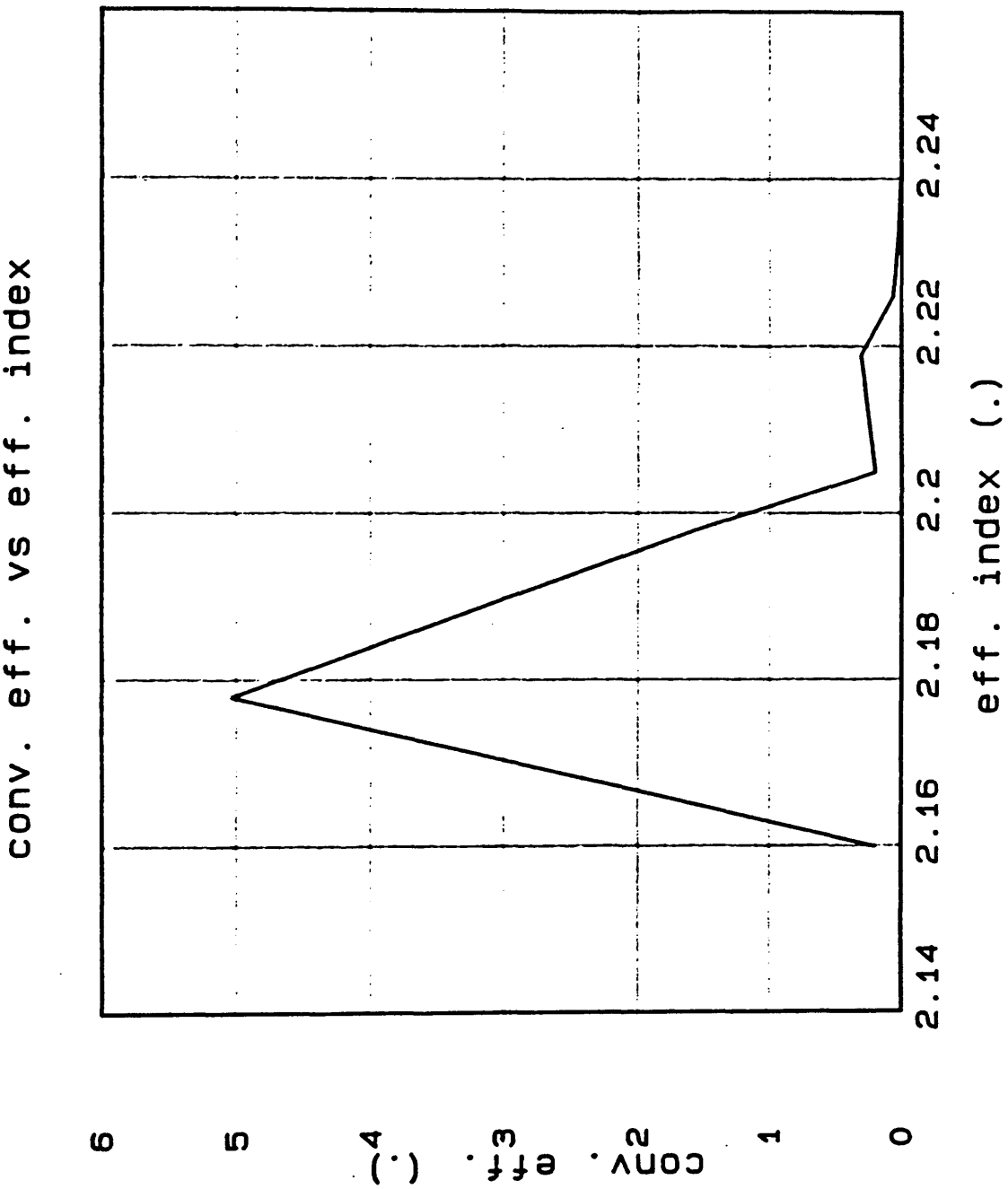

figure 4.8 experimental plot of conversion efficiency for waveguides fabricated using pyrophosphoric acid with a congruent substrate

4.4.4 Second harmonic generation in MgO– lithium niobate

As in the previous section, two sets of waveguides were fabricated in MgO– lithium niobate. The conversion efficiencies were measured and normalised and are plotted in Figs. 4.9 and 4.10. It can be seen that the curves are again very similar. The value of the maximum normalised conversion efficieny for the benzoic acid in this case was around 2.5 times that of the phosphoric acid waveguide. The reason for this is not clear, but may have been due to a systematic error when the measurements were taken on that particular series of waveguides. Inspection of the experimental results indicated that the measured fundamental powers were higher than those of the other sets of waveguides. This may indicate poor coupling into the waveguide due to contamination of the prism. The fundamental power levels were consistent for each waveguide in the set. For the benzoic acid waveguides the maximum normalised conversion efficiency was comparable to the value measured in 4.4.3 for the congruent material.

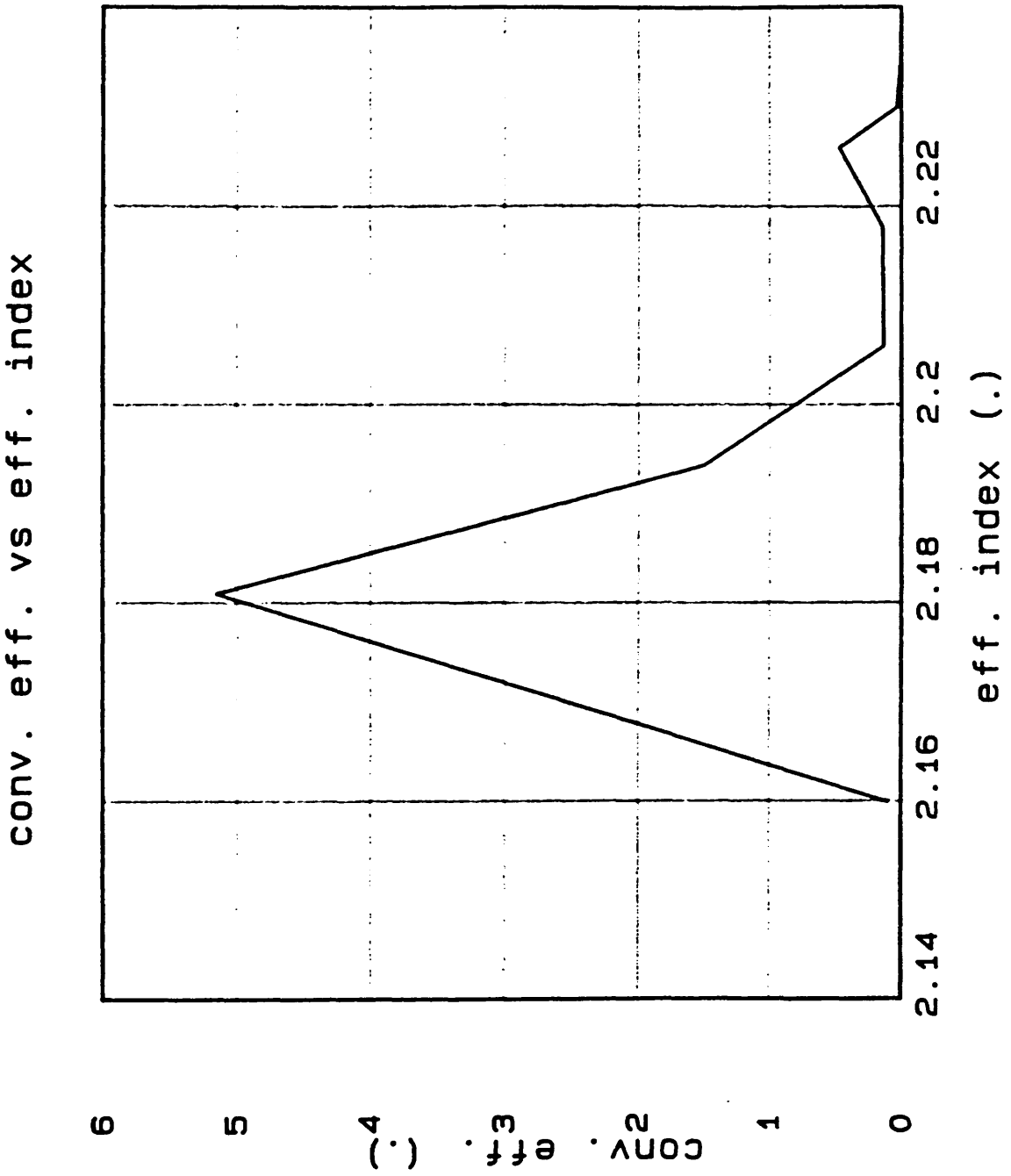

figure 4.9 experimental plot of conversion efficiency for waveguides fabricated using benzoic acid with a MgO-doped substrate

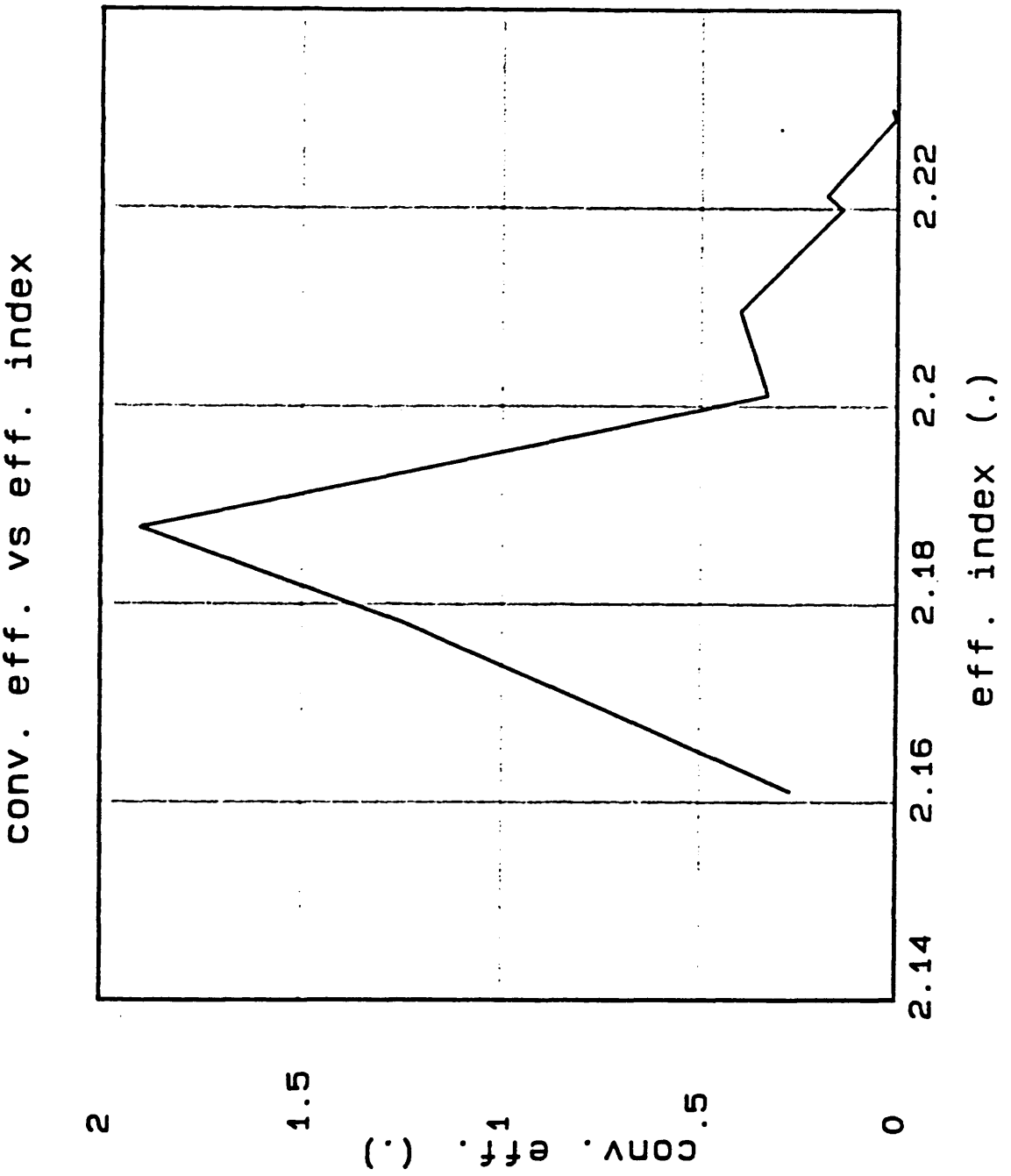

figure 4.10 experimental plot of conversion efficiency for waveguides fabricated using pyrophosphoric acid with a MgO-doped substrate

4.5 Conclusions

Second harmonic generation in waveguides fabricated using pyrophosphoric acid as the protonic source has been studied. In general, the conversion efficiency is slightly higher than that measured in waveguides fabricated using benzoic acid. The theory presented in chapter 2 predicted an increase of 18% (with respect to benzoic acid waveguides). Experimentally, an increase of 16% was measured. MgO– lithium niobate substrates have also been used. It was found that the conversion efficiencies were comparable to those obtained using congruent material as expected from the model. For all of the waveguides, the dependence of the conversion efficiency on waveguide depth was, at least qualitatively, in agreement with the predictions of the model.

The results of proton–exchange using pyrophosphoric acid indicate that the diffusion coefficients are very nearly equal to those of benzoic acid as expected. However, in disagreement with Yamamoto and Taniuchi and Pun et al, the increase in the refractive index was found to be 0.134 at $\lambda = 0.6328$ μm, and not 0.145 as quoted by these authors.

4.6 References

[1]. K. Yamamoto and T. Taniuchi, *"New proton–exchange technique for $LiNbO_3$ waveguide fabrication"*, Technical digest O.F.C. 1987, paper ThU2.

[2]. G. Zhong, J. Jian and Wu Zhong–Kang, 11th International Quantum Electronics Conference, IEEE Cat. No. CH 1561–0, p. 631, 1980.

[3]. T. Maciak, *"$LiNbO_3$ optical waveguides obtained by proton–exchange in oleic acid"*, Int. Jnl. Optoelectronics, 5(3), pp.227–234, 1990.

[4]. G. A. Bogert and D. T. Moser, *"Sulfuric acid proton–exchanged channel waveguides fabricated in $LiNbO_3$"*, IEEE Photonics Technology Letters, 2(9), pp.632–633, 1990.

[5]. J. T. Cargo, A.J. Filo, M.C. Hughes, V.C. Kannan, F.A. Stevie, J.A. Taylor and R.J. Holmes, *"Characterization of sulfuric acid proton–exchanged $LiNbO_3$"*, Jnl. Appl. Phys., 67(2), pp.627–633, 1990.

[6]. T. Taniuchi and K. Yamamoto, *"Second harmonic generation using proton–exchanged $LiNbO_3$ waveguide"*, Optoelectronics – Devices and Technologies, 2(1), pp.53–58, 1987.

[7]. N. Goto and G. L. Yip, *"Characterization of proton–exchange and annealed $LiNbO_3$ waveguides with pyrophosphoric acid"*, Applied Optics, 28(1), pp.60–65, 1989.

[8]. E.Y.B. Pun, T.C. Kong, P.S. Chung and H.P. Chan, *"Index increase of proton–exchanged waveguides in $LiNbO_3$ using pyrophosphoric acid"*, Electronics Letters, 26(2), pp.81–82, 1990.

[9]. N. A. Sanford and J. M. Connors, *"Optimisation of the Cerenkov second harmonic generation in proton–exchanged $MgO–LiNbO_3$"*, Jnl. Appl. Phys., 65(4), pp.1429–1437, 1989.

[10]. J. L. Jackel, *"Proton–exchange in MgO–doped $LiNbO_3$"*, IEE Electronics Letters, 21, pp.509–510, 1985.

[11]. M. Digonnet, M. Fejer and R.L. Byer, *"Characterization of proton–exchanged waveguides in $MgO:LiNbO_3$"*, Optics Letters, 10, pp.235–237, 1985.

[12]. M. A. Foad, *"Proton–exchanged $LiNbO_3$ optical waveguides made from phosphoric acids: detailed studies and comparisons with guides made with benzoic acid"*, Integrated Optics and Optoelectronics, SPIE Proceedings 1177, paper 05, 1989.

[13]. A. Loni, R.W. Keys, R.M. De La Rue, M.A. Foad and J.M. Winfield, *"Optical characterization of z–cut proton–exchanged $LiNbO_3$ waveguides fabricated using orthophosphoric and pyrophosphoric acid waveguides"*, IEE Proceedings 136, Part J, No. 6, pp.297–300, 1989.

[14]. D. A. Bryan, R.R. Rice, R. Gerson, H.E. Tomaschike, K.L. Sweeney and L.E. Halliburton, *"Magnesium–doped $LiNbO_3$ for higher optical power applications"*, Opt. Eng., 24(1), pp.138–143, 1985.

[15]. A. Loni, R.W. Keys and R.M. De La Rue, *"Characterisation of waveguides formed by proton–exchange in MgO–doped and Nd:MgO–doped $LiNbO_3$: A comparison with congruent material"*, Jnl. Applied Physics, 67(9), pp.3964–3967, 1990.

[16]. G. Arvidsson and F. Laurell, *"Nonlinear optical wavelength conversion in $Ti:LiNbO_3$ waveguides"*, Thin Solid Films, 136, pp.29–36, 1986.

[17]. F. Laurell and G. Arvidsson, *"Frequency doubling in $Ti:MgO:LiNbO_3$ channel waveguides"*, Jnl. Optical Society of America, 5(2), pp.292–299, 1988.

[18]. R.C. Sckardt, H. Masuda, Y.X. Fan and R.L. Byer, *"Absolute and relative nonlinear optical coefficients of KDP, KD*P, BaB_2O_4, LiO_3, $MgO:LiNbO_3$ and KTP measured by phasematched SHG"*, IEEE jnl. Quant. Elec., 26(5), pp.922–933, 1990.

CHAPTER 5

GRATING STRUCTURES AND THE d_{33} NONLINEAR COEFFICIENT.

5.1 Introduction.

This chapter describes the work which was carried out to investigate two of the properties of the nonlinear coefficient d_{33} and how these properties may be affected by device fabrication. Firstly, by a suitable technique, it has been found that the sign of the d_{33} coefficient can be reversed periodically, opening up the possibility of very efficient second harmonic generation. The experimental techniques for producing such periodic gratings, developed by the author in conjunction with co-workers at the University of Sussex, are discussed in some detail.

The waveguide fabrication technique used exclusively throughout this project was proton-exchange. It was known from earlier studies that the proton-exchange process leads to a reduction in the electro-optic coefficients, but that subsequent annealing of the waveguide could lead to a substantial or complete restoration of the effect [1,2]. As the electro-optic and nonlinear effects are related material parameters, it was apparent that proton-exchange might also reduce the intrinsic nonlinearity of the lithium niobate crystal. Using a grating diffraction technique, developed both theoretically and experimentally by Suhara et al [3], the magnitude of the nonlinear coefficient d_{33} has been measured. The effects of annealing on the magnitude of the nonlinearity have also been measured.

Both of these topics are discussed in this chapter. As the subjects can be treated separately, the chapter naturally splits into two sections. The first half of the chapter describes the fabrication and characterisation of the domain reversed gratings, whilst the second half of the chapter will discuss the measurement of the nonlinear coefficient of lithium niobate.

5.2.1 Grating structures for nonlinear optics.

The technique whereby phase-matching is achieved via a grating structure is called quasi phase-matching (QPM) [4]. There are at least two situations where grating structures are important for nonlinear optical applications;

(1) Some materials, for example II-VI and III-V compounds, possess large

second order nonlinearity but lack birefringence. This precludes the use of conventional phase–matching for second harmonic generation. Materials such as ZnS and ZnSe (II–VI) and GaAs (III–V) have second order coefficients comparable to those of lithium niobate but cannot be phase–matched conventionally.

(2) In many materials some of the nonlinear coefficients are not phase–matchable conventionally. For example, the largest nonlinear coefficient of lithium niobate, d_{33}, is not phase–matchable conventionally. This is because the d_{33} coefficient will only couple together a fundamental and a harmonic wave of similar polarisations. Since the phasematching condition requires that the refractive indices at the fundamental and harmonic wavelengths be equal, this requires that the dispersion of the material be zero. This is not the case for lithium niobate so that phasematching via d_{33} cannot be achieved (in the wavelength range of interest to the work of this thesis). For the lithium niobate system this is unfortunate because d_{33} is about 6 times larger than d_{31} and, therefore, the use of d_{33} would lead to a 36–fold increase in the conversion efficiency for second harmonic generation (everything else being equal).

5.2.2 Periodic structures for quasi phase–matched second harmonic generation.

The potential of periodic structures for quasi phase–matched second harmonic generation was probably first described by Bloembergen and Severs [4] in 1970. They proposed growing a periodic lattice of GaAs and GaP with a suitable choice of lattice parameters and predicted that nonlinear optical interactions, including second harmonic generation, could be phase–matched.

Periodic structures for nonlinear optical interaction in lithium niobate can be realised in two ways. The first, and most efficient, way is to modulate the nonlinear coefficient periodically [5]. The second is to modulate the linear refractive index profile periodically [5]. The conversion efficiency which can be achieved via a periodic modulation of the linear refractive index profile is lower than that which can be achieved via a modulation of the nonlinear coefficient. A modulation of the refractive index profile also creates a grating coupler effect in the waveguide region and therefore potentially increases the optical propagation losses. For these two reasons most of the work on periodic structures has concentrated on a modulation of the nonlinear effect and the work of this thesis was concerned with developing a technique for this purpose, so no further mention will be made of the refractive index modulation approach.

All things being equal (overlap integral etc.), phase–matching by modulation of the nonlinear coefficient is not as efficient for second harmonic generation as conventional phase–matching. This can be shown as follows. Let us assume that second harmonic generation at a fundamental wavelength λ is achieved by periodic modulation of the nonlinear coefficient and not by conventional phase–matching (i.e. temperature tuning of the birefringence). In this case the nonlinear coefficient must be considered as some periodic function of z, where z is the propagation direction, Fig. 5.1.

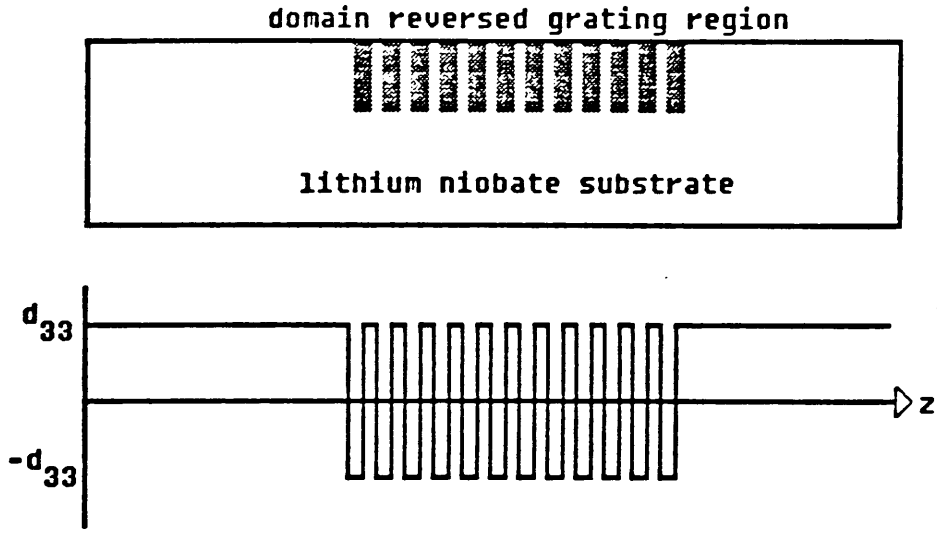

figure 5.1 modulation of the nonlinear coefficient caused by periodic domain reversal

In the ideal case, the periodic function would be a sine wave where there would be no reduction in the nonlinear coefficient; however in practice it is more realistic to produce a square wave modulation i.e.:–

$$d(z) = d \qquad \text{for } 0 < d < \Lambda / 2 \text{ and}$$
$$d(z) = -d \qquad \text{for } \Lambda / 2 < d < \Lambda \qquad (5.1)$$

where Λ is "wavelength" of the grating structure. A square wave modulation of the nonlinear coefficient can be expressed in terms of a Fourier series as:–

$$d(x,y,z) = \sum_q d_q(x,y).\exp(-jmKz) \qquad (5.2)$$

where $K = 2\pi/\Lambda$ is the spatial frequency of the grating and m is known as the grating order, m = 0,1,2,... etc. The Fourier series expansion implies that the

nonlinear coefficient can be regarded as a summation over an infinite number of spatial harmonics of the "nonlinear coefficient", each with a spatial frequency mK

For a phase–mismatch of Δk, only the Fourier component of the grating modulation with spatial frequency $m.K = \Delta k$ will be phasematched for second harmonic generation. Since only one Fourier component is involved in the interaction, the nonlinear coefficient is effectively reduced (relative to the bulk nonlinear coefficient) by a factor which depends on which order of the Fourier component is phasematched. For the square wave modulation described above the bulk nonlinear coefficient d is reduced by the factor $2/(m\pi)$ [6], i.e. the effective nonlinear coefficient is:–

$$d_{eff} = 2.d/(m\pi) \qquad (5.3)$$

Since only one spatial component of the nonlinear coefficient is phasematched, the conversion efficiency for second harmonic generation will be reduced. This can be shown as follows. Let the conversion efficiency for conventionally phasematched second harmonic generation be given by:–

$$\eta = C.d^2 \qquad (5.4)$$

where C contains all other parameters such as overlap integral, refractive indices etc. (see chapter 2). For the case of quasi phase–matching the conversion efficiency is given by:–

$$\eta = C.4.d^2/(m.\pi)^2 \qquad (5.5)$$

The best possible case is realised by using a first order grating (m = 1) and Eq. 3 becomes:–

$$\eta = C.4.d^2/\pi^2 \qquad (5.6)$$

Comparing Eqs. 4 and 6 it can be seen that the conversion efficiency is reduced by a factor of $4/\pi^2$ for quasi phase–matching.

It has been shown that conventional phase–matching is more efficient than quasi phase–matching. So why is quasi– phase–matching important? As was stated in the introduction, the importance of the quasi phase–matching technique is that it makes possible the use of nonlinear coefficients which are not conventionally

phase–matchable. For lithium niobate, the d_{33} coefficient is larger than the conventionally used d_{31} coefficient but is not phase–matchable. The relative magnitude of d_{33} to d_{31} is:–

$$d_{33} / d_{31} = 34 / 5.95 = 5.7 \qquad (5.7)$$

where the magnitude of the nonlinear coefficients is given in units of pm/V. The potential increase in the conversion efficiency which may be derived by exploiting the d_{33} coefficient is thus:–

$$(4/\pi^2)\cdot(d_{33} / d_{31})^2 = 13.7 \qquad (5.8)$$

The periodicity, Λ, of the grating required for phasematching can be found by defining a quantity known as the "coherence length" [5]. The coherence length, l_c, is defined as the propagation length over which the fundamental and harmonic waves become π radians out of phase. If the phase–mismatch, Δk, is defined by:–

$$\Delta k = k_{2\omega} - 2.k_{\omega} \qquad (5.9)$$

then the "coherence length", l_c, is given by:–

$$l_c = \pi / \Delta k \qquad (5.10)$$

Phasematching implies:–

$$m.K + \Delta k = 0 \qquad (5.11)$$

i.e., from Eqs. 10 and 11, we find:–

$$\Lambda = 2.m.l_c \qquad (5.12)$$

For bulk lithium niobate the coherence length is 6 μm for a fundamental wavelength of 1.06 μm.

5.2.3. Methods for producing a modulation of the nonlinear coefficients

Quasi phase–matched second harmonic generation via a periodic modulation of the d_{33} coefficient of lithium niobate has been reported by several research

groups [7–13]. In a later section of this chapter the origin of the intrinsic nonlinearity of the lithium niobate crystal will be discussed in some detail. It is well known that the nonlinearity is related to the spontaneous dielectric polarisation vector associated with the permanent electric dipole moment of the ferroelectric lithium niobate crystal. In order to achieve a reversal of the nonlinear effect it is necessary to reverse the direction of the spontaneous polarisation vector of the lithium niobate crystal. In chapter 1, it was stated that the spontaneous polarisation vector of the lithium niobate crystal is aligned either during or after the growth process. The crystal is then regarded as being *single domain*. If by some means the domain structure of the crystal could be reversed periodically, this would provide a suitable technique for the reversal of the nonlinearity. In terms of the crystal structure, domain reversal is equivalent to reversing the stacking order of the crystal sites. This reversal is illustrated in Fig. 5.2.

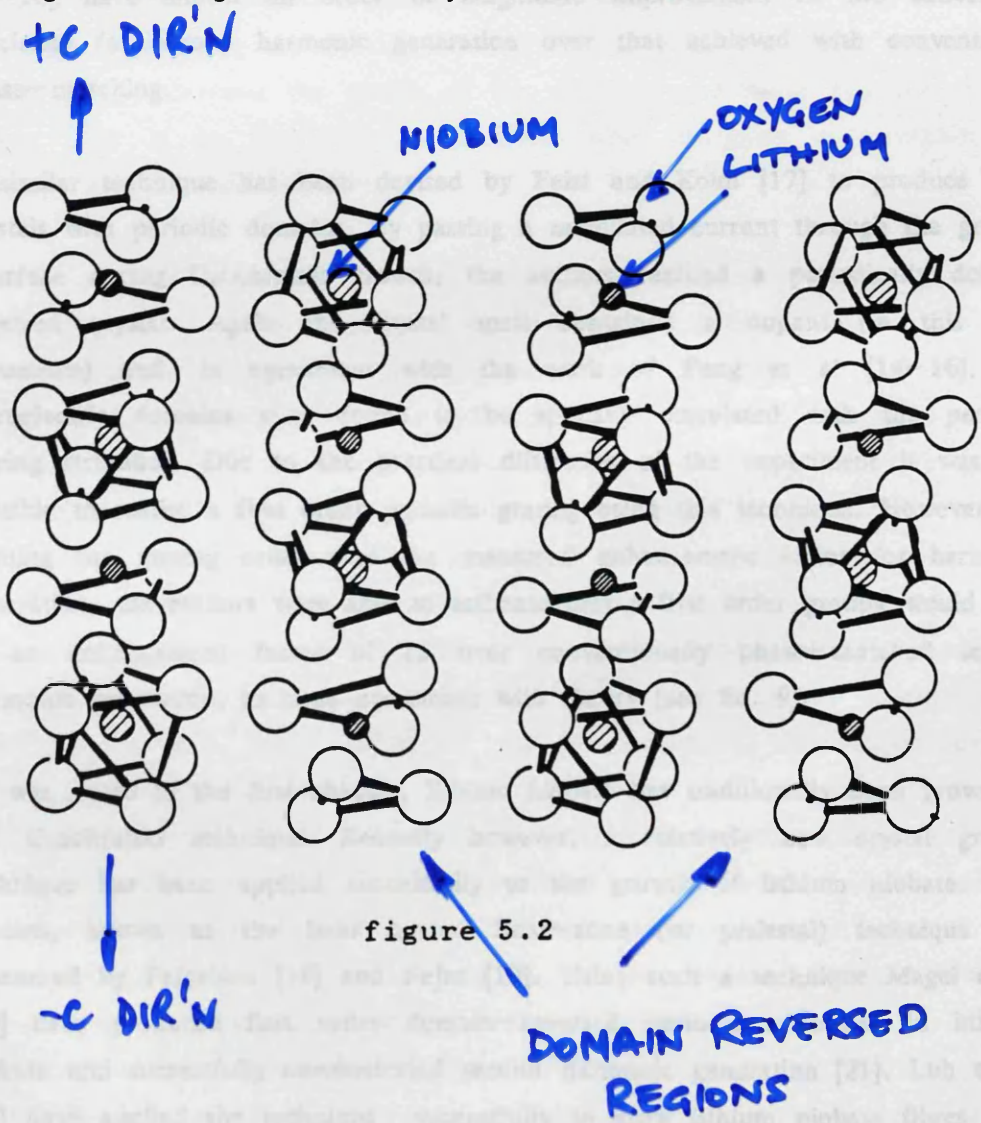

figure 5.2

groups [7–13]. In a later section of this chapter the origin of the intrinsic nonlinearity of the lithium niobate crystal will be discussed in some detail. It is well known that the nonlinearity is related to the spontaneous dielectric polarisation vector associated with the permanent electric dipole moment of the ferroelectric lithium niobate crystal. In order to achieve a reversal of the nonlinear effect it is necessary to reverse the direction of the spontaneous polarisation vector of the lithium niobate crystal. In chapter 1, it was stated that the spontaneous polarisation vector of the lithium niobate crystal is aligned either during or after the growth process. The crystal is then regarded as being *single domain*. If by some means the domain structure of the crystal could be reversed periodically, this would provide a suitable technique for the reversal of the nonlinearity. In terms of the crystal structure, domain reversal is equivalent to reversing the stacking order of the crystal sites. This reversal is illustrated in Fig. 5.2.

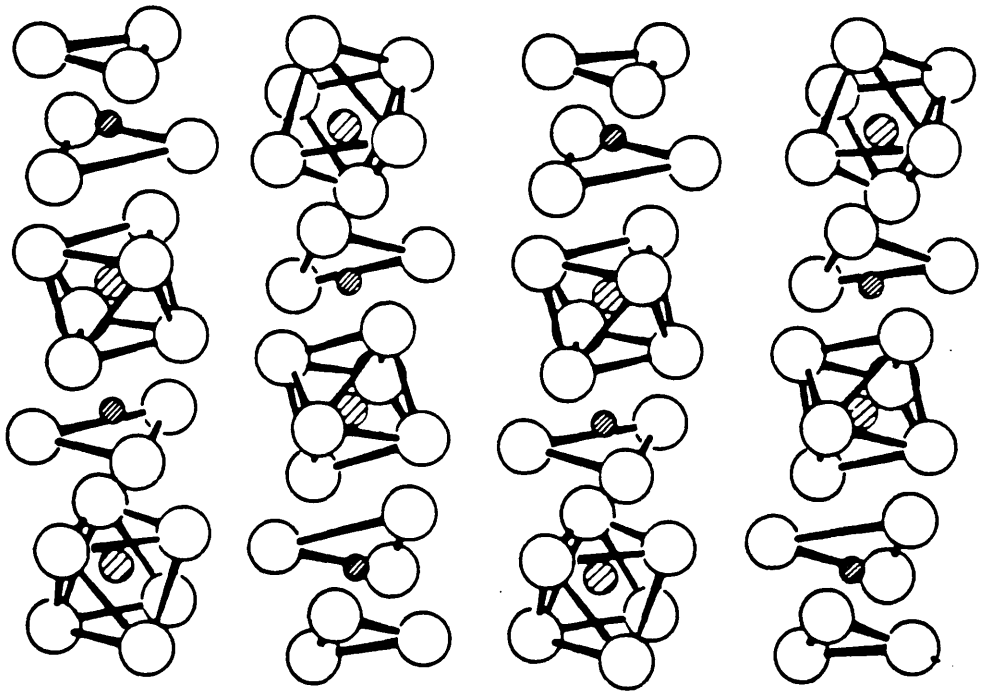

figure 5.2

In bulk crystals, periodically domain–reversed crystals have been grown by inducing periodic temperature fluctuations during Czochralski growth [14]. The periodic fluctuations were further enhanced by introducing 1% of yttrium into the melt during the growth process, with the result that the crystal had a dopant profile which varied sinusoidally along the growth axis. The periodic domain structure correlates with the periodic dopant profile. The mechanism for domain reversal would thus appear to be the periodic dopant concentration gradient. The concentration gradient sets up an electric field within the crystal (and consequently a polarisation field) which is (periodically) opposed to the direction of the spontaneous polarisation field of the crystal. In order to achieve a consistent domain structure throughout the crystal, very careful control of the rotation and pulling rates was necessary. Using crystals grown by this technique, Feng et al [14–16] have shown an order of magnitude improvement in the conversion efficiency for second harmonic generation over that achieved with conventional phase–matching.

A similar technique has been devised by Feist and Koidl [17] to produce bulk crystals with periodic domains. By passing a modulated current through the growth interface during Czochralski growth, the authors realised a periodically domain reversed crystal. Again the crystal melt contained a dopant (in this case chromium) and, in agreement with the work of Feng et al [14–16], the ferroelectric domains were found to be spatially correlated with the periodic doping striations. Due to the practical difficuties of the experiment it was not possible to realise a first order periodic grating using this technique. However, by plotting the grating order with the measured enhancement factor for harmonic generation, the authors were able to estimate that a first order grating would lead to an enhancement factor of 15 over conventionally phase–matched second harmonic generation, in close agreement with theory (see Eq. 9).

As was stated in the first chapter, lithium niobate has traditionally been grown by the Czochralski technique. Recently however, a relatively new crystal growth technique has been applied successfully to the growth of lithium niobate. This process, known as the laser heated float–zone (or pedestal) technique was pioneered by Feigelson [18] and Fejer [19]. Using such a technique Magel et al [20] have produced first order domain–reversed periodic structures in lithium niobate and successfully demonstrated second harmonic generation [21]. Luh et al [22] have applied the technique successfully to grow lithium niobate fibres with periodic domain structures. These fibres have also been used to produce second harmonic generation [23]. This technique for growing crystals is very controllable

and highly flexible and to date crystals have been grown with domain reversals every 1 μm. As well as the short domain periods which can be achieved, the domains are highly regular, which is essential for efficient harmonic generation.

The techniques described in the three preceding paragraphs allow the growth of bulk crystals with quasi phase-matching properties. For waveguide applications it would be ideal to produce periodic domain reversed crystal regions localised to the substrate surface. By localising the regions of domain reversal, it would become possible to realise integrated optic substrates which are capable of a number of different functions, one of which is second harmonic generation. A simple example of such a multi-function device would be a self-frequency doubled rare-earth doped lithium niobate laser incorporating electro-optic switching devices for control of the laser output (Q-switching etc) [24]. A second advantage of localising the domain reversed regions is that it allows optimisation of the overlap between the profile of the nonlinear coefficient and the optical modes. This is an important consideration when designing a waveguide to maximise the conversion efficiency.

In order to produce periodic domain reversed gratings in a waveguide geometry, two techniques have been used. It is well known that indiffusion of titanium into the +c-face of lithium niobate at temperatures near the Curie point of the bulk crystal can lead to domain inversion [25-26]. The actual mechanism which causes the domain reversal is not known but the most probable cause is, again, a dopant concentration gradient (in the case of titanium) [27-29]. Because of the dopant concentration gradient there exists a gradient of the Curie temperature and, hence, a gradient of the spontaneous polarisation vector. Assuming that the equivalent electric field is anti-parallel to the titanium concentration gradient it is then parallel to the spontaneous polarisation on the -c-face and antiparallel to it on the +c-face. This is consistent with the observation that domain reversal by titanium indiffusion has only been observed on the +c-face of lithium niobate [29]. During domain reversal, as the temperature of the crystal approaches the Curie point, the magnitude of the spontaneous polarisation field is reduced. At some temperature the field associated with the concentration gradient will exceed the spontaneous polarisation field and domain reversal will occur. On the -c-face the field associated with the concentration gradient is always in the same direction as the spontaneous polarisation field and so domain reversal cannot occur. As well as the concentration gradient, other effects may contribute to domain reversal. These effects are mainly related to the temperature at which the fabrication process takes place [30]. It has been shown [30] that out-diffusion of

lithium oxide (Li_2O) can lead to domain reversal.

Both of these techniques have recently been applied to produce periodic domain reversed grating structures for quasi phase-matching [7-13]. Lim et al have fabricated gratings by the indiffusion of a periodic titanium grating to produce a periodic modulation of the d_{33} coefficient on the +c-face of lithium niobate [7]. A planar waveguide was then fabricated by proton-exchange. With this stucture they achieved quasi phase-matched second harmonic generation of fundamental c.w. Nd:YAG laser radiation at $\lambda = 1.06\mu m$. The conversion efficiency realised using this structure was 5% /(W/cm^2). Since this first demonstration, improved design and fabrication techniques have allowed efficient quasi phase-matched second harmonic generation of blue radiation with a (normalised (by them) to a fundamental power of 1 W and a beam spot size of 1 cm^2) conversion efficiency of 37%/(W/cm^2) [7-10].

Webjorn et al [11-13] have developed a technique whereby they could control spatially the out-diffusion of lithium (for brevity, "lithium" refers to the Li_2O species). To do this, they deposit a layer of silicon dioxide on the +c-face of the crystal, and form a periodic mask in the silicon dioxide. The substrate is heated to 1100^{0}C in a furnace and then allowed to cool. Lithium out-diffusion is apparently suppressed under the silicon dioxide masked regions. The domains formed by this fabrication procedure have been shown to be triangular in shape [11]. Since the nonlinear coefficient has a triangular distribution function, it must now be included as a factor within the overlap integral calculations [13]. (Recall the case of the overlap integral calculations in chapter 2 where the nonlinear coefficient was regarded as constant along the propagation direction and could be taken outside the integration. For a square wave the nonlinear coefficient is still constant but is reversed in sign every coherence length). By suitable choice of fabrication parameters, the conversion efficiency for quasi phase-matched second harmonic generation can be optimised but is always reduced with respect to the square wave case [13]. Using a laser diode operating at a wavelength of 833nm as the fundamental, Laurell et al. have achieved conversion efficiencies of 0.4% /W/cm^2 with such structures.

There are several drawbacks to both of these techniques for producing periodic domain reversed gratings. These are:-

(1) The resulting domains may not be rectangular in shape, i.e. with a modulation function which can be represented as a "square" wave (see Fig. 5.1).

For the case of the lithium out−diffused case, it has already been stated that the domains are triangular in shape. The consequence of non−rectangular domains is a lower available conversion efficiency through a reduced ovelap between the nonlinear coefficient and the optical fields [13].

(2) Both the in−diffusion of titanium and the out−diffusion of lithium lead to a periodic modulation of the refractive index profile along the propagation direction. This modulation of the refractive index profile may increase the propagation losses due to modal mis−match, with a consequent reduction in the conversion efficiency (see chapter 2).

(3) It is well known that regions of titanium in−diffused lithium niobate are susceptible to optical damage [31]. This susceptibility to damage may place an upper limit on, essentially, the harmonic power which can be generated, thus limiting the conversion efficiency. The use of a proton−exchanged waveguide region will lower the susceptibility to optical damage. However, high conversion efficiencies for second harmonic generation have been demonstrated using this technique [7−10], with no signs of optical damage.

(4) Domain reversal can only be achieved on the +c−face of the lithium niobate, but for waveguide applications it is, traditionally, the −c−face which is the preferred crystal face [28]. If the domain reversal is due to the concentration gradient, the use of the −c−face is precluded.

(5) In−diffusion/out−diffusion processes necessarily take place at elevated temperatures close to the Curie temperature. At these temperatures there exists a danger of exceeding the local Curie point of the crystal in regions outside that where domain−reversal is to be produced intentionally, thus causing the crystal to become multi−domain.

The ideal domain reversed grating should have rectangular shaped domains with a uniform refractive index profile along the propagation direction. The fabrication process should also cause no increased susceptibility to optical damage, should produce domain reversal on the −c−face and should take place at low temperatures (c.f. Curie temperature).

5.2.4 Fabrication of periodic domains by electron beam bombardment of lithium niobate

An alternative technique for achieving domain reversal in bulk lithium niobate was demonstrated by Haycock and Townsend [32], for which they have offered the following explanation. The technique involves generating a temporary, or transient, vacancy in the oxygen triangle, thereby opening a pathway for lithium ion motion. If an electric field is then applied along the c− axis, as in conventional poling, the fixed site occupancy of the lithium ions with respect to the oxygen triangle will be removed and the lithium ions will move to form an unpoled intermediate state followed by an ordered, i.e. poled, structure in the opposite direction.

The key step in the process is to generate the transient vacancy in the oxygen plane. Figure 5.3 explains diagrammatically what is meant by the phrase "transient vacancy in the oxygen plane". Townsend and Haycock considered that if the oxygen ions were excited by ionising radiation then a possible relaxation route would be the formation of a metastable oxygen molecular ion. In this configuration, the physical size of an oxygen molecule is comparable with the size of a separate oxygen ion and hence a vacancy in the oxygen triangle may appear. The ionic radius of an oxygen ion is typically 0.135 nm, and in molecular oxygen the separation of the nuclei is 0.121 nm. To reverse the direction of the spontaneous polarization the lithium ions need only be moved approximately 0.05 nm to cross the oxygen plane and thus the metastable molecular oxygen state need only exist for a few picoseconds [32]. Figure 5.4 is a diagrammatic representation of the domain reversal process. The process can be carried out using energetic electrons as the source of ionising radiation. In order to re− pole the crystal, an electric field was applied along the crystal c− axis. The electron beam was normal to the −c− face of the crystal and covered the entire surface area of the −c− face. For a crystal of thickness 1 mm, an electron beam energy of 1.8 MeV was sufficient to traverse the whole of the sample. Domain reversal was demonstated at temperatures as low as 600 °C, using electric fields of the order of 10 Vcm^{-1}, with electron currents in the range 1−3 μA.

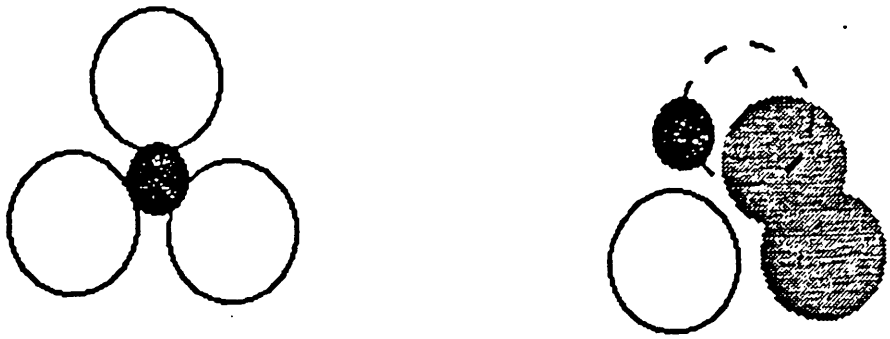

figure 5.3 Illustration of the mechanism for the formation of a transient vacancy in the oxygen triangle.

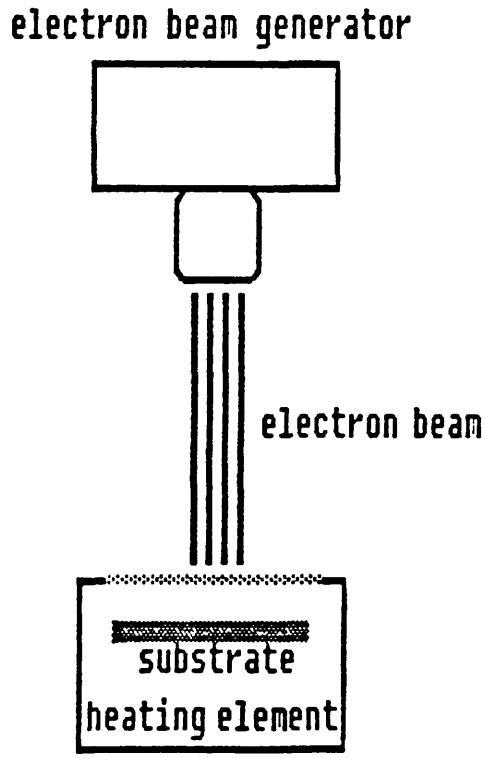

figure 5.4 schematic of apparatus for performing electron beam domain reversal

This technique has significant potential advantages for domain reversal in lithium niobate for nonlinear device applications:-

(1) At temperatures close to the Curie point, any fluctuations in the local temperature distribution may cause domain reversal to take place. These randomly formed domains are equivalent to fluctuations in the domain periodicity and lead to a non-uniform grating. For domain reversal at lower temperatures, the formation of random domains is less likely, so that it may be possible to produce highly regular domain-reversed gratings. Also, at these lower temperatures,

out–diffusion of lithium, which would cause (unwanted) domain reversal, should be less significant (although out–diffusion of oxygen may be a problem).

(2) There is no need for the in–diffusion of any transition metal species, thus reducing the risk of increasing the optical damage susceptibility of the lithium niobate substrate.

(3) The domain reversal can be localised by photolithographically defining an appropriate area in a suitable metallic masking layer. By defining a periodic grating in a suitable masking layer, a periodic, domain–reversed region may be produced.

Points (1) and (2) also mean that there should be much less modulation of the refractive index than is found for the case of titanium–indiffused or lithium oxide out–diffused domain–reversal. For quasi phase–matched second harmonic generation applications, there are two further important aspects to this process. These are:–

(1) that it allows domain reversal to take place on the –c–face of the substrate, usually the preferred face for waveguide fabrication, and that,

(2) by suitable choice of electron energy, the depth of penetration of electrons into the substrate material can be controlled. This potentially allows the depth of the domain reversed regions to be defined and controlled. The depth of domain reversal can then be chosen to optimise the conversion efficiency [13].

Using the electron bombardment technique, this author (and co–workers) has demonstrated that periodic domain–reversed gratings can be fabricated on the –c–face of a lithium niobate wafer [33]. The gratings were realised by photolithographically defining a metallic grating mask on the –c–face of the substrate. The domain reversal was carried out by Dr. B. Luff and Professor P. Townsend at the University of Sussex using a similar technique to that of Haycock and Townsend. The electron energies were suitably reduced so that the electrons would penetrate only a short distance into the substrate.

The interaction of an electron beam with a solid is a complex interaction. Before ultimately losing all its energy or escaping from the material, the electron may undergo hundreds or thousands of scattering events, which may be either elastic or inelastic processes. However, the many ways in which a given electron could

complete the sequence of interactions precludes the construction of a detailed analytical model. In order to model the passage of an electron subject to these random scattering processes, a mathematical technique known as the Monte–Carlo method can be used. Monte–Carlo techniques use random numbers as a means of predicting the magnitude of various events and as a way of selecting between the various scattering events.

The Bethe relation describes the rate of energy loss of an electron as it passes through a solid. It relates the rate at which an electron loses energy via the various scattering events to the density, atomic number, the mass number and the ionisation potential of the element. The relation is written formally as [34]:–

$$\partial_s E \quad (\text{keV/cm}) = -78500.(\rho.Z/A.E).\log(1.166.E/J) \qquad (13)$$

where E is the initial energy of the electron, $\partial_s E$ represents the derivative of energy of the electron with respect to penetration distance s, ρ is the density of the element, Z and A are the atomic and mass numbers repectively and J is the ionisation potential given by:–

$$J\ (\text{keV}) = \{9.76.Z + (58.5 / Z^{0.19})\}.10^{-3} \qquad (14)$$

A Monte–Carlo simulation of the Bethe relation [34] was used to calculate the electron penetration depth as a function of electron energy. In the model it was assumed that the electrons undergo only elastic scattering events and that the electrons lose energy continuously at a rate determined by the Bethe relation. The author is indebted to Dr G. Sinclair, Dept. of Physics and Astronomy, University of Glasgow, for providing the program and for invaluable advice on the validity of the program.

The Bethe relation is strictly only valid for electron ranges calculated in elementary condensed materials. In the model, the penetration depth is dependent on the atomic number and mass number of the element and also on the ionisation potential of the element (which is itself related to the atomic number). To calculate the electron range in lithium niobate, the compound was treated as a single element, in which the atomic number, the mass number and the ionisation potential were approximated by calculating a weighted average for each using the appropriate values for the atomic numbers and mass numbers for lithium, niobium and oxygen respectively. The weighted average for the atomic number is used to calculate the weighted average ionisation potential via Eq. 14.

Figure 5.5 shows a graph of penetration depth as a function of incident electron energy. The calculation does not take the temperature of the substrate into account and it would be expected that, at the temperatures to be used for domain reversal, the electron energies required will be greater than those indicated by the analysis, due to increased scattering.

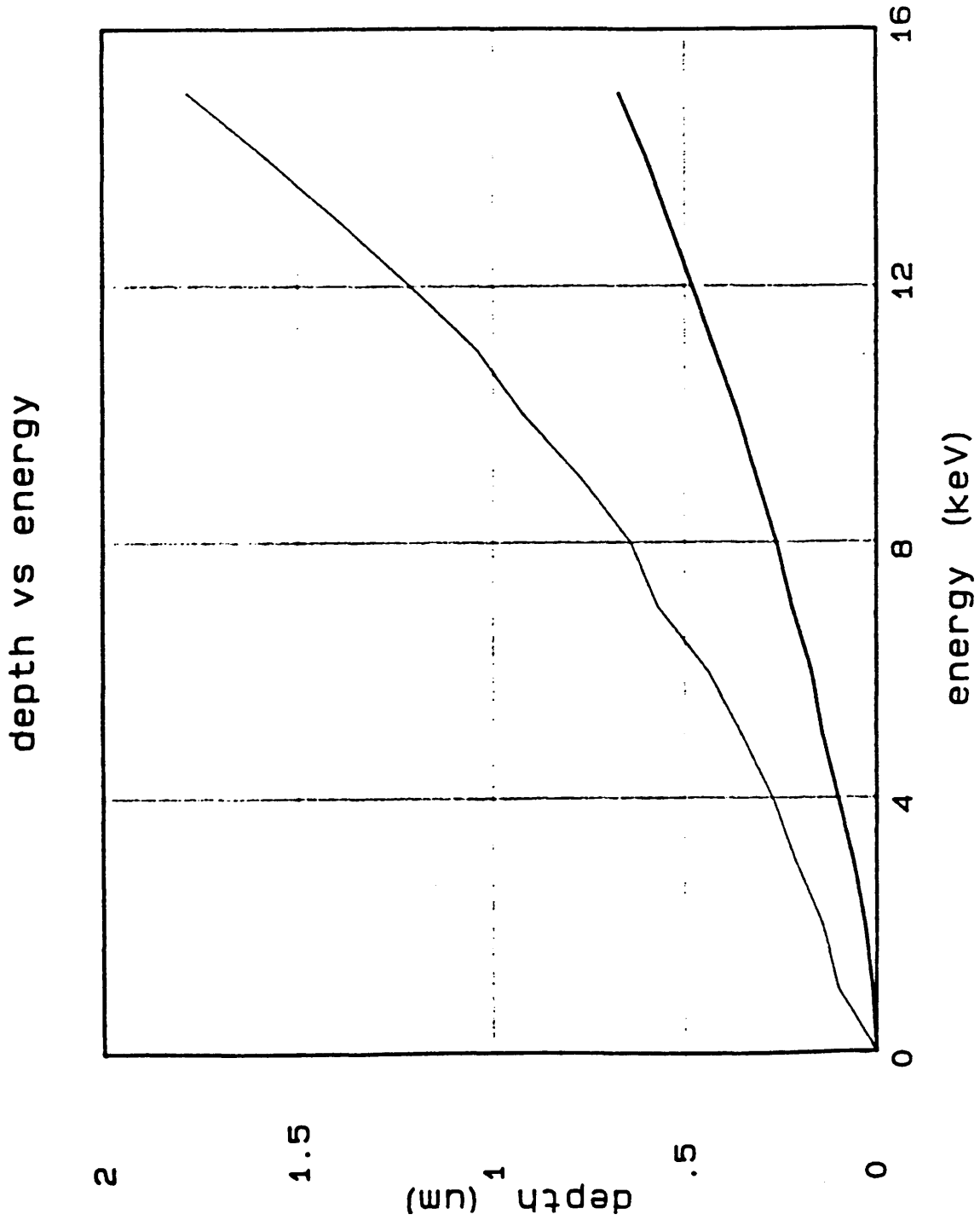

figure 5.5 electron penetration depth as a function of energy for Gold (lower curve) and lithium niobate (upper curve)

Also shown in Fig. 5.5 is the penetration depth of electrons into gold. Gold was chosen as the masking layer for three reasons;

(1) It is compatible with standard photolithographical techniques.

(2) It is an efficient absorber of electrons and so only a thin layer is required. For the grating dimensions to be used in the experiment, as thin as possible an absorbing layer is an essential requirement as it allows the height to width ratio of the metallic grating to be minimized, simplifying the photolithography.

(3) It is an electrical conductor and therefore facilitates application of the poling field to the crystal.

5.2.5 Fabrication of grating structures.

This section is split into four sub-sections, each of which deals with a different part of the grating fabrication process.

5.2.5.(i) Determination of the grating period required.

Before any fabrication details could be decided on, it was necessary to establish the grating period required to provide first order quasi phase-matching at a fundamental wavelength of $\lambda = 1.06$ μm. The grating period is dependent on the depth of the proton-exchanged waveguide used because of the dependence of the effective refractive index on the depth of the waveguide region. In chapter three it was shown that the conversion efficiency for second harmonic generation via Cerenkov radiation was a maximum at a waveguide depth of around 0.75 μm. As a first approximation it was assumed that the conversion efficiency in the quasi phase-matched case will be optimised for the same waveguide depth (or a depth close to this value). From Eq. 3, the required grating period is:-

$$l_c = \pi / \Delta k \qquad (5.15)$$

where $\Delta k = 2.k_0.(N_{2\omega} - N_{\omega})$ (5.16)

i.e.:-

$$l_c = \pi / \{2.k_0.(N_{2\omega} - N_{\omega})\} \qquad (5.17)$$

In Eq. 12, k_0 is the wavevector of the fundamental wavelength in free space and $N_{2\omega}$ and N_{ω} are the refractive indices of the guided modes at frequencies 2ω and ω respectively.

The required grating period was determined by fabricating a series of neat melt proton–exchanged waveguides with depths covering a range around the predicted required depth i.e.:–

$$0.65 \lesssim d \lesssim 0.85 \ \mu m \qquad (5.18)$$

(here d is the waveguide depth, not the nonlinear coefficient).

For each waveguide, the prism coupling technique was used to measure the effective index of the zeroth order waveguide mode at the fundamental wavelength of $\lambda = 1.06$ μm and at the harmonic wavelength of 0.53 μm. The harmonic wavelength was in fact generated by frequency doubling the fundamental beam in a proton–exchanged waveguide. Figure 5.6 shows an experimental graph of the effective index of both the fundamental and harmonic wavelengths as a function of waveguide fabrication time (in minutes).

A waveguide depth of 0.75 μm was found to correspond to a fabrication time of 22 minutes for a (benzoic) acid temperature of 235 °C. From the graph, the index difference between the fundamental and harmonic waves is 0.154. The corresponding grating period, calculated from Eq. 17 is 3.44 μm. It can also be seen from the graph that, within the range of fabrication times investigated, the grating period is approximately constant for each waveguide depth (see Fig. 5.7). Having established the period of the grating, it was decided that the depth of the domain reversed region should be approximately 1 μm. This depth was chosen to be greater than the waveguide depth, but not so deep that too thick a layer of gold was required for the mask. From Fig. 5.5, the thickness of gold required was 0.4 μm.

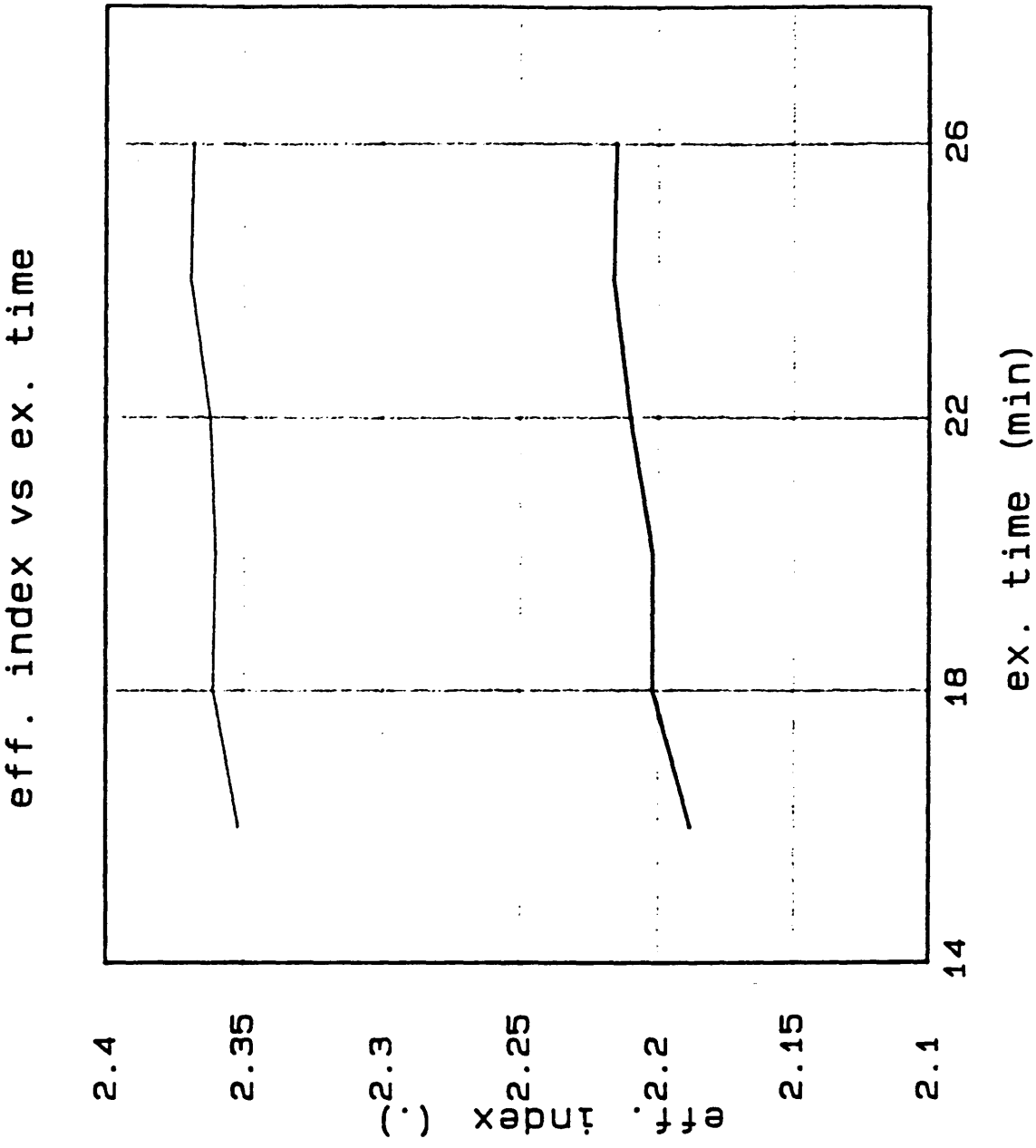

figure 5.6 effective index of zeroth order waveguide modes as a function of exchange time for both 1.06 um (lower curve) and 0.53 um (upper curve) radiation

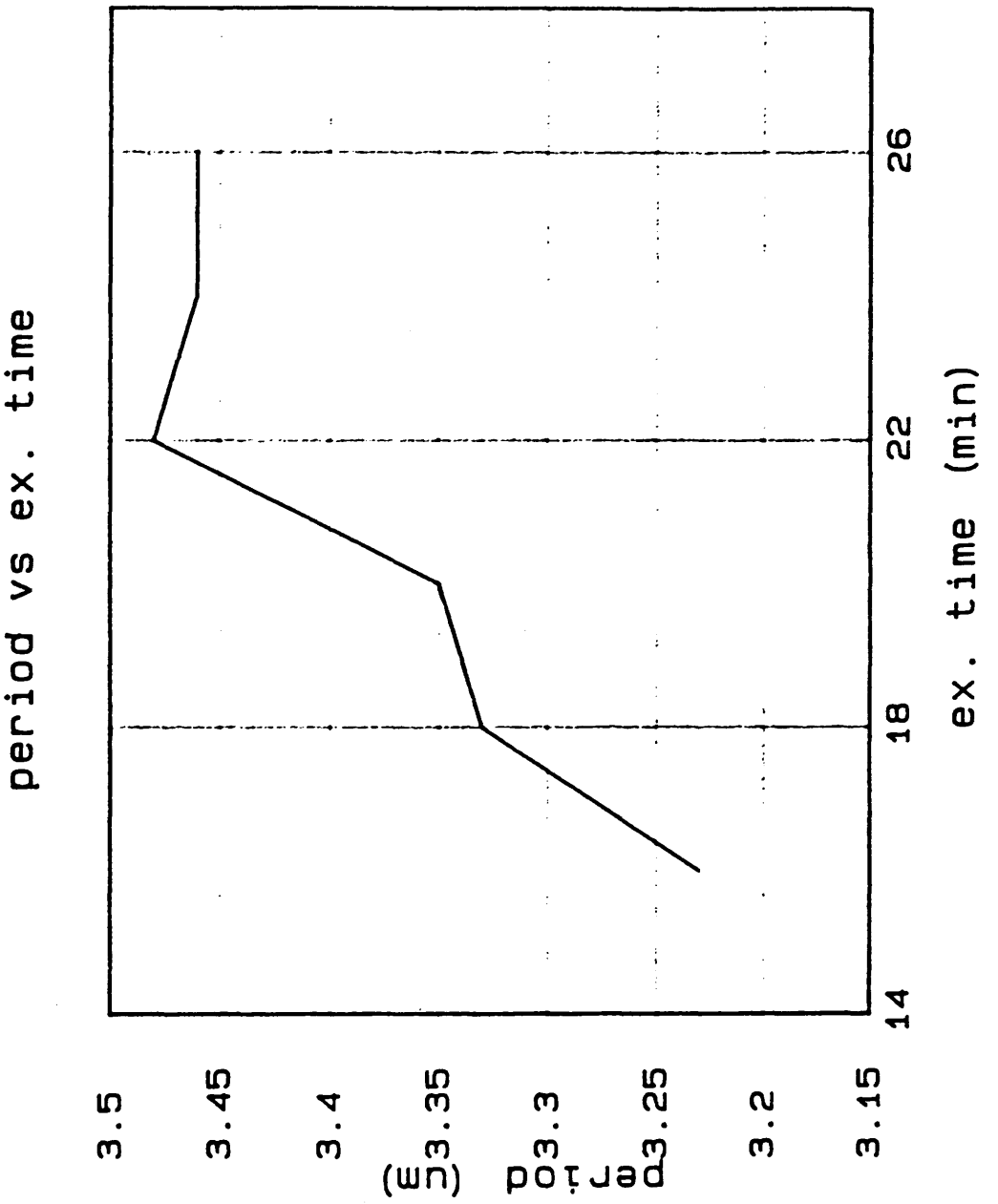

figure 5.7 grating period for zeroth order grating as a function of exchange time (derived from figure 5.6)

5.2.5.(ii) Grating fabrication procedure.

The grating fabrication procedure is outlined in this section. A more detailed step–by–step recipe is given in the appendix at the end of the chapter.

A dark–field (positive) mask was prepared with a period of 3.4 μm, with a total of 295 periods and with a transverse width of 1 mm. The substrates used in the experiment were polished on the –c–face but not on the +c–face. There was no specific reason for using an unpolished +c–face, but the surface roughness appeared to promote good adhesion between the substrate and the metal. A thin layer (50 nm) of "chromel", (90:10 nichrome:chromium), was first evaporated onto the +c–face of the lithium niobate. This layer was used to act as an adhesion "buffer" between the gold and the lithium niobate. The adhesion of gold to lithium niobate is poor, but it does adhere to a thin layer of chromel. The evaporation of the chromel was followed by the evaporation of 200 nm of gold. These metal layers were to provide electrical contact to the rear face. On the –c–face a thin layer of chromel was again evaporated, followed by the 400 nm of gold required to prevent the electrons penetrating the lithium niobate. The grating was then defined in photoresist and etched. This was carried out by wet chemical etching in a saturated solution of potassium iodide in iodine solution, diluted 1:1 with RO water to slow the etching process down and make the process more controllable. The chromel layer performed a second function since, after the gold was etched to produce the grating, the chromel buffer layer served to provide electrical contact to the –c–face. The resulting grating structure is shown schematically in Fig. 5.8.

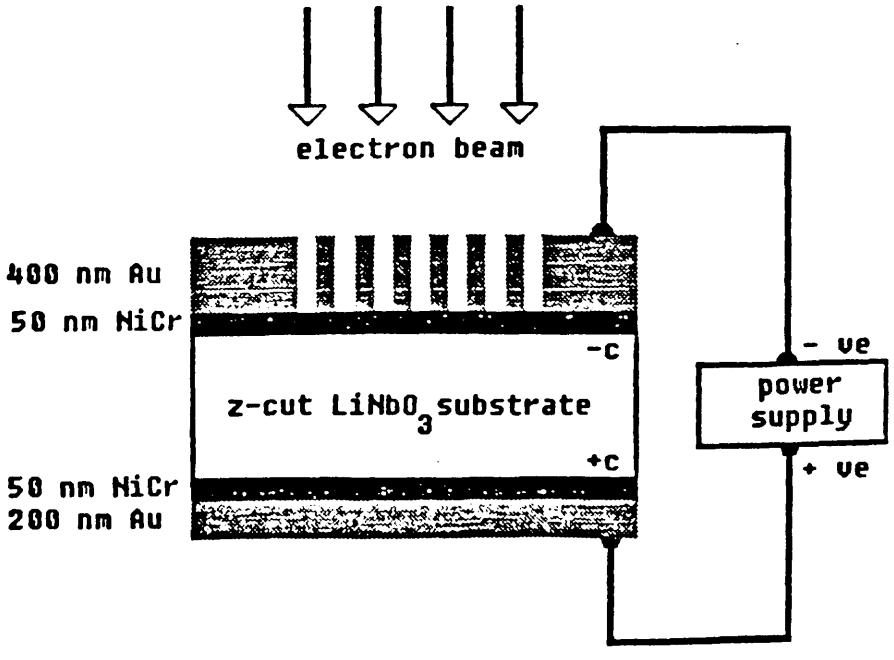

figure 5.8 details of processed substrate and applied voltage conditions for domain reversal

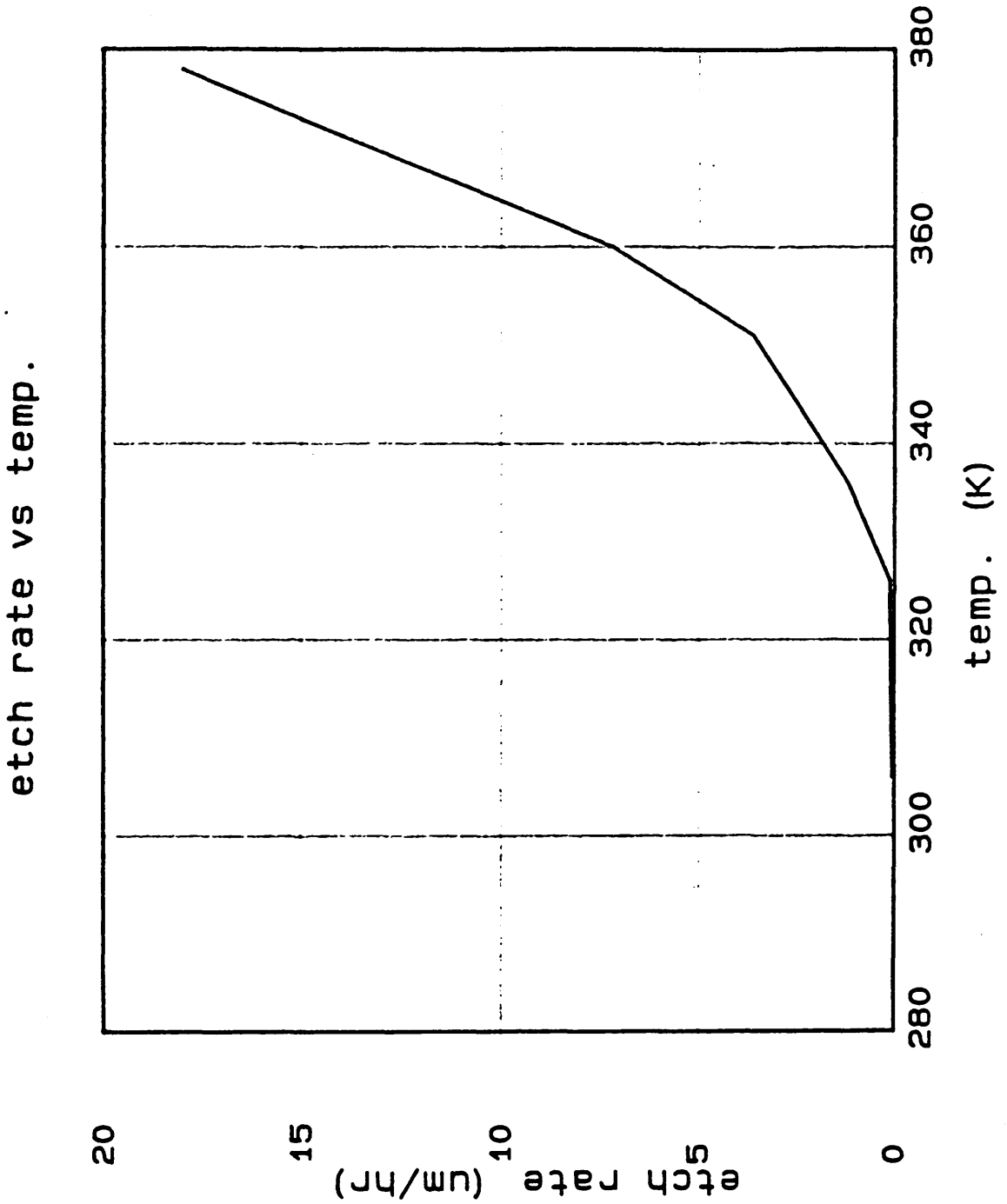

figure 5.9 etch rate of lithium niobate (by HF/HNO_3) as a function of etchant temperature

5.2.5.(iii). Domain reversal procedure.

An outline of the domain reversal process has already been given. For the samples used to fabricate domain reversed gratings the fabrication conditions were as follows. The nominal temperature of the substrate was 580 °C. A poling field of 10 Vcm^{-1} was used, with an electron beam energy of 10 keV and beam spot size of 9 mm^2. The electron beam current used was 8 μA for a period of 1 hour, and a total dose of approximately 10^{17} electrons was used.

5.2.5.(iv). Test for domain reversal.

The gold and chromel layers were first removed from the substrate by wet chemical etching (see appendix for details of the etchants). At temperatures of around 580 °C in vacuo, the lithium niobate was partially reduced and therefore, after removal of the metal layers, the sample was annealed in air for 5 hours at 650 °C to replace the lost oxygen. The domain reversed regions of lithium niobate could then be revealed by etching in a 1:2 mixture of hydrofluoric and nitric acids. This etchant attacks the −c− face, whilst the +c− face remains unetched. Domain−reversed regions were therefore shown up because of the differences in the etch rates. This is the most common test for domain reversal [35], although other tests based on the pyroelectric effect or the piezoelectric effect [36] have also been used. Given the dimensions of the grating structures involved in this work, the last two techniques are not easy to implement as a check for domain reversal.

The acid temperature used for the etching was in the 30−40 °C temperature range. It was found that in this temperature range the etch rate was well controlled, resulting in etch times of 5−10 minutes. Figure 5.9 shows a graph of the measured etch rate versus acid temperature. At high temperatures, etching of the substrate was rapid, resulting in an over−etching of the substrate. Also, from a safety aspect, it was preferable to carry out the etching at lower temperatures. Figure 5.10 shows a scanning electron micrograph of part of the grating structure after etching, with the domain reversed−regions clearly visible. Generally similar features were observed optically.

A number of samples were produced over a period of several weeks to check the reproducibility of the process. Although the photolithography involved is tedious and time consuming, if care is taken the process is highly repeatable. After the photolithography stages a yield of around 40−50% was obtained of samples which

were suitable for domain reversal. After the conditions had been established for the domain reversal process, each fabrication was apparently successful. A total of 6 samples was prepared.

figure 5.10

5.2.6 Quasi phase– matched second harmonic generation.

Of the six samples that were prepared, three were used for etching, rendering them useless for second harmonic generation. The final three did not arrive in the laboratory until after the author had left. This was unfortunate because, although a successful process for domain reversal has been established, it has not been possible to confirm that the samples could be used to produce second harmonc generation in the quasi phase– matched mode.

5.3.1. Measurement of the d_{33} coefficient of proton– exchanged lithium niobate.

As was stated in the introduction to this chapter and also in chapter one, the electro– optic coefficients of proton– exchanged lithium niobate are, in some cases,

were suitable for domain reversal. After the conditions had been established for the domain reversal process, each fabrication was apparently successful. A total of 6 samples was prepared.

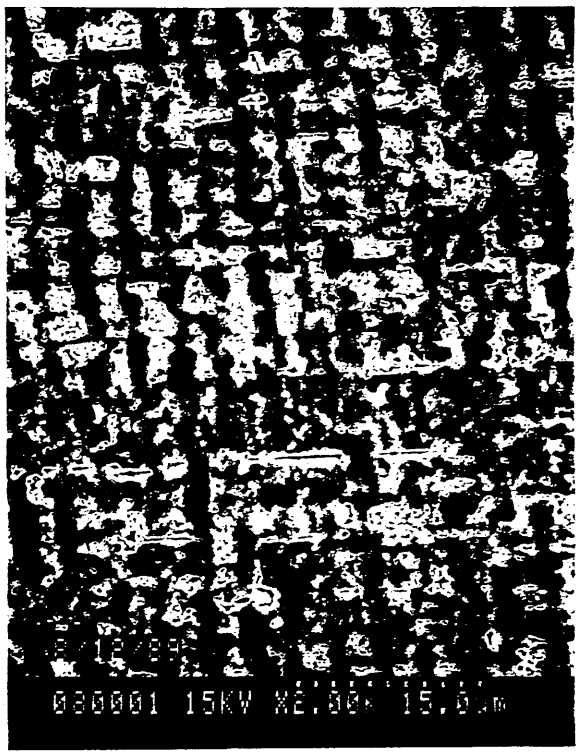

figure 5.10

5.2.6 Quasi phase– matched second harmonic generation.

Of the six samples that were prepared, three were used for etching, rendering them useless for second harmonic generation. The final three did not arrive in the laboratory until after the author had left. This was unfortunate because, although a successful process for domain reversal has been established, it has not been possible to confirm that the samples could be used to produce second harmonc generation in the quasi phase– matched mode.

5.3.1. Measurement of the d_{33} coefficient of proton– exchanged lithium niobate.

As was stated in the introduction to this chapter and also in chapter one, the electro– optic coefficients of proton– exchanged lithium niobate are, in some cases,

reduced significantly with respect to those of bulk lithium niobate. The electro–optic and nonlinear coefficients are closely related material parameters through the second order susceptibility tensor (for the arguments presented in the following discussion the nonlinear coefficient is taken to mean the relevant d_{ijk} tensor component of lithium niobate). This observed reduction in the electro–optic coefficient indicates that the nonlinear coefficient may also be reduced by the proton–exchange process.

A knowledge of the magnitude of the nonlinear coefficients of the proton–exchanged lithium niobate is therefore necessary for at least two reasons from a device point of view:–

(1) If the nonlinearity of the waveguide region is reduced by proton–exchange then the conversion efficiency for second harmonic generation will be different from that which might be expected (assuming no degradation of the nonlinear effect). If the second harmonic generation is phasematched either by the material birefringence or by a grating structure then the conversion efficiency will be reduced by the decrease in the nonlinearity. If the second harmonic generation is phasematched via Cerenkov radiation then the conversion efficiency will be increased by the decrease in the nonlinearity. For conventional phasematching the reduction can be understood by referring to Eq. 4. If the nonlinear coefficient of the "ideal" waveguide region (with no degradation of the intrinsic nonlinearity) is denoted by d and of the actual waveguide (with a degradation of intrinsic nonlinearity) is denoted by d^*, with $d > d^*$ then the conversion efficiencies are given by:–

$$\eta = C.d^2 > C.(d^*)^2$$

For the case of Cerenkov second harmonic generation, a recent publication by Li et al [37] has shown that the conversion efficiency for second harmonic generation is proportional to the difference between the nonlinear coefficients of the waveguide and substrate regions. For certain combinations of waveguide parameters, reducing the nonlinearity of the waveguide region *increases* the difference between the nonlinearities of the waveguide and substrate regions, thus potentially increasing the conversion efficiency. (For a more detailed discussion of this see chapters two and three).

(2) If the nonlinearity of the proton–exchanged layer is reduced then it may provide an alternative way of fabricating a periodic modulation of the nonlinear

coefficient for quasi phase-matched second harmonic generation. For example it could be envisaged that, superimposed onto a titanium-indiffused waveguide for example, a periodic proton-exchanged grating could be fabricated. A fundamental wave propagating along the titanium-indiffused waveguide would then experience a periodic modulation of the nonlinear coefficient (see Fig. 5.1).

From the above discussion, it should be clear that a measurement technique to determine the nonlinear coefficient of proton-exchanged lithium niobate is desirable. There are many experimental techniques for the measurement of the nonlinear coefficients of a crystal [38]. Among these techniques, the most commonly used and most well developed are phase-matched second harmonic generation [39], the wedge technique [40], Maker fringes [41], and optical parametric fluorescence [42]. All of the techniques require a bulk sample of the material for the measurement. Unfortunately, proton-exchanged lithium niobate, in the form of $H_xLi_{1-x}NbO_3$, has apparently not been produced in bulk single crystal form. Phase-matched second harmonic generation and optical parametric fluorescence techniques could, in principle, be used in a waveguide geometry. In order to evaluate the nonlinear coefficient, a knowledge of the electric fields of the waveguide modes is required. Consequently, the difficulty of evaluating the absolute optical intensity profile in the optical waveguide precludes their use in this way. In a recently published paper [3] Suhara, Tazaki and Nishihara have demonstated a technique whereby non-phase-matched second harmonic generation in a grating structure can be used to measure the d_{33} coefficient of proton-exchanged lithium niobate. Using this technique they have estimated that the d_{33} coefficient is reduced to 0.45 of that of bulk lithium niobate.

In the second half of this chapter, the theory and experimental technique developed by Suhara et al [3] will be outlined. The nonlinearity is measured by non-phase-matched second harmonic generation in a wedged-shaped substrate with a proton-exchanged grating region. Using the grating technique, this author has repeated the experiment of Suhara, and has further extended the experiment by measuring the effect of annealing on the nonlinearity. It was confirmed that the proton-exchange process does reduce the nonlinearity of the lithium niobate. Furthermore, the experimental results were in close agreement with those of Suhara et al [3]. It was also found that annealing the proton-exchanged layer tended to restore the nonlinearity of the proton-exchanged region, a result not unexpected from previous work on electro-optic coefficients.

Following a description of the work and analysis of the results, a section will be

devoted to a discussion of the possible mechanism for the reduction of the nonlinearity of the lithium niobate substrate after proton–exchange.

5.3.2 Measurement of d_{33} by the grating diffraction technique.

In this section the theory of the measurement will be outlined, followed by a description of the experimental technique. Only an outline and the final results of the theory will be given, followed by some results generated by a computer calculation using the theory of Suhara et al [3]. No details of the theory will be given because, firstly, it is not original work by this author, and secondly, although an attempt was made to derive the results, the author could not reach the same final results as published by Suhara et al [3]. The published equations of Suhara et al were taken as correct, and the inconsistency with this author's own derivation attributed to his lack of insight into solving the Maxwells equations with the relevant boundary conditions. The justification for accepting the theory of Suhara et al is the agreement between the theoretical model and the experimental results. Further confidence was engendered by the agreement of the computer–generated results obtained by the author with those of Suhara et al.

Consider non–collinear second harmonic generation in a thin slab of lithium niobate of thickness T (see Fig. 5.11).

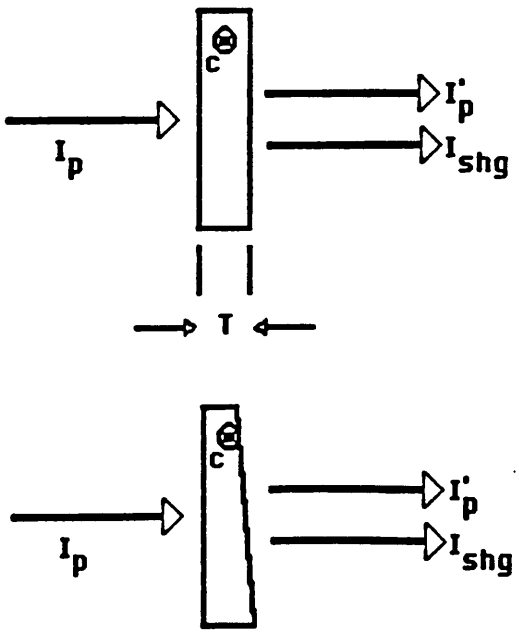

figure 5.11 SHG in a thin slab (top) and in a wedge shaped (bottom) substrate

The fundamental beam is polarised along the c− axis of the crystal. The intensity of the second harmonic, with the same polarisation as the fundamental, is given by:−

$$I = C^2 . I_p^2 . \sin^2(\pi T/l_c) \qquad (5.19)$$

where C is a constant proportional to d_{33}, I_p is the fundamental intensity, and l_c is the coherence length. For the case of second harmonic generation in a wedged shape sample, the harmonic intensity is averaged over the thickness T, and is given by:−

$$I = C^2 . I_p^2 / 2 \qquad (5.20)$$

The intensity of the second harmonic wave generated in a wedge with a thin proton− exchanged surface layer (of thickness t), as in Fig. 5.12a, can be calculated by connecting the wave equation solutions at the proton− exchanged layer/substrate interface, and averaging the intensity over T. The result can be written as:−

$$I_a = C^2 \frac{I_p^2}{4} \{1 + |1 + j.2.\frac{dn_{LN}}{dn_{PE}}.x.\sin(\varphi_t dn_{PE}).e^{j(\varphi_t dn_{PE})}|^2$$

$$I_a = C^2 \frac{I_p^2}{4} \{1 + |1 + j.2.\frac{dn_{LN}}{dn_{PE}}.x.\sin(\varphi_t dn_{PE}).e^{j(\varphi_t dn_{PE})}|^2 \qquad (5.21)$$

where

$$\varphi_t = 2.\pi.t/\lambda$$

$$\delta n = n_{PE}^{\omega} - n_{LN}^{\omega}$$

$$dn_{LN} = n_{LN}^{\omega} - n_{LN}^{2\omega}$$

$$dn_{PE} = n_{PE}^{\omega} - n_{PE}^{2\omega}$$

with n the extraordinary refractive index , and λ and ω the wavelength and frequency of the fundamental beam.

Fig. 5.12b shows second harmonic generation in a wedge with a thin proton− exchanged grating layer (of thickness t and period Λ). The pump beam is diffracted into many orders by the periodic index modulation in the grating layer and, simultaneously, second harmonic waves of many diffraction orders are

generated by the periodic modulation of the d coefficient.

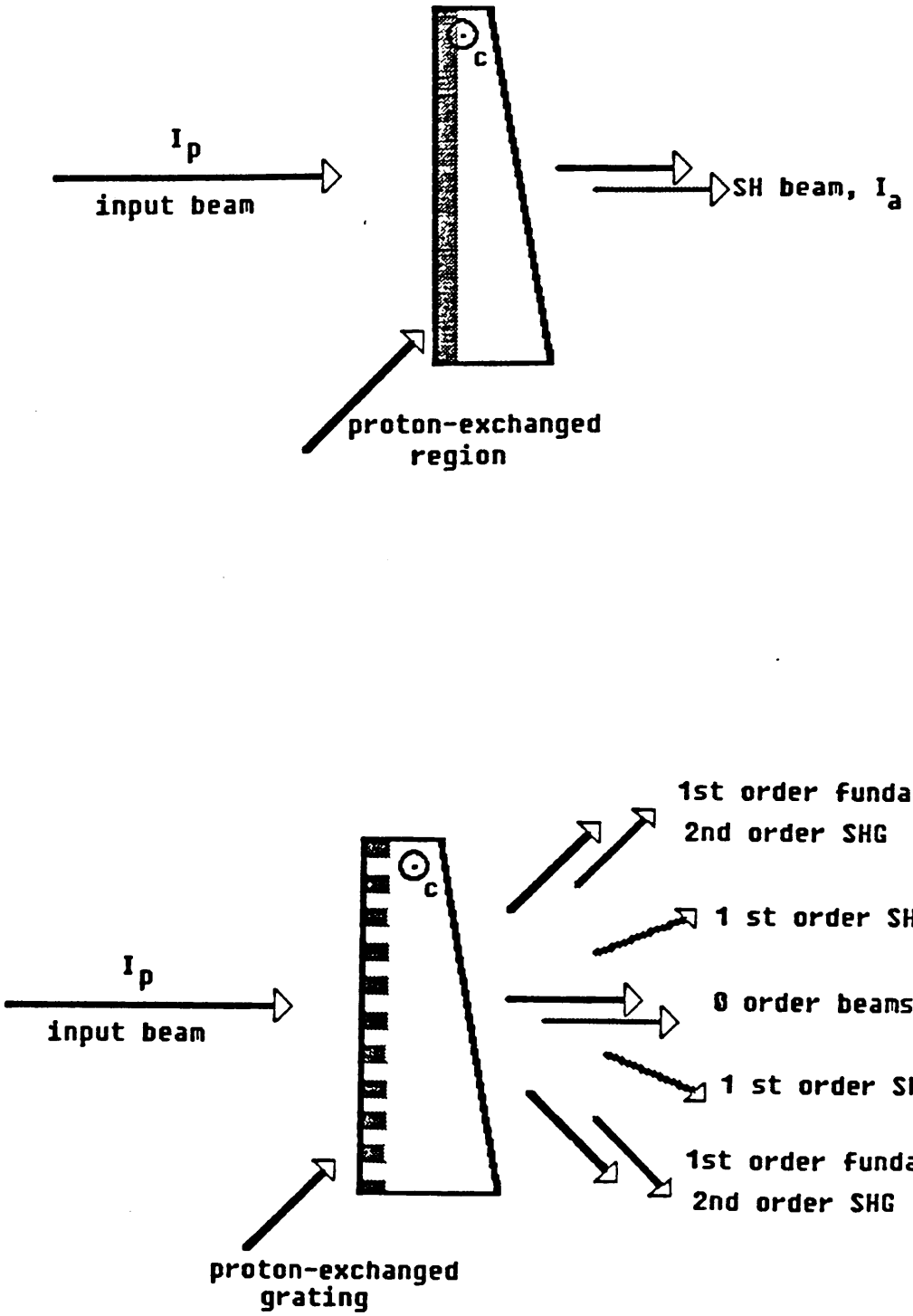

figure 5.12 SHG in a wedge shaped substrate with planar PE region (top) and grating PE region (bottom)

The nonlinear coupling of the zeroth and first order fundamental frequency beams in the substrate generates a second harmonic beam which propagates at an angle exactly matching that of the first-order, second harmonic, beam yielded by the grating. Thus the second harmonic beam detected at this angle is a superposition of second harmonic diffraction in the grating and noncollinear two-beam pump second harmonic generation in the substrate. When the grating is thin, i.e. in the Raman-Nath diffraction regime ($Q = 2\pi\lambda t/n\Lambda^2 << 1$), the second harmonic intensity can be calculated by :-

(1) deriving expressions for the pump and second harmonic wave amplitudes through a thin extended layer of lithium niobate, of thickness t, and deriving similar expressions for the proton-exchanged layer,

(2) expressing the fundamental and second harmonic waves at the grating/substrate interface in a Fourier series consisting of spatial harmonics

(3) using the first order second harmonic diffraction amplitude as the initial value to integrate the wave equation for the noncollinear second harmonic generation in the substrate and

(4) averaging the second harmonic intensity over the thickness T.

The result can be written as:-

$$I_b = C^2.I_p^2.\frac{\sin(a\pi)}{\pi}.\{|Z(x) - Z_0|^2 + |Z_0|^2\} \qquad (5.22)$$

where:-

$$Z(x) = x.\frac{dn_{LN}}{dn_{PE}}\sin(\varphi_t dn_{PE}).e^{j\varphi_t(dn_{PE} - 1.5\,\delta n)} - \sin(\varphi_t dn_{LN}).e^{j\varphi_t(0.5\,\delta n + dn_{LN})}$$

and

$$Z_0 = 2.\sin(\varphi_t.0.5\,\delta n).|1 - \{.2.a.\sin(\varphi_t.0.5\,\delta n).\exp^{-j\varphi_t(0.5\,\delta n)}|$$

In Eqs. 5.21 and 5.22 above, a is the ratio of the proton exchanged stripe width to grating period.

It is the parameter x which is important and is defined as:-

$$x = d_{33}PELN \;/\; d_{33}LN \qquad (5.23)$$

i.e. the ratio of the d_{33} coefficients of the proton-exchanged lithium niobate and the bulk lithium niobate. The x value can be determined by comparing the measured ratio of I_b/I_a, with the calculated x dependence of I_b/I_a. It should be noted that I_b/I_a does not depend on the pump intensity, so that the measurements should give reliable results even when using a pulsed fundamental beam with a nonuniform (Gaussian) profile. Eqs. 5.21 and 5.22, based on the equations of Suhara et al [3], were solved numeriaclly on a computer. Fig. 5.13 illustrates a typical calculated relationship between x and the ratio I_b/I_a.

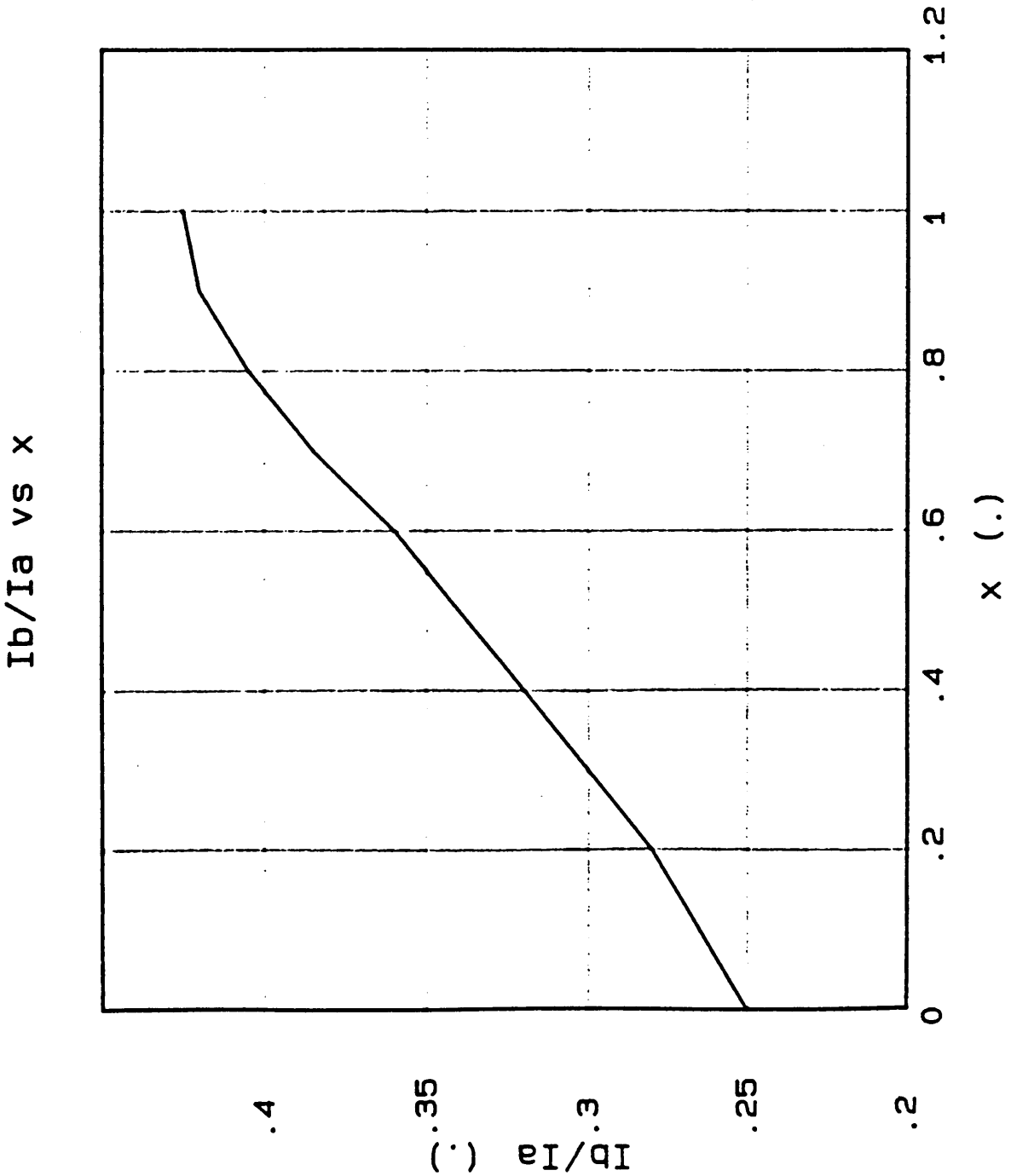

figure 5.13 theoretical plot to determine the reduction in d33 from the measured harmonic radiation intensities

The value of the parameters a and t for this curve were 0.5 and 2.0 μm respectively. The shape of the curve and the magnitude of the ratio of intensities (plotted on the y-axis as I_b/I_a) are very similar to those of the published curve of Suhara et al [3]. Based on this close agreement, the published results of Suhara et al [3] were taken as correct. A series of experiments was then carried out to measure x for both an unannealed waveguide and a waveguide annealed under specific annealing conditions.

5.3.3 Experimental determination of d_{33}.

The proton-exchanged layers were fabricated in neat melt benzoic acid at an acid temperature of 235°C. For an exchange time of 1 hour, the depth of the proton-exchanged layer should be on the order of 2 μm. One sample was masked by photolithographically defining an aluminium film with a grating of period 24 μm. The other sample was exchanged without masking to produce a uniform proton-exchanged layer. The two samples were coated with aluminium on the rear face to prevent the creation of a second proton-exchanged layer on that face. Both samples were polished into a wedge with a 2° angle. The waveguide depth and refractive index were estimated before and after each annealing stage in a reference planar waveguide fabricated under identical conditions. Using an IWKB analysis [43], the initial waveguide depth was measured to be 1.95 μm, close to the estimated depth of 2 μm. By illuminating the grating with a He-Ne laser (λ= 0.6328 μm) and measuring the relative intensities of the diffraction orders, the ratio of the width of the proton-exchanged layer to the grating periodicity (stripe-to-period ratio) was estimated. The ratio was estimated to be 0.51 for the unannealed grating. This value was expected from the photolithographic definition of the aluminium mask and was also anticipated from early work on lithographic definition of proton-exchanged structures where lateral diffusion of proton-exchanged stripes was small [44].

The output of a Q-switched Nd:YAG laser was used as the fundamental beam (λ= 1.06 μm). The Q-switched pulses of 200 ns duration with a repetition rate of 1 kHz were used. Although the beam was collimated, there was no need for any form of spatial filtering because, as has been discussed, the measurement is independent of the intensity of the fundamental beam. The experimental set up is shown in Fig. 5.14. For an (estimated) initial proton-exchanged layer depth of 1.95 μm, it was found that there was no second harmonic wave for the zeroth diffraction order. This was not completely unexpected because, for an initial

proton–exchange depth of 1.95 μm, there is almost π phase difference between the optical path lengths of the second harmonic wave generated in adjacent proton–exchanged and bulk regions of the grating structure. This can be

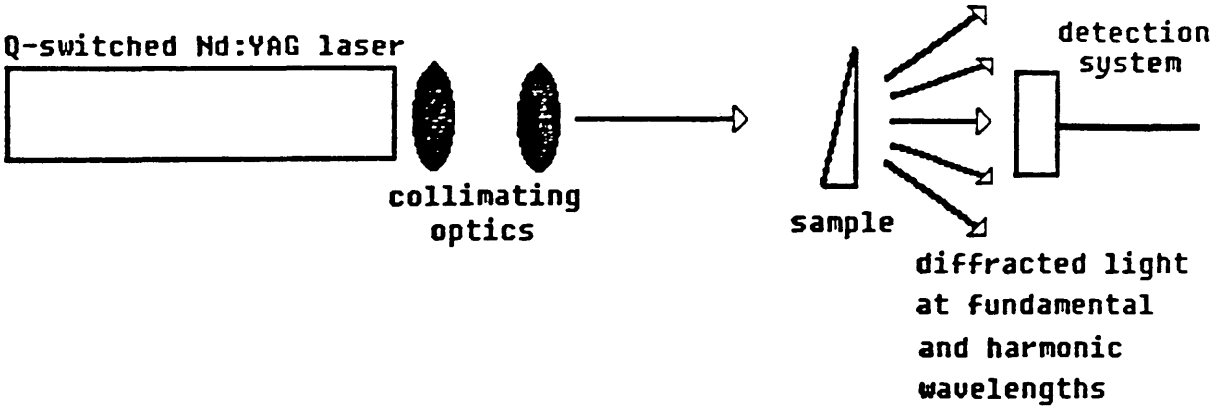

figure 5.14 experimental arrangement used in the measurement of d_{33}

justified by the following argument. Denote the phase of the harmonic wave in the proton–exchanged region by φ_1 and in the lithium niobate region by φ_2. The optical path difference, δ, between the harmonic waves after propagating a distance equal to the depth, d, of the proton–exchanged region is then:–

$$\delta = (d/\lambda).(n_{PE} - n_{LN}) \qquad (5.24)$$

$$= (d/\lambda).(2.37 - 2.25) = 0.45 \simeq 0.5$$

Thus there is almost a π phase difference between the harmonic waves generated in adjacent proton–exchanged and lithium niobate regions. As the grating was annealed, this phase difference was reduced and the intensity of the zeroth order harmonic beam *increased*.

For the initial, unannealed, proton–exchanged layer, the value of x was found to be 0.45 (±0.05). This value agrees with that measured by Suhara et al. and indicates a substantial reduction in the nonlinear coefficient of the proton–exchanged layer relative to the bulk value.

5.3.4 Effect of annealing on d_{33}

After the first set of measurements, both the planar proton–exchanged samples and the proton–exchanged grating sample were annealed at 275 °C for 10 min, followed by annealing at 350 °C for successive periods of 5 min, 5 min, and 10 min. Any further annealing was expected to give a significantly graded–index profile which is not desirable for second harmonic generation applications (see chapter 3) and therefore no further annealing was carried out. After each annealing stage the waveguide depth and refractive index change were measured in the plane sample and the grating stripe–to–period ratio was re–measured in the wedged sample. Over the annealing period of 30 min, the waveguide depth increased from 1.95 μm to 3.06 μm and the estimated refractive index changed by less than 1%. The waveguide depths and refractive index were estimated by an inverse WKB fit to the measured effective refractive indices of the guided modes at λ = 0.6328 μm. From the measurements of the relative intensities of the diffraction pattern of the He–Ne laser light, the measured grating stripe–to–period ratio appeared to remain constant over the annealing period. It might have been expected that, due to lateral diffusion of the proton–exchanged region, the stripe–to–period ratio would increase with progressive annealing. Assuming that the effective diffusion coefficient for annealing is equal in both the lateral and depth directions (valid as a first approximation), then annealing should increase the proton–exchanged stripe width from 12.0 to 14.6. For a pure phase grating, this may not be enough to have a measurable impact on the diffraction pattern envelope (at least with this experimental arrangement) and consequently the measured stripe–to–period width would appear to remain constant.

After each annealing stage the new values for waveguide depth and refractive index were substituted into the analysis and a new curve for I_b/I_a calculated. As an example, Fig. 5.15 shows the curve for I_b/I_a after annealing for a total of 15 min. As the annealing progressed it was found that the nonlinearity of the proton–exchanged layer increased. Figure 5.16 shows the increase in the measured value of d_{33} as a function of annealing time. The estimated value of x increases from an initial value of 0.45 (±0.05) to a value of 0.65 (±0.02) after 30

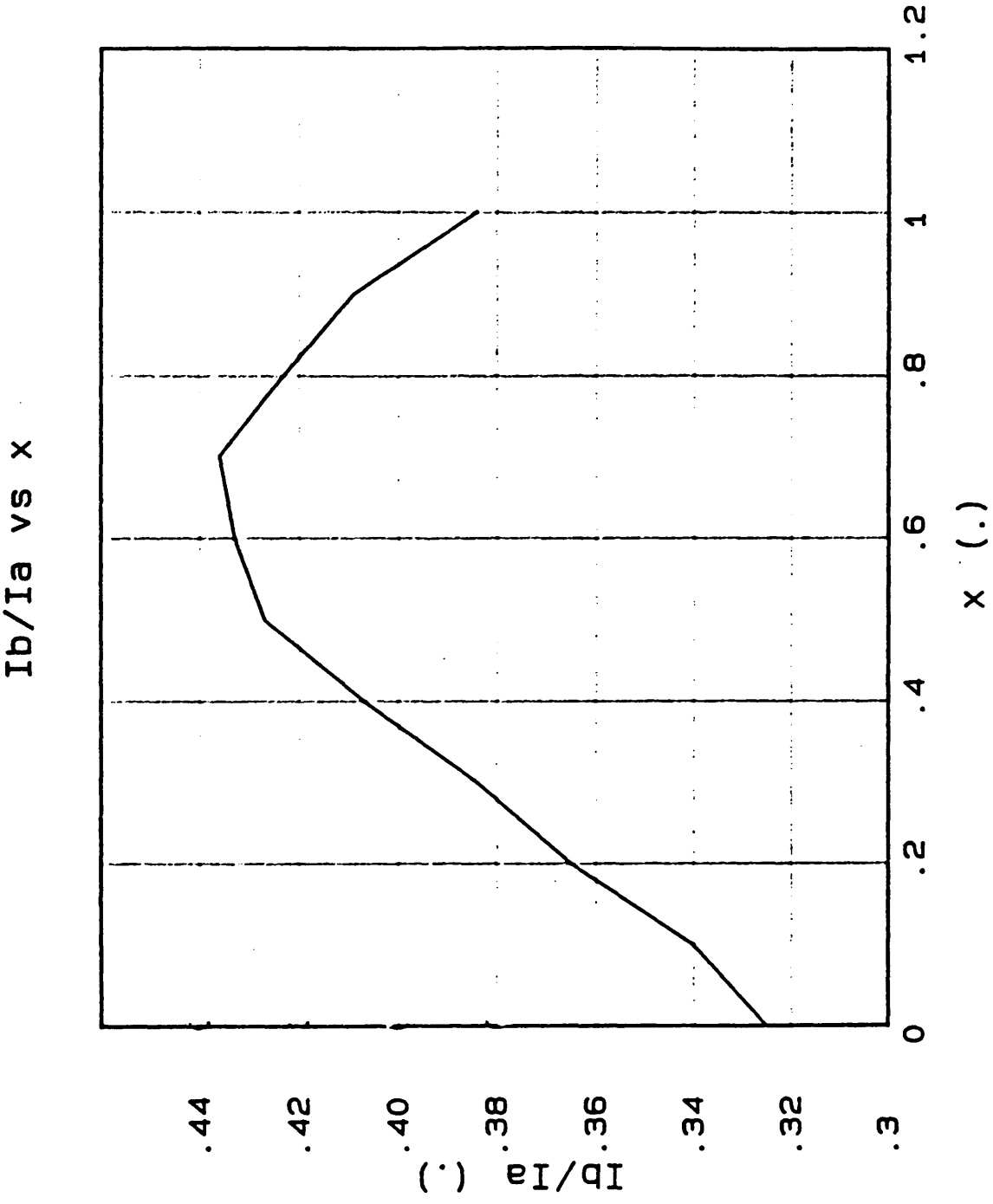

figure 5.15 experimental plot of the harmonic radiation intensities for the determination of d_{33}

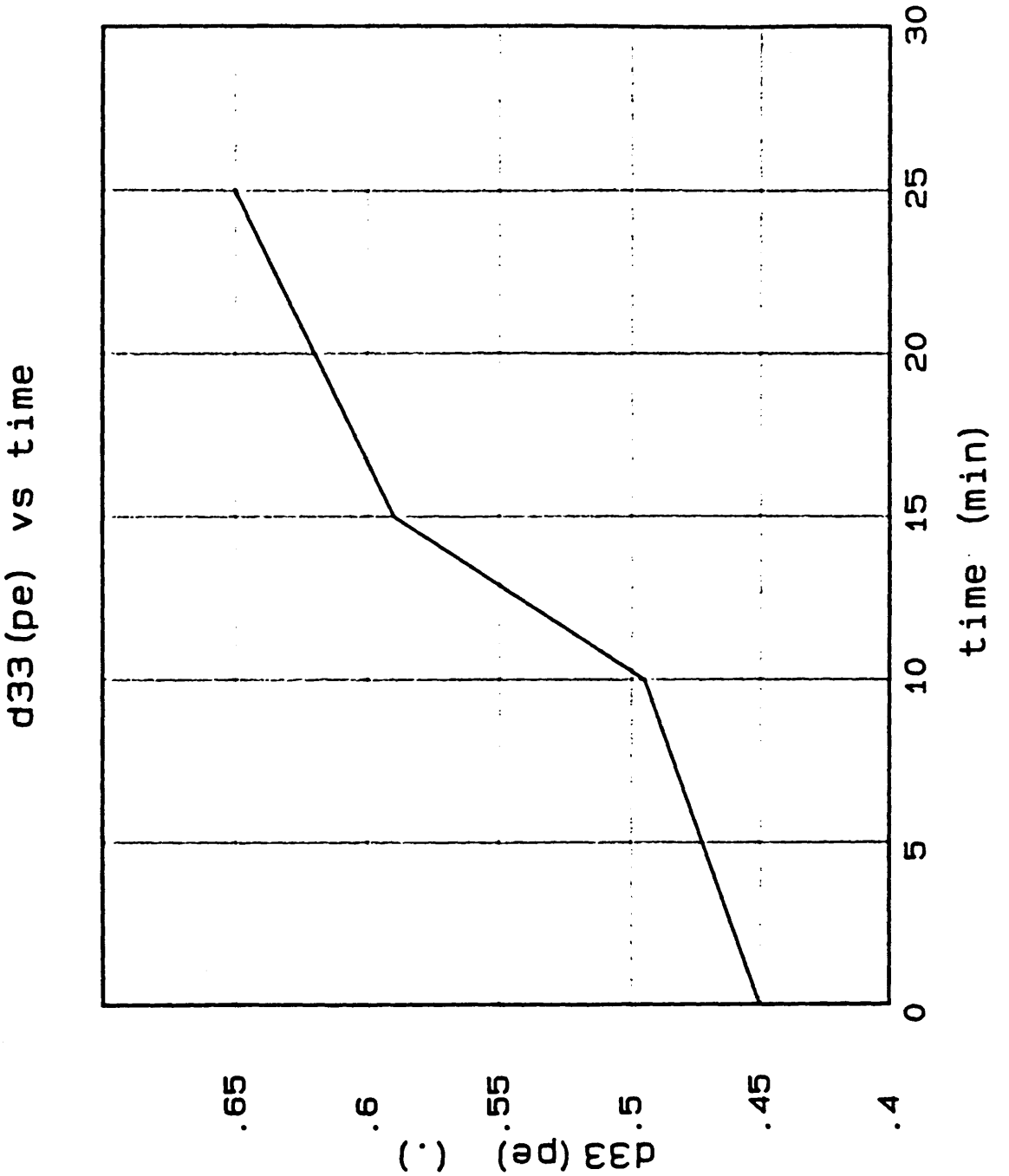

figure 5.16 plot of measured reduction in d_{33} as a function of annealing time

min of annealing. If the effective diffusion coefficients in the lateral and vertical directions are assumed to be equal, and the stripe width increases to 14.6 μm after the final annealing stage, the final value for x would be 0.67. This is close to the estimated value of 0.65. Figure 5.17 shows a curve of the magnitude of the d_{33} coefficient of proton–exchanged lithium niobate as a function of annealing time, assuming a value of 34.4 pm/V for the d_{33} coefficient of bulk lithium niobate.

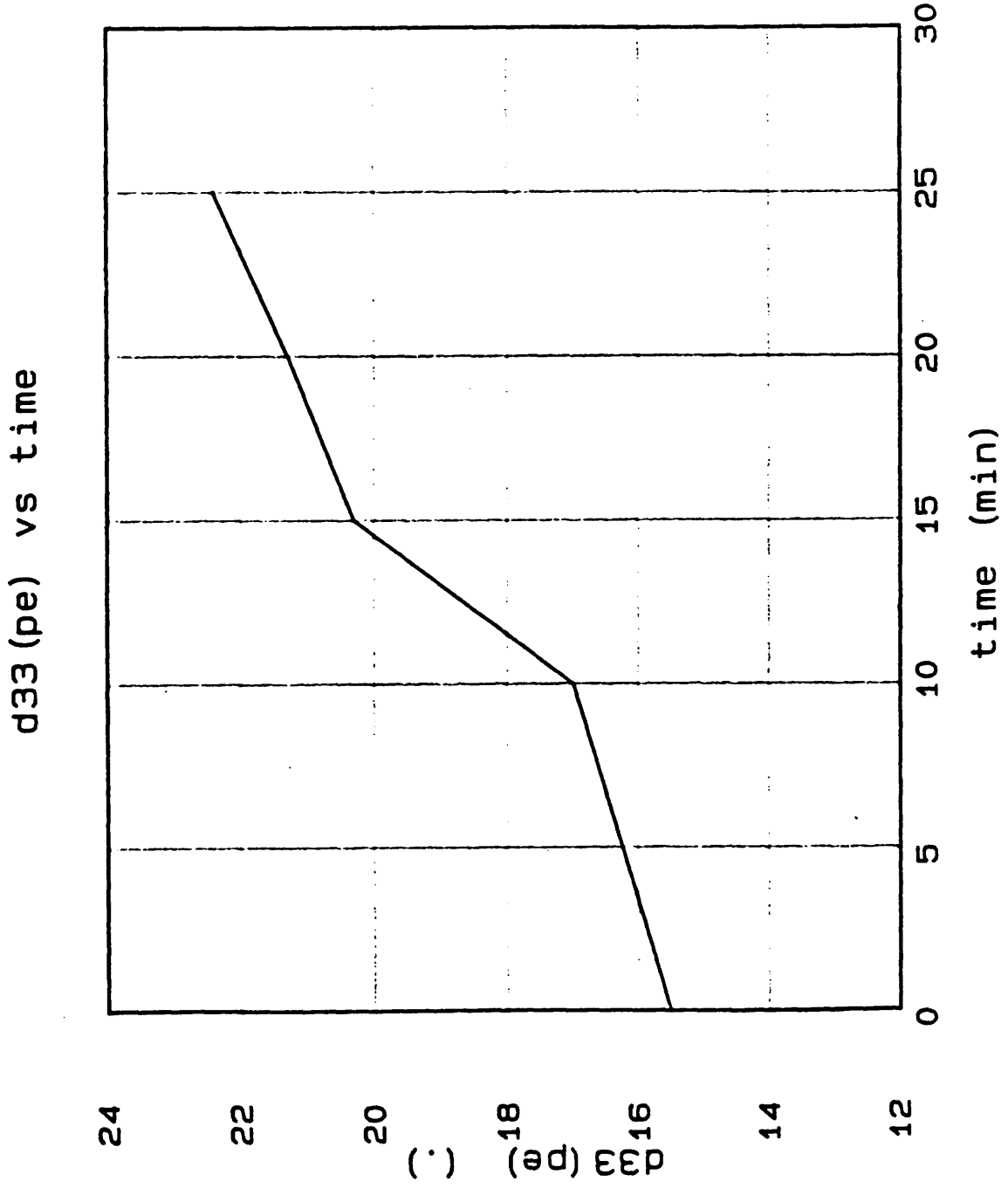

figure 5.17 plot of absolute value of d33 of proton exchanged lithium niobate as a function of annealing time

5.3.5 Mechanism for the reduction in nonlinearity.

Before a possible mechanism for the reduction in the nonlinearity of lithium niobate due to proton–exchange can be discussed, the origin of the nonlinearity of lithium niobate crystals must be established. There are several theoretical models which calculate the magnitude of the nonlinearity of crystals such as lithium niobate. Only one model will be discussed, namely the model of Jeggo and Boyd, [45]. This model decribes the nonlinearity in terms of the polarisabilities of the Nb – O bonds within the unit cell of the crystal.

In the model of Jeggo and Boyd, ("the model"), the macroscopic nonlinearity of the crystal is related to the microscopic nonlinear polarisability of the chemical bonds within the unit cell. For lithium niobate there are two independent tensor coefficients of the polarisability – $\beta_{||}$ and $\beta_{\perp}$ where:–

$\beta_{||} = \beta_{zzz}$ and $\beta_{\perp} = \beta_{xxz} = \beta_{yyz}$.

It has been shown [46] that $\beta_{||} \gg \beta_{\perp}$ (by a factor of about 30) and so $\beta_{\perp}$ can be neglected.

If a bond i has direction cosines (l_i, m_i, n_i) then the second harmonic coefficients are given by:–

$$d_{311} = V^{-1}.\Sigma n_i.l_i^2.\beta_i \qquad (5.25a)$$

$$d_{333} = V^{-1}.\Sigma n_i^3.\beta_i \qquad (5.25b)$$

$$d_{222} = V^{-1}.\Sigma m_i^3.\beta_i \qquad (5.25c)$$

where the sum is taken over all the bonds in the unit cell of volume V.

In the lithium niobate unit cell there are twelve "covalent" Nb – O bonds, six of length 0.211 nm and six of length 0.189 nm. The lithium atoms are bound "ionically" to the oxygen atoms. Consequently, the electrons in the Li – O bond are only weakly polarizable. A valid assumption therefore is that the polarizability of the crystal is due solely to the twelve Nb – O bonds. Ascribing polarizabilities β_1 and β_2 to the 0.189 nm and 0.211 nm bonds repectively, the three nonlinear coefficients can then be written [45] as:–

$$d_{311} = d_{31} = V^{-1}(1.104.\beta_1 - 1.106.\beta_2) \qquad (5.26a)$$

$$d_{333} = d_{33} = V^{-1}(0.643.\beta_1 - 1.796.\beta_2) \qquad (5.26b)$$

$$d_{222} = d_{22} = V^{-1}(0.396.\beta_1 - 0.195.\beta_2) \qquad (5.26c)$$

It can be seen that in lithium niobate the magnitude of the d_{33} coefficient is dependent on the geometry of the unit cell which in turn determines the unit cell volume and the length of the Nb − O bond. In a more detailed derivation of the bond polarizability (see, for example [38] for a detailed model of nonlinear polarizabilities) it is found that the coefficients β_1 and β_2 are strongly dependent on the Nb − O bond length.

The origin of the reduction in the d_{33} coefficient can be related to the change in the structure of the unit cell as the proton exchange process proceeds. As was discussed in chapter 1, the proton−exchange process can be described by the equation:−

$$H + LiNbO_3 \text{ ---> } Li_{1-x}H_xNbO_3 \qquad (5.27)$$

As the reaction proceeds and the value of x increases, the strain in the crystal increases, changing the unit cell from a rhombohedral−like unit cell structure to a more tetragonal unit cell structure [1]. Microscopically, the structural changes have the following effects:−

(1) The induced strain $\Delta c/c = 0.45\%$ [1] increases the volume of the unit cell, which in turn leads to a reduction in the nonlinear coefficients through Eqs. 26(a−c).

(2) Changes in the unit cell shape will lead to changes in the bond angles and therefore in the direction cosines l_i, m_i, n_i. The changes will also lead to a change in the nonlinearity, a change which could be either positive or negative. The direction of the change can only be derived from a detailed calculation of the direction cosines, a calculation which would require a detailed knowledge of the structure of $Li_{1-x}H_xNbO_3$.

In order to evaluate fully the reasons for a change in the nonlinear coefficients of proton−exchanged lithium niobate a more detailed knowledge of the crystal structure of the material is required. To the author's knowledge, the crystal structure of proton−exchanged lithium niobate is still unknown and no theoretical calculations of the type detailed above have been carried out to calculate the nonlinear coefficients of proton−exchanged lithium niobate. This structure must first be determined before the reasons for a reduction in the nonlinear and

electro–optic coefficients can be fully quantified and understood.

5.4 References.

[1]. M. Minakata, K. Kumagai, S. Kawakami, *"Lattice constant changes and electro–optic effects in proton–exchanged $LiNbO_3$ waveguides"*, Appl. Phys. Letts., 49(16), pp.992–994, 1986.

[2] S. McMeekin and R.M. De La Rue, *"Novel transverse electro–optic waveguide phase modulator realised in titanium–indiffused and proton–exchanged $LiNbO_3$"*, Electronics Letters, 25, pp853–854, 1989.

[3]. T. Suhara, H. Tazaki, H. Nishihara, *"Measurement of reduction in SHG coefficient of $LiNbO_3$ by proton–exchange"*, Electronics Letters, 25, pp.1326–1328, 1989.

[4]. N. Bloembergen and A.J. Sievers, *"Nonlinear optical properties of periodical laminar structures"*,Appl. Phys. Letts, 17(11), pp.483–485, 1970.

[5]. B. Jaskorzynska, G, Arvidsson, F. Laurell, *"Periodic structures for phase–matching in SHG in titanium $LiNbO_3$ waveguides"*, Proceedings Integrated Optical Circuit Engineering III, SPIE Volume 651, 1986.

[6]. M.M. Fejer, G.A. Magel and E.J. Lim, *"Quasi phase–matched interactions in $LiNbO_3$"*, Proceedings of Nonlinear Optical Properties of Materials, SPIE volume 1148, 1989.

[7]. E.J. Lim, M.M. Fejer and R.L Byer, *"SHG of blue and green light in periodically–poled planar $LiNbO_3$ waveguides"*, Technical digest Topical Meeting on Nonlinear Guided wave Phenomena: Physics and Applications, Paper PD3–1, Houston, Texas, 2–4 February 1988.

[8]. E.J. Lim, M.M. Fejer and R.L Byer, *"SHG of green light in periodically–poled planar $LiNbO_3$ waveguides"*, Electronics Letts., 25(3), pp.174–175, 1989.

[9]. E.J. Lim, M.M. Fejer and R.L Byer, *"SHG of green light in periodically–poled planar $LiNbO_3$ waveguides"*, Proceedings Conference on Lasers and Electro–optics, Paper THQ4, 1989.

[10]. E.J. Lim, M.M. Fejer, R.L Byer and W. Kovlovsky, *"Blue light generation by frequency doubling in periodically–poled $LiNbO_3$ channel waveguides"*, Electronics Letts., 25(11), pp.731–732, 1989.

[11]. J. Webjorn, F. Laurell and G. Arvidsson, *"Periodically domain–inverted lithium niobate channel waveguides for SHG"*, Technical digest Topical Meeting on Nonlinear Guided wave Phenomena: Physics and Applications, Paper THA2–1, Houston, Texas, 2–4 February 1988.

[12]. J. Webjorn, F. Laurell and G. Arvidsson, *"Blue light generated by frequency doubling of laser light in a $LiNbO_3$ channel waveguide"*, IEEE Photonics Tech. Letts., 1(10), pp.316–318, 1989.

[13]. G. Arvidsson and B. Jaskorzynska, *"Periodically domain–inverted waveguides in $LiNbO_3$ for SHG: influence of domian boundary on the conversion efficiency"*, Proceedings Conference Materials for Nonlinear and Electro–optics, Inst. Phys. Conf, series 103: Pt. 1, Cambridge 1989.

[14]. D. Feng, N. Ming, J. Hong, Y. Yang, J. Zhu, Z. Yang and Y. Wang, *"Enhancement of SHG in $LiNbO_3$ crystals with periodic laminar ferroelectric domains"*, Appl. Phys. Letts., 37(7), pp.607–609, 1980.

[15]. N. Ming, J. Hong and D. Feng, *"Growth striations and ferroelectric domain structures in Czochralski–grown $LiNbO_3$ single crystals"*, Jnl. Mat. Sci., 17, pp.1663–1670, 1982.

[16]. D. Feng, *"Ferroelectric crystals with periodic laminar domains: a new type of nonlinear optical material"*, Proceedings Conference on Lasers and Electro–optics, Paper TUGG1, 1987.

[17]. A. Feisst and P. Koidl, *"Current induced periodic ferroelectric domain structures in $LiNbO_3$ for efficient nonlinear optical frequency mixing"*, Appl. Phys. Letts., 47(11), pp.1125–1127, 1985.

[18]. R.S. Fiegelson, *"Preparation of single crystal fibres"*, Proceedings Conference Materials for Nonlinear and Electro–optics, Inst. Phys. Conf, series 103: Pt. 1, Cambridge 1989.

[19]. M.M. Fejer, *"Single crystal fibres: Growth dynamics and nonlinear optical applications"*, Ph.D. dissertation, Univ. of Stanford, Stanford, 1986.

[20]. G.A. Magel, M.M. Fejer and R.L. Byer, *"SHG of blue light in periodically poled $LiNbO_3$"*, Proceedings Conference on Lasers and Electro–optics, Paper THQ3, 1989.

[21]. G.A. Magel, M.M. Fejer and R.L. Byer, *"Quasi phase–matched SHG of blue light in periodically poled $LiNbO_3$"*, Appl. Phys. Letts., 56(2), pp.108–110, 1990.

[22]. Y.S. Luh, R.S. Fiegelson, M.M. Fejer and R.L. Byer, *"Ferroelectric domain structures in $LiNbO_3$ single crystal fibres"*, Jnl. Cryst. Growth, 78, pp.135–143, 1986.

[23]. G.A. Majel, S. Sudo, A. Cordova–Plaza, M.M. Fejer, H.J. Shaw and R.L. Byer, *"SHG in $LiNbO_3$ fibres"*, paper WR3, Jnl. Opt. Soc. Am. (A), p.77, 1987.

[24]. T.Y. Fan, A. Cordova–Plaza, M.J.F. Digonnet, R.L. Byer and H.J. Shaw, *"Nd:MgO:$LiNbO_3$ spectroscopy and laser devices"*, Jnl. Opt. Soc. Am. (B), pp.140–148, 1986.

[25]. S. Miyazawa, *"Ferroelectric domain inversion in Ti–indiffused $LiNbO_3$ optical waveguides"*, Jnl. Appl. Phys., 50, pp.4599–4603, 1979.

[26]. S. Thaniyavern, T. Findlaky, D. Booher and J. Moen, *"Domain inversion effects in Ti–$LiNbO_3$ integrated optic devices"*, Appl. Phys. Letts., 46, pp.933–935, 1985.

[27]. A. Rauber, *"Doping modulation by electric currents in $LiNbO_3$ during crystal growth"*, Mat. Res. Bull., 11, p.497, 1976.

[28]. J.C. Peuzin, Comment on *"Domain inversion effects in Ti–$LiNbO_3$ integrated optic devices"*, Appl. Phys. Letts., 48(16), p.1104, 1986.

[29]. S. Miyawa, Response to [28], *ibid.*

[30]. K. Nakamura, H. Ando and H Shimuzu, *"Ferroelectric domain inversion caused in $LiNbO_3$ plates by heat treatment"*, Appl. Phys. Letts., 50, pp.1413–1414, 1987.

[31]. R.A. Becker, *"Comparison of guided–wave interferometric modulators fabricated on $LiNbO_3$ via titanium–indiffusion and proton–exchange"*, Appl. Phys. Letts., 43, pp.131–133, 1983.

[32]. P.W. Haycock and P.D. Townsend, *"A method of poling $LiNbO_3$ and $LiTaO_3$ below T_C"*, Appl. Phys. Letts., 48(11), pp698–700, 1986.

[33]. R.W. Keys, A. Loni, R.M. De La Rue, C.N. Ironside, J.H. Marsh, B.J. Luff and P.D. Townsend, *"Fabrication of domain reversed gratings for SHG in $LiNbO_3$ by electron beam bombardment"*, Electronics Letts., 26(3), pp188–190, 1990.

[34]. R.L. Myklebust, D.E. Newbury and H. Yakowitz, *"The NBS Monte–Carlo electron trajectory program"* in K.F.J. Heinrich (ed) " The use of Monte–Carlo calculations in EPMA and SEM", NBS special publication/460, p.105, 1979.

[35]. K. Nassau, H.J. Levenstein and G.M. Loiacano, *"The domain structure and etching of ferroelectric $LiNbO_3$"*, Appl. Phys. Letts., 6, pp.228–230, 1965.

[36]. See, for example, A. Rauber, *"Chemistry and physics of lithium niobate"* and references therein; Current Topics in Materials science, Vol. 1, Ed. E. Kaldis, North–Holland, 1978.

[37]. M.J. Li, M. De Micheli, Q. He and D.B. Ostrowsky, *"Cerenckov SHG in proton–exchanged $LiNbO_3$ guides"*, IEEE Jnl. of Quant. Elecs., 26(8), pp.1384–1393, 1990.

[38]. See, for example, Y.R. Shen, *"The Principles of Nonlinear Optics"*, John Wiley and Sons, 1984.

[39]. R.C. Eckardt, H. Masuda, Y.X. Fan and R.L. Byer, *"Absolute and relative nonlinear optical coefficients of KDP, KD*P, BaB_2O_4 $LiIO_3$, $MgO:LiNbO_3$ and KTP measured by SHG"*, IEEE Jnl. of Quant. Elecs., 26(5), pp.922–933, 1990.

[40]. M.M. Choy and R.L. Byer, *"Accurate second–order susceptibility measurements of visible and infrared crystals"*, Phys. Rev. B, 14(4), pp.1693–1706, 1976.

[41]. J. Jerphagnon and S.K. Kurtz, *"Maker fringes: A detailed comparison of theory and experiment for isotropic and uniaxial crystals"*, Jnl. Appl. Phys., 41(4), pp.1667–1681, 1970.

[42]. R.L. Byer and S.E. Harris, *"Power and bandwidth of spontaneous parametric emmission"*, Phys. Rev., 168, pp.1064–1068, 1968.

[43]. J. Finak, H. Jerominek Z. Opilski and K. Wotjala, *"Planar diffusion glass waveguides obtained by immersion in KNO_3"*, Optica Acta, XII, pp.11–17, 1982.

[44]. E.Y.B. Pun, K.K. Wong, I. Andonovic, P. Laybourn and R.M. De La Rue, *"Efficient waveguide Bragg–deflection grating on $LiNbO_3$"*, Electronics Letts., 18,pp.740–742,1982.

[45]. C.R. Jeggo and G.D. Boyd, *"Nonlinear optical polarisability of the*

niobium–oxygen bond", Jnl. Appl. Phys., 41, pp.2741–2743, 1970.

[46]. J.G. Bergman, *"Molecular mechanics of the ferroelectric to paraelectric phase transition in $LiNbO_3$ via optical SHG"*, Chem. Phys. Letts., 38(2), 1976.

Appendix.

This appendix presents, in detail, the steps involved in the fabrication of the grating structures.

(1) Cleaning.

The substrates were cleaned by scrubbing with a sponge in soapy water followed by successive ultrasonic baths in trichloroethylene, methanol, acetone and finally water.

(2) Photolithography (rear face).

A metal electrical contact was required on the rear face. The sequence of steps was:–

Spin on Shipley 1400–31 photoresist for 30 seconds at 4000rpm.

Bake for 30 minutes.

Expose and develop resist using the rectangular mask. (This mask was just smaller in size than the substrate. This was to ensure electrical isolation of the side walls).

Rinse in RO water and dry completely.

Evaporate 50nm of chromel followed by 200nm of gold.

Lift–off in acetone.

Spin on 1400–31 on rear face to protect the gold metal.

(3) Photolithography (front face).

Ensure that the –c– face of the wafer is spotlessly clean.

Evaporate 50 nm of chromel followed by 400 nm (or more) of gold.

Spin on Shipley 1400–17 photoresist for 30 seconds at 4000rpm.

Ensure that the mask is clean by soaking for 5 minutes in an etch consisting of 1:7 hydrogen peroxide to sulphuric acid (each time the mask was used it was re–cleaned in the etch to remove any residual photoresist).

Expose the grating for 2.25 minutes.

Develop for 60 seconds.

Etch gold in 1:1 saturated potassium iodide in iodine solution and RO water for 30–60 seconds.

Remove the remaining resist and dry the sample completely.

The nichrome etch was a mixture of hydrochloric acid and RO water in the ratio 4:1.

CHAPTER 6

CONCLUSIONS AND FUTURE WORK

6.1 Summary and conclusions

This thesis has reported a theoretical and experimental study of second order nonlinear effects in optical waveguides farmed by proton–exchange in lithium niobate. Chapter one served as a general introduction to nonlinear optics with special attention to second order nonlinear effects in both bulk and waveguide materials. It also reviewed the crystal structure of lithium niobate with respect to second order nonlinear effects and also introduced the proton–exchange process for the fabrication of optical waveguides in lithium niobate.

In chapter two a more detailed explanation of second order nonlinear effects in optical waveguides was presented, including second harmonic generation via the Cerenkov effect. The bulk of the chapter was devoted to outlining a model derived for the case of second harmonic generation via Cerenkov radiation in proton–exchanged waveguides. The difficulty in modelling the radiation modes of the harmonic light was dealt with by using a theory developed previously for electro–optic coupling to radiation modes, used in d3evices such as cut–off modulators. Although the theory is simplistic, it nevertheless allows a qualitative understanding of the problem and models fairly well the shape of the conversion efficiency/waveguide depth curve.

Chapter three was devoted to reporting the experimental work carried out to measure and characterise the Cerenkov second harmonic generation process in proton–exchanged waveguides.It was found that the optimum depth of waveguide fpr maximising the conversion efficiency of second harmonic generation in planar waveguides was of the order of 0.7 um. Using a Q–switched Nd:yag laser a maximum conversion efficiency of 1 $\%W^{-1}$ was measured. It was found that there were two peaks in the conversion efficiency /waveguide depth curve (at least to the maximum waveguide depth used in the work), in agreement to the predicted behaviour. After annealing the waveguides, known to restore the electro–optic effect in proton–exchanged waveguides (and also shown in a susequent chapter of the thesis to restore the nonlinear coefficient), led, in most cases, to a reduction in the conversion efficiency. It was argued that this reduction was probably a result of changing the overlap integrals and the increase in the nonlinear coefficient. The reduction in the conversion efficiency post–annealing was predicted by the simple model of chapter two. Second harmonic generation was also carried out in stripe waveguides with both a c.w. Nd:yag laser and a c.w. high output power semiconductor laser. The increase in the power densitywithin the waveguides allowed conversion efficiencies as high as 2.4

%W^{-1} for the Nd:yag laser and 2.8%W^{-1} for the semiconductor laser.

It has been reported by several independent research groups that proton-exchanged waveguides fabricated using phosphoric acids exhibit a higher refractive index difference and have lower propagation losses than waveguides formed using benzoic acid. Waveguides formedwith phosphoric acid could potentially give a higher conversion efficiency for second harmonic generation. A series of waveguides was fabricated using both benzoic acid and pyrophosphoric acids. It was found that the diffusion coefficients were the same for both acids, in contradictionto some reports, and that the refractive index change was only slightly higher in pyrophosphoric waveguides. The difference between the two refractive increases was not found to be as high as in other reports. Using the model developed in chapter two, it was calculated that the pyrophosphoric acid waveguides would produce more efficient second harmonic generation but only by a factor of 20% or so. This was confirmed experimentally using planar waveguides fabricated using each acid. Also reported in this chapter was experimental work carried out to investigate second harmonic generation in MgO-doped lithium niobate crystals. These crystals have a reduced susceptibility to optical damage with respect to undoped lithium niobate . The crystals can therefore be used with higher optical powers without causing optical damage to the crystal. This potentially would allow higher conversion efficiences to be attained. The crystals are especially useful in applications involving second harmonic generation with titanium-indiffused waveguides where optical damage can be a significant hindreance to high conversion efficiences. The inherently superior optical damage performance of proton-echanged waveguides means that optical damage was not found to be a problem. However, second harmonic generation in MgO-lithium niobate was investigated, again using benzoic acid and pyrophosphoric acid. It was found , in agreement with other authors, that the diffusuion coefficient was lower for the doped material and again the diffusion coefficient was the same for both acids, consistent with the observed diffusion constants in the undoped substrates. The measured conversion efficiences were similar to those obtained with the undoped substrates and it was concluded that there is no significant advantage to be gained by using the doped material under the experimental conditions used in the work.

Grating structures have a significant role to play in nonlinear optics. They can be used to provide the "extra" wavevector to allow phasematching in otherwise non-phasematchable crystals. One increasingly important application for nonlinear integrated optics in lithium niobate is the use of grating structures for quasiphasematching, i.e. phasematched second harmonic generation using the nonlinear d_{33} coefficient. Several techniques are known whereby a periodic modulation of the nonlinear d_{33} coefficient can be derived. Unfortunately they either require specialised crystal growth or can only be realised on the +c-face of the lithium niobate crystal which is not the preferred crystal orientation. A

technique was therefore developed whereby, for the first time, a local periodic modulation of the nonlinear d_{33} coefficient could be produced on the $-c-$face of the crystal. The technique involved photolithographically defining a grating structure on a gold masking layer deposited onto the $-c-$face. The crystal was then heated up to a temperature of 580^{0}C. The sample was then irradiated with a total dose of 10^{17} electrons at an energy of 20 keV for a period of one hour with a poling field of 10 Vcm^{-1} used to produce domain reversed gratings of the correct period for quasi-phasematched second harmonic generation of Nd:YAG laser radiation in a planar proton-exchanged waveguide. A second use was made of the properties of a grating structure to measure the magnitude of the nonlinear d_{33} coefficient. The nonlinear coefficient was measured by comparing the diffraction pattern of the harmonic radiation generated in a wedge shaped substrate with a planar waveguide region to that produced from a similar wedge with a periodic proton-exchanged region. It was found that, in agreement with published results, the nonlinear d_{33} coefficient was reduced to a value of 0.45 times that of the bulk value by proton-exchange. Extending this work to investigate the effect of annealing it was found that the magnitude of the nonlinear d_{33} coefficient increased with increasing annealing time.

As was suggested in the thesis outline one application for Cerenkov frequency doubled semiconductor lasers is in the field of optical storage. In my opinion the resulting beam quality of such a device makes there use prohibitive. It would seem far more realistic however that guided wave frequency doubled devices are very good candidates for such a practical application. The excellent beam quality from such devices (which can be focussed down to a diffraction limited spot) mean that they should find widespraed use in optical data storage systems at least until the practical demonstration of a blue laser.

6.2 Suggestions for future work

There are several aspects of the thesis which warrant further investigation. Firstly, a more rigorous theory should be developed by solving directly the wave equation under the given boundary and with more explicit expressions for the radiation modes. Such a theory would aid the waveguide fabrication and design to maximise the conversion efficiency with the available fundamental power. In order to improve the conversion efficiency for second harmonic generation the possibility of fabricating a resonant cavity at the fundamental wavelength could be investigated. This would involve depositing high reflectivity mirrors for the fundamental wavelength on the polished crystal end faces to confine the light in the stripe waveguide. Sohler et al have estimated that such an approach could increase the efficiency by 4- to 10-fold.

The domain reversal process should be further refined and optimised. The lithography

stages are tedious to perform and a new approach may produce better and more reproducible results. Such an approach might include laser beam writing of grating structures. It is important that domain reversed gratings are used in quasi–phasematching experiments. This would be an important test of the feasibilty of this appraoch for the production of domain reversed regions.

Although it was shown that the nonlinear d_{33} coefficient is reduced by the proton–exchange process further work should be undertaken to investigate the effect of processing conditions on the magnitude of the reduction. Also an investigation into the correlation (if any) between the increase in the nonlinear coefficient, a change in overlap integral and a change in the conversion efficiency as a function of annealing time and temperature. Such an in–depth study would give a greater scope for optimizing the waveguide parameters to maximise the conversion efficiency for second harmonic generation.

Several of the above ideas could be gathered together in a single experiment to demonstrate the feasibility of a self–frequency doubled laser. By doping the lithium niobate with either neodymium or erbium an efficient laser crystal can be realised. The lithium niobate waveguide laser crystal is an idealmedium for the realization of a miniature laser source. By fabricating a waveguide structure the laser threshold is reduced. Dichroic mirrors could be coated onto the end faces to provide suuficient feedback, whilst an electro–optic modulator would allow Q–switching/frequency control. With a domain reversed region inclyded on the substrate an all–integrated green laser could be fabricated with excellent spatial and temporal characteristics suitable for many applications.

Relevent Publications

[1]. *"Influence of annealing on the conversion efficiency for SHG by Cerenkov radiation in proton–exchanged $LiNbO_3$ waveguides"*, G. Arvidsson, F. Laurell, B. Jaskorzynska, A. Loni, R. W. Keys and R.M. De La Rue, Paper ThA3, Procs. Topical Meeting Nonlinear Guided Wave Phenomenon: Physics and Applications, Houston, Texas, 1989, O.S.A.

[2]. *"Characterization of proton–exchanged waveguides for second harmonic generation using Q–switched Nd:YAG laser pulses"*, R.W. Keys, A. Loni and R.M. De La Rue, Procs. IEE Colloquium Applications of Ultra–short Pulses for Optoelectronics, May 1989.

[3]. *"Cerenkov second harmonic generation in proton–exchanged waveguides"*, R.W. Keys, A. Loni and R.M. De La Rue, Poster paper, 9–th National Quantum Electronics Conference, Oxford, 18–22 September 1989.

[4]. *"Proton–exchanged lithium niobate optical waveguides made from phosphoric acids: detailed studies and comparisons with guides made with benzoic acid"*, M.A. Foad, A. Loni, R.W. Keys, J.M. Winfield, R.M. De La Rue, Presented at Integrated Optics and Optoelectronics, SPIE Procs. 1177, Paper 05, 1989.

[5]. *"Cerenkov second harmonic generation in proton–exchanged lithium niobate waveguides"*, R.W. Keys, A. Loni and R.M. De La Rue, Jnl. of Modern Optics, 37(4), pp.545–553, 1990.

[6]. *"Optical characterisation of Z–cut proton–exchanged $LiNbO_3$ waveguides fabricated using orthophosphoric and pyrophosphoric acid"*, A. Loni, R.W. Keys, R.M. De La Rue, M.A. Foad and J.M. Winfield, IEE Procs. Vol. 136, Pt. J, pp.297–300, 1989.

[7]. *"Fabrication of domain reversed gratings for SHG in $LiNbO_3$ by electron beam bombardment"*, R.W. Keys, A. Loni, R.M. De La Rue, C.N. Ironside, J.M. Marsh, B.J. Luff and P.D. Townsend, Electronic Letts., 26(3), pp.188–190, 1990.

[8]. *"Measurement of the increase in the SHG coefficient of proton–exchanged $LiNbO_3$ after annealing using a grating diffraction technique"*, R.W. Keys, A. Loni, R.M. De La Rue, ibid., 26(10), pp.624–626, 1990.

[9]. *"Characterization of waveguides formed by proton-exchange in MgO-doped and Nd:MgO-doped $LiNbO_3$: A comparison with congruent material"*, A. Loni, R.W. Keys and R.M. De La Rue, Jnl. Appl. Phys., 67(9), pp.3964-3967, 1990.